



Norwegian  
Meteorological Institute  
met.no

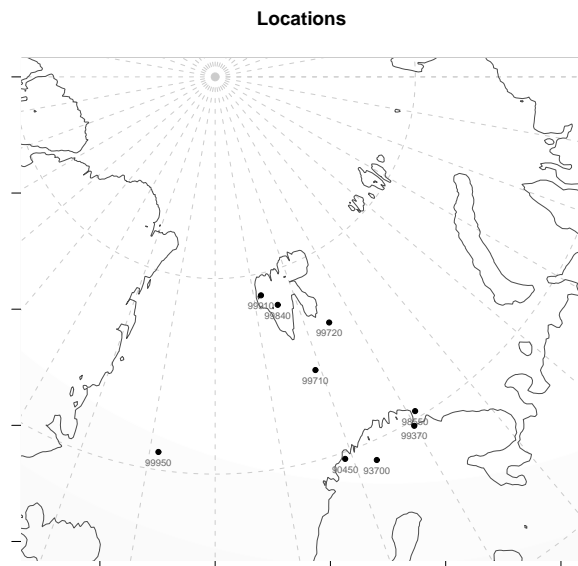
**met.no report**

no. 10/2008

Climate

# **Empirical-Statistical Downscaled Arctic Temperature & Precipitation Series**

Rasmus E. Benestad





Norwegian  
Meteorological Institute  
met.no

# report

<b>Title</b> Empirical-Statistical Downscaled Arctic Temperature & Precipitation Series	<b>Date</b> November 18, 2008
<b>Section</b> Climate	<b>Report no.</b> 10/2008
<b>Author</b> R.E. Benestad	<b>Classification</b> <input checked="" type="radio"/> Free <input type="radio"/> Restricted <b>ISSN</b> 1503-8025 <b>e-ISSN</b> 1503-8025
<b>Client(s)</b> NorACIA (The Norwegian Research Council) & met.no	<b>Client's reference</b>

## Abstract

Empirical-Statistical downscaling is carried out for monthly mean temperature and precipitation totals for a selection of Norwegian Arctic sites, based on the most recent global climate model simulations described in the Intergovernmental Panel on Climate Change (IPCC) fourth assessment report (AR4) from 2007. The downscaling analysis incorporated multi-model ensembles based on 50 integrations for temperature and 43 runs for precipitation, following the SRES emission scenario A1b for the future or '20C3M' for the past. The analysis involved new ways of combining results from the 20th century (CTL) with results for the 21st century (SCE), and a quality control was used to 'weed out' global climate models with a poor climate reproduction. The results were found to be sensitive to the choice of predictor domain, but smaller domains were taken to be more reliable.

## Keywords

Empirical-Statistical downscaling, Arctic temperature and precipitation, Climate change scenarios.

Disciplinary signature	Responsible signature
Inger Hanssen-Bauer	Eirik Førland

**Postal address**  
PO Box 43 Blindern  
N-0313 OSLO  
Norway

**Office**  
Niels Henrik Abels vei 40

**Telephone**  
+47 2296 3000

**Telefax**  
+47 2296 3050

**e-mail:** met.inst@met.no  
**Internet:** met.no

**Bank account**  
7694 05 00601

**Swift code**  
DNBANOKK

# Contents

<b>1</b>	<b>Introduction</b>	<b>4</b>
1.1	The problem . . . . .	4
1.2	Introduction to downscaling . . . . .	4
<b>2</b>	<b>Data</b>	<b>6</b>
2.1	Predictors: calibration . . . . .	6
2.2	Predictors: GCMs . . . . .	6
2.3	Predictand . . . . .	7
<b>3</b>	<b>Methods</b>	<b>9</b>
3.1	Related work . . . . .	9
3.2	ESD tool . . . . .	9
3.2.1	Common EOFs & 'finger printing'	9
3.2.2	ESD model . . . . .	10
3.2.3	Calibration & assessment . . . . .	10
3.2.4	Trend fits . . . . .	10
3.2.5	Known problems & fixes . . . . .	11
3.2.6	Quality check . . . . .	12
<b>4</b>	<b>Results</b>	<b>12</b>
4.1	Temperature . . . . .	13
4.1.1	Bjørnøya & Hopen . . . . .	13
4.1.2	Limitations, biases & uncertainties associated with sea-ice . . . . .	13
4.1.3	Quality checks . . . . .	14
4.2	Precipitation . . . . .	25
4.2.1	Trends . . . . .	25
4.2.2	Quality checks . . . . .	25
<b>5</b>	<b>Discussion &amp; Conclusions</b>	<b>38</b>

# 1 Introduction

The objective of this report is primarily to document a set of calculations done for the 'NorA-CIA' project (*Førland et al.*, 2008). This report have much in common with *Benestad* (2008b,c,a) and *Engen-Skaugen et al.* (2008, 2007), and hence, the introduction of this report is copied from these earlier reports. The focus will be on the methodological details and the results. However, a short introduction to background is also provided for the readers who are new to the subject. The lay-out of the report is as follows: a brief introduction, description of the data, methods, the results, discussion, conclusion and an appendix.

## 1.1 The problem

Since the industrial revolution, the levels of atmospheric concentrations of long-lived greenhouse gases such as CO<sub>2</sub> have risen (IPCC, 1995; Houghton et al., 2001; Solomon et al., 2007) and the most recent estimate suggests that the global mean surface temperature on Earth has increased by  $0.74 \pm 0.18^\circ\text{C}$  over the last 100 years (Solomon et al., 2007). It has been well-known within the scientific community for a long time that the effect of raised levels of atmospheric CO<sub>2</sub> will lead to a surface warming (Weart, 2003; Peixoto & Oort, 1992; Fleagle & Businger, 1980; Houghton, 1991; Solomon et al., 2007; Houghton et al., 2001; IPCC, 1995, 1990), and that future increases in the levels of greenhouse gases will warm the surface further (Meehl et al., 2007; Christensen et al., 2007a).

## 1.2 Introduction to downscaling

Global Climate models (GCMs) represent the most important tool for simulating Earth's climate, but they do not give a realistic description of the local climate in general (*Benestad et al.*, 2008)<sup>1</sup> because they tend to have a coarse spatial resolution (Figure 1) and are unable to represent aspects with spatial scales smaller than the grid box size. The GCMs are also unable to account for substantial variations in the climate statistics within a small region, such as the temperature differences over short distances (e.g. within a valley or on a hill side). Neither do the GCMs give a perfect description of the real climate system, as they include 'parameterisations' that involve simple statistical models giving an approximate or ad-hoc representation of sub-grid processes.

It is therefore common to downscale the results from the GCMs, either through a (i) nested

---

<sup>1</sup>Early version of the compendium also available at <http://www.gvc2.gu.se/ngeo/rcg/edu/esd.pdf>

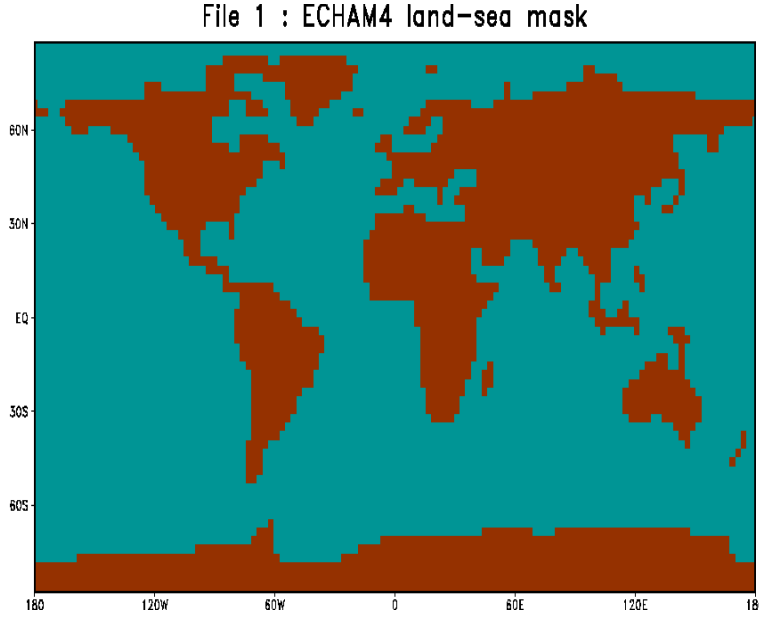


Figure 1: An example of land-sea mask of a general circulation model (GCM) with  $\sim 2^\circ \times 2^\circ$  spatial resolution (T42). Notice that Italy and Denmark are not represented in the model.

high-resolution regional climate model (RCM) (Christensen & Christensen, 2002; Christensen et al., 2001, 1998; Haugen et al., 2000; Haugen & Ødegaard, 2003) or (ii) through empirical/statistical downscaling (von Storch et al., 1993a; Rummukainen, 1997; Easterling, 1999; Benestad, 2004; Wilby et al., 2004; Hanssen-Bauer et al., 2005; Fowler et al., 2007; Benestad et al., 2008). The latter is henceforth referred to as 'empirical-statistical downscaling', or the abbreviation 'ESD'.

Here we will define downscaling as *the process of making the link between the state of some variable representing a large space* (henceforth referred to as the 'large scale') *and the state of some variable representing a much smaller space* (henceforth referred to as the 'small scale').

Another view of ESD is that it is an advanced statistical analysis of the model results.

The large-scale variable may for instance represent the circulation pattern over a large region whereas the small scale may be the local temperature as measured at one given point (station measurement).

It is important to keep in mind the limitations of statistical downscaling, especially when applied to model results from greenhouse gas (GHG) integrations using GCMs. The statistical models are based on historical data, and there is no guarantee that the past statistical relationships between different data fields will hold in the future.

One should also be concerned about the uncertainties associated with the GCM results as well as those of the downscaling methods themselves (Wilby et al., 1998). It is well known that low resolution GCMs are far from perfect, and that they have problems associated with for in-

stance cloud representation, atmosphere-ocean coupling, and artificial climate drift (*Bengtsson*, 1996; *Anderson & Carrington*, 1994; *Treut*, 1994; *Christensen* et al., 2007b).

Part of the problems are due to incomplete understanding of the climate system. The important mechanisms causing variability such as El Niño Southern Oscillation (ENSO) and the North Atlantic Oscillation (NAO) for instance are probably still not completely understood (*Sarachik* et al., 1996; *Anderson & Carrington*, 1994; *Philander*, 1989; *Christensen* et al., 2007b). In addition, it is unlikely that the global GCMs will simulate regional details realistically due to discretisation and gridding of data, (*Crane & Hewitson*, 1998; *Zorita & von Storch*, 1997; *von Storch* et al., 1993b; *Robinson & Finkelstein*, 1991).

However, because a wide range of global GCMs predict observed regional features (e.g. the NAO, ENSO, the Hadley Cell, atmospheric jets), it is believed that the GCMs may be useful for predicting large scale features.

## 2 Data

### 2.1 Predictors: calibration

Monthly gridded data from the ERA40 (*Bengtsson* et al., 2004; *Simmons & Gibson*, 2000) were used as predictors for training the statistical models.

### 2.2 Predictors: GCMs

The multi-model ensemble of global climate model (GCM) simulations used here represents a range of different GCMs and is referred to as 'MMD' (also referred to as 'CMIP3'). These simulations are reported in Intergovernmental Panel on Climate Change (IPCC) fourth assessment report (AR4) (*Meehl* et al., 2007), and the data are freely available from Program for Climate Model Diagnosis and Intercomparison<sup>2</sup>. This model ensemble includes both simulations for the 20th century (20C3M) and scenario runs for the 21th century following the Special Report Emission Scenarios (SRES) A1b<sup>3</sup> (*Nakicenovic* et al., 2000). Some of the GCMs have been

---

<sup>2</sup>PCMDI; <https://esg.llnl.gov:8443/index.jsp>

<sup>3</sup>The A1 storyline and scenario family describes a future world of very rapid economic growth, global population that peaks in mid-century and declines thereafter, and the rapid introduction of new and more efficient technologies. Major underlying themes are convergence among regions, capacity building and increased cultural and social interactions, with a substantial reduction in regional differences in per capita income. The A1 scenario family develops into three groups that describe alternative directions of technological change in the energy system. The three A1 groups are distinguished by their technological emphasis: fossil intensive (A1FI), non-fossil energy sources (A1T), or a balance across all sources (A1B) (where balanced is defined as not relying too heavily on one particular energy source, on the assumption that similar improvement rates apply to all energy supply and end-use

used to make several parallel runs, differing only by using different initial conditions (starting point).

The ESD was applied to the MMD ensemble for both the 20th century and the 21st century simulations separately. Tables 3–4 in the appendix provide a complete list of the GCMs and runs (integrations) included in this analysis. The choice of the GCMs was somewhat arbitrary, as (*i*) results from some models were not available on-line at the time of the downloads, (*ii*) there has been several rounds of fetching GCM data, (*iii*) the impact of adding further GCM results was not expected to add much new information about the inter-model spread, and (*iv*) there was no attempt to have a systematic strategy for a complete set of GCMs and runs (the reason - see points *i*–*iii*). However, most of the CMIP3 GCMs are included in the 'super-ensemble'.

### 2.3 Predictand

The station data (the predictand) were taken from the Norwegian climate data archive ('Klima-DataVareHuset'), and retrieved using the function KDVH4DS in the R-package `met.no`. The station numbers were: 90450, 93700, 94260, 97250, 98550, 99370, 99710, 99720, 99840, 99910, and 99950, and the locations of the sites are shown in Figure 2. For Svalbard Lufthavn (air port; station number 99840) extended data series were provided by Inger Hanssen-Bauer (precipitation) and Øyvind Nordli (temperature). Furthermore, the temperature record from Ny Ålesund (99910) was provided by Hanssen-Bauer, as opposed to using a shorter series from climate data archive. The longer Ny Ålesund temperature series spanned the period 1935–2008 (as opposed to 1972–2008 provided by the climate data archive), but this temperature record also differed from the climate data archive record during the late 1990s. The shorter climate data archive had a gap in 1997–1999, and the longer record had a slight systematic positive bias before 1990 compared to the climate data archive record. The bias, however, had little impact on the calibration of the ESD model, but was more pronounced during summer and spring/autumn and is possibly related to different ways of estimating the daily mean temperature (using different 'K-values').

---

technologies). (source: <http://www.ipcc.ch/ipccreports/tar/vol4/english/099.htm>)

## Locations

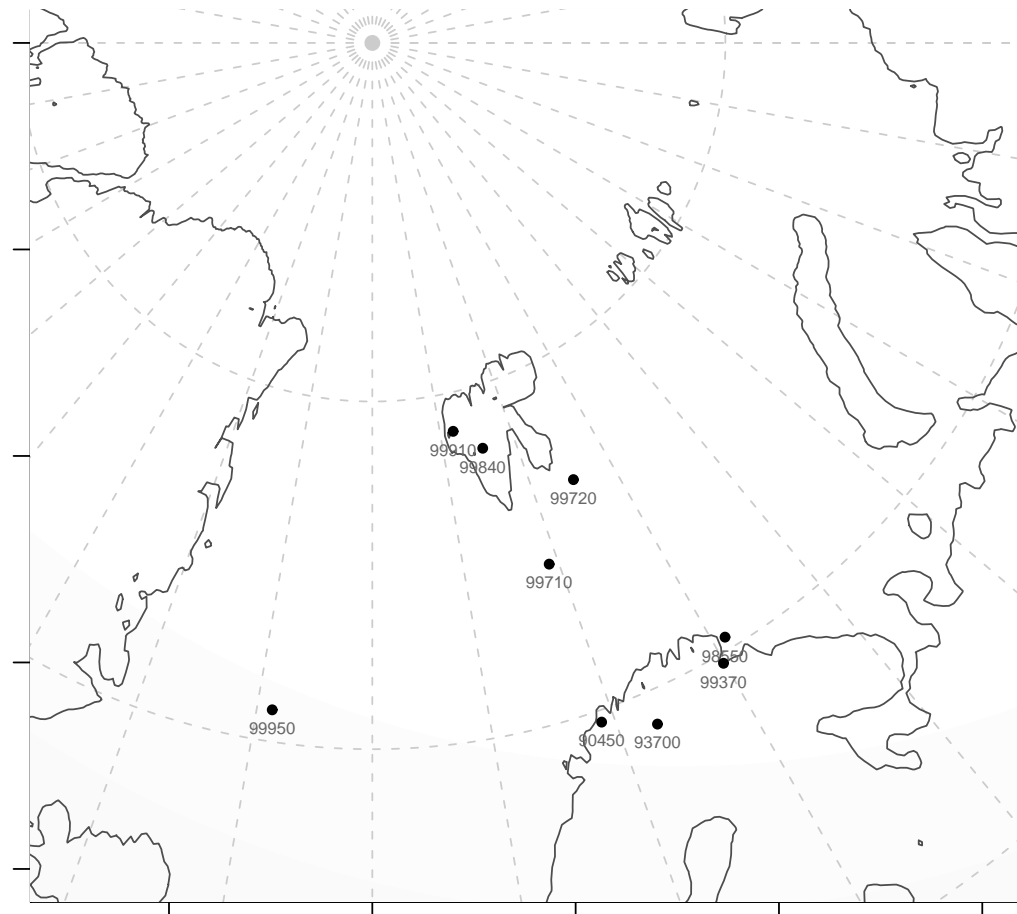


Figure 2: Maps showing the location of the temperature measurements.

## 3 Methods

### 3.1 Related work

The method on which these results are based has been used in several previous studies and is therefore well-documented. This study uses similar approach as those used in *Benestad* (2008b) to downscale Norwegian regional climate series, *Engen-Skaugen* et al. (2007) to downscale river run-off, and *Engen-Skaugen* et al. (2008) where catchment-scale temperature and precipitation were downscaled. Thus, much of the introduction of those reports are recited here. The implementation of the ESD is also documented in *Benestad* (2005), explaining how each GCM were downscaled for each calendar month separately. Large-scale precipitation was used to downscale the local precipitation, as in *Benestad* et al. (2007), and large-scale temperature was used to estimate the local temperature.

### 3.2 ESD tool

The tool clim.pact (*Benestad*, 2003, 2004; *Benestad* et al., 2008) was used to carry out the calculations, using a common empirical orthogonal function (EOF) based framework (*Benestad*, 2001) and linear multiple regression as a basis for the empirical-statistical model.

The ESD was based on a 'finger-print' type technique whereby spatial patterns describing the large-scale anomalies correlated with the local variations were identified in the gridded observations (re-analysis) and then matched with the same spatial structures found in the model results.

#### 3.2.1 Common EOFs & 'finger printing'

A common EOF framework combined large-scale gridded temperature or precipitation anomalies estimated from the ERA40 re-analysis with corresponding anomalies from a simulation performed by a GCM (interpolated onto the same grid as the former). An ordinary EOF analysis is applied to this combined data set. The common EOF framework yields both the spatial structures (referred to as 'EOFs' or 'modes') as well as weights describing their temporal evolution/variation (referred to as 'principal components').

By combining anomalies rather than the total values, constant biases are removed, however, the constant level of the end results become more arbitrary. Thus, when analysing the final results, the 'traditional' approach has been to focus on trends and long-term transient behaviour, rather than the initial level (e.g. the first 10 years) of the downscaled time series. Here, the

analysis was based on absolute values after the ESD results for the 20st century (SCE) has been combined with the 20th century (CTL), as described below.

The principal components (PCs) describing the temporal variations of the different modes (dominant spatial temperature or precipitation pattern) represent exactly the same spatial structures for GCMs and the ERA40.

### 3.2.2 ESD model

A step-wise regression analysis was employed that used the part of the PCs describing the ERA40 data together with the predictand (temperature or precipitation series) to calibrate the model. This calibration returns  $R^2$ -statistics, describing how well the local series can be reproduced with the statistical model if the ERA40 data is used as predictor.

### 3.2.3 Calibration & assessment

The `clim.pact` tool makes predictions based on the calibration data (here ERA40) as well as the GCM (here either 20th century or the 21st century). However, the ESD-results derived from ERA40 are not independent and only serves as a visual check of the quality of the statistical downscaling model. The downscaling for the 20th century, on the other hand, provides independent data which can be used in the validation against the actual observations. This validation will test whether the ESD-model is good (here the  $R^2$ -statistic is also a measure of skill).

### 3.2.4 Trend fits

In order to ensure representative values, the downscaled scenarios were adjusted so that the starting point of the scenarios (SCE) match the final parts of the matching simulations  $i$  of the past (CTL). This adjustment was done on calendar month-by-calendar month  $m$  basis similar to the adjustment in *Benestad* (2008b) (first doing the adjustment for all January months, then for all February months, etc).

But whereas the adjustment in *Benestad* (2008b) was based on the first and last 3 data points of the 20th (CTL) and 21st (SCE) centuries for GCM  $i$  and calendar month  $m$  ( $y_{i,m,\text{SCE}}(t) = y_{i,m,\text{SCE}}(t) - \overline{y_{i,m,\text{SCE}}(t \in [1, 2, 3])} + \overline{y_{i,m,\text{CTL}}(t \in [n-2, n-1, n])}$ ), the adjustment here was performed by first fitting a quadratic trend and then matching the starting point of the SCE trends to end points of the CTL trends. However, before the stitching of the SCE and CTL series, the CTL runs were adjusted so that they had the same 1961–1990 mean as the observations. The reason for this change was that the mean level of the 3 first and last data points could fluctuate randomly, thus resulting in unrealistic outliers. For instance, if the last 3 January temperatures

in the CTL results were dominated by internal variations such as a dip and the 3 first in SCE were part of a peak in the natural variations, then the level of the SCE temperatures may be set to be spuriously low (which could result in apparent cooling between 1961–1990 and 2070–2099). The 3-end-points matching also generates a wider range of results (i.e. widens the confidence intervals) compared to a more optimal adjustment.

The new trend-matching is now default in the `ESD.results()`-call in the `met.no` package version 1.2-0 (September 12 2008) or later, as opposed to the earlier versions of `met.no`<sup>4</sup>. Specifically, the default part of the `ESD.results()`-code matching the CTL with SCE runs looks like

```
tr1 <- predict(lm(y1 ~ I(t) + I(t^2)))      # Quadratic trend firt for CTL
tr2 <- predict(lm(y2 ~ I(t) + I(t^2)))      # Quadratic trend firt for SCE
offset <- tr1[length(tr1)] - tr2[1]        # Difference between the CTL-trend end-point and SCE-trend
                                                # start-point
batch2[ii,im,] <- batch2[ii,im,] + offset # Adjust the mean level of the SCE series
```

Those runs that did not have a 20th century match were pooled together, and the median of the 3 first years for entire set of unmatched runs were set to the median of the 3 last years of the entire set of CTL runs, as in *Benestad* (2008b).

Then trends were estimated for the observations and scenarios respectively, taking the best-fit to a fifth-order polynomial for the ensemble median or quantile for the confidence bounds, as in *Benestad* (2008b).

### 3.2.5 Known problems & fixes

Due to suspect recordings of precipitation amounts at Hopen and Kautokeino after 1990 (station relocation), the values after 1989 were set to missing prior to calibration of the ESD model (thus excluding these from the model training).

Some GCMs had the year wrong in the data files, which has been corrected for in `met.no_1.1-0` (Version: June 12, 2008). The plume plots exclude those GCM runs that give a standard deviation outside the range of [0.5, 3.0] for temperature and [0.3, 3.0] for precipitation of that of the corresponding observed standard deviation. In this case,  $\sigma$  for the SCE runs was estimated for the time interval 2010–2091 (this is implemented in the `met.no` package version 1.1-0, as of Jun 12 2008).

---

<sup>4</sup>The old approach can still be implemented by setting the argument `stitch="endpoints"` in the call to `ESD.results()` - see the manual for the function for more details.

### 3.2.6 Quality check

An additional quality control applied to the temperature, for which there was no matching series in the 20C run and the scenario, involved weeding out the time series for which the first mean of the 3 first years (each month was tested individually, thus involving three point averages) was more than 3 standard deviations away from the corresponding ensemble mean for the 3 last corresponding values from the 20C run.

The predictor domain for most of the stations was automatically defined from objective means within the location of the site  $\pm 50^\circ$  of longitude ( $\theta$ ) and the latitude ( $\phi$ )  $10^\circ$  to the north and  $30^\circ$  to the south of the site, but this extensive area was problematic for the Svalbard sites where the temperature correlated with the sea-ice edge. The GCMs did not reproduce the location of the sea-ice edge accurately, and therefore failed to provide a realistic description of the local temperature for these sites. But the problem was partly avoided ('swept under the carpet') by using a predictor domain that was constrained to smaller area for the stations Svalbard lufthavn (99840) and Hopen (99720) ( $\pm 50^\circ$  of longitude and  $5^\circ$  to the north and  $20^\circ$  to the south), and for Ny Ålesund (99910) temperature this search was further limited to  $\theta \pm 15^\circ$  and  $\phi - 15^\circ$  to  $\phi + 5^\circ$ . Thus, the results for these three locations are associated with less confidence than for other sites.

For precipitation, the predictor domains were constrained to  $\pm 15^\circ$  north-south and east-west of the location of the station. Larger domains would result in spurious results as the spatial scales associated with the local series are in fact quite small. A large domain resulted in a slightly negative winter trend for precipitation in Tromsø. The dependency of trend estimates to predictor domains was addressed by *Benestad* (2001) and the relationship between the spatial scales and domain size is discussed in *Benestad* et al. (2008). Thus, the choice of predictor domain introduced additional uncertainty.

The complete listing of the R-script used to make the computations presented here is given in the Appendix.

## 4 Results

The following figures are shown to provide a quick idea of the main features present in the downscaled results. These should be considered as part of the documentation of these results together with the tables. The results in the figures speak for themselves: there is a general tendency towards warmer climate in the future and there is a considerable spread in the values derived from the different GCM.

Here 'winter' is taken as December–February, 'spring' is March–May, 'summer' June–August, and 'autumn' is September–November.

## 4.1 Temperature

Figures 3–11 show the ESD results for temperature at the NorACIA stations in Figure 2, and the 2070–2099 climatological values for the different seasons are summarised in Table 1. The plume plots presented in Figures 3–11 indicate the presence of pronounced temperature spikes for some or unrealistically weak year-to-year variability for other stations discussed below.

### 4.1.1 Bjørnøya & Hopen

The September–November results for Bjørnøya (Figure 7) exhibited some 'spike' characteristics for some of the ESD results, possibly due to near-singularities in the matrix operations (linear algebra) involved in the singular value decomposition (*Strang*, 1988; *Press et al.*, 1989). The spikes (extremely high or low values) are thought to be caused by near-singularities in the matrix inversion or the performance of the singular value decomposition (SVD). The SVD was mainly performed with the routine DSVDC from the LINPACK library, but sometimes this algorithm failed, and the LAPACK routines DGESDD and ZGESVD were used instead.

A large number of GCM runs were also weeded out in the automatic quality check for the March–May scenario results (the blue shaded region is dramatically reduced). However, the lines marking the 10-year low-passed individual series of the individual runs seem to follow a realistic course, albeit with weak year-to-year variability (one of the criteria for weeding out the ESD results).

Original ESD-results for summer temperature at Hopen exhibit large variance differences between the 20th and 21st centuries (not shown), but a re-run with a smaller domain and a new strategy for matching C20 and C21 series gave results more in line with observations and expectations (more diagnostics are presented in the appendix).

### 4.1.2 Limitations, biases & uncertainties associated with sea-ice

It was found that the most pronounced observed temperature anomaly in the Greenland–Iceland–Norwegian Sea (GIN Sea) region was associated with changes in the sea-ice border east of Greenland, temperatures in the Greenland interior, and north-western Russia. The leading common EOF pattern, however, had greater resemblance with the leading EOF for the GCM than ERA40, and with different structures along the sea-ice border to that seen in the observations.

It has been found that the position of the sea-ice has a strong influence of the local temperature, and many GCMs which do not use flux correction have large systematic errors in the description of the sea-ice extent (*Benestad et al., 2002*).

#### 4.1.3 Quality checks

Quality test and further diagnostics (presented in the appendix) indicate that the  $R^2$ -metric used to describe the quality of the analysis (the variance that can be accounted for by the multiple regression) yields low values for some calendar months. Low values for  $R^2$  can suggest weak correlation between the large-scale temperature anomalies embedded in the ERA40 re-analysis and the local station series.

The Ny Ålesund (Spitsbergen, Svalbard) and Hammerfest series from the Norwegian Institute's climate data archive were shorter than e.g. the Tromsø temperature, but the former was replaced by a longer series (Hanssen-Bauer, pers. comm) whereas the latter gave questionable results and is therefore not included in this report.

The ESD is hampered by systematic model biases in the Arctic region and disimilarities between the spatial modes predicted by the GCM and those found in the ERA40 re-analysis. To provide a simple assessment of the ability of the GCMs to predict the spatial patterns, the leading EOFs derived from the ERA40 temperature was compared with the leading EOF of an arbitrary selected GCM simulation (HadGEM1 run 1) and the leading common EOF. One should keep in mind that the HadGEM1 may be one of the most skillful GCMs and that the higher order modes, which may be more relevant for the actual prediction of the local temperature, may differ more than the leading mode.

The predictor patterns can reveal unrealistic or accidental relationships between the local and larger scales. The January pattern for Svalbard-Lufthavn (99840) reveals weights in the sea-ice edge region, which is where the GCMs tend to misrepresent the local sea-ice conditions and hence the temperature. The predictor domain for Svalbard-Lufthavn (99840) and July was selected to be smaller than for January, yielding results with higher variance.

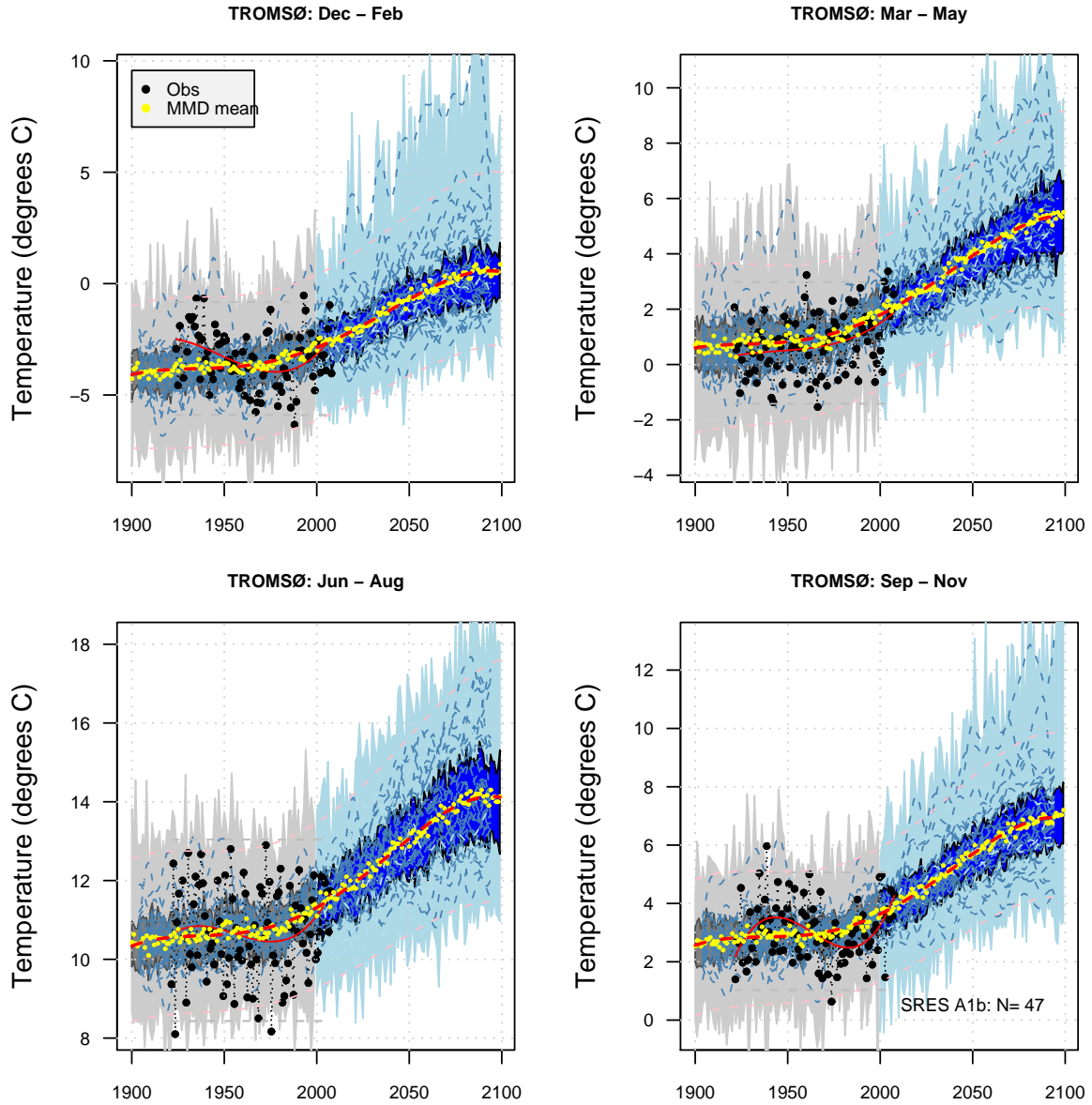


Figure 3: Plume plot for Tromsø (90450), showing the time evolution of the observed values (black), the 20th Century simulations (grey), and the future scenarios (blue). The light shading shows the minimum–maximum range for the ensemble, and the darker shading marks the inter-quartile range (25%–75%). The yellow symbols mark the ensemble mean values and the thick red-dashed is the polynomial trend fit to these. The thin pink lines show best-fit polynomial to the 5 and 95 percentiles, and the dashed blue lines show 10-year low-pass filtered (Gaussian filter) of the individual runs.

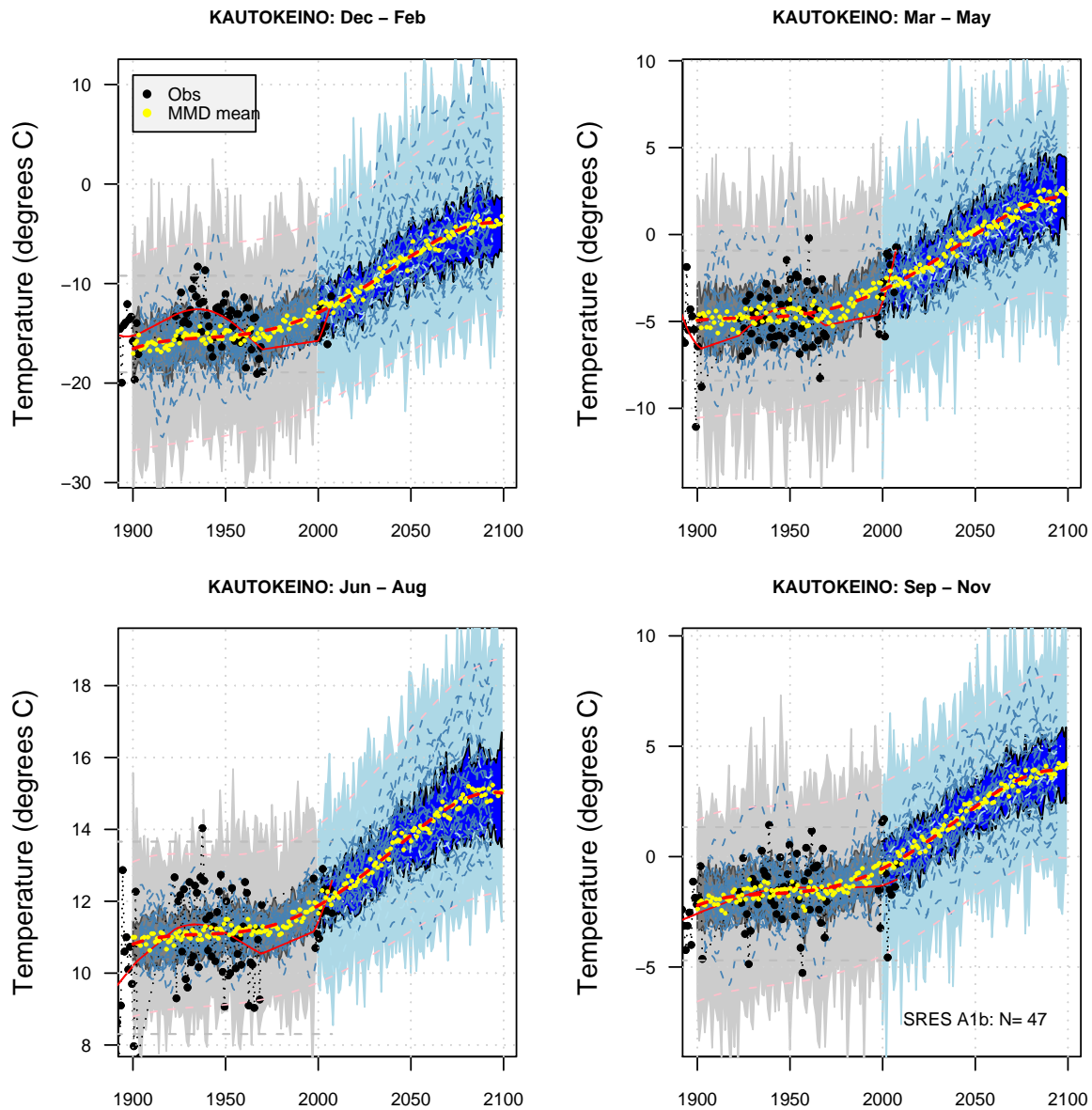


Figure 4: As in Figure 3, but for Kautokeino (93700).

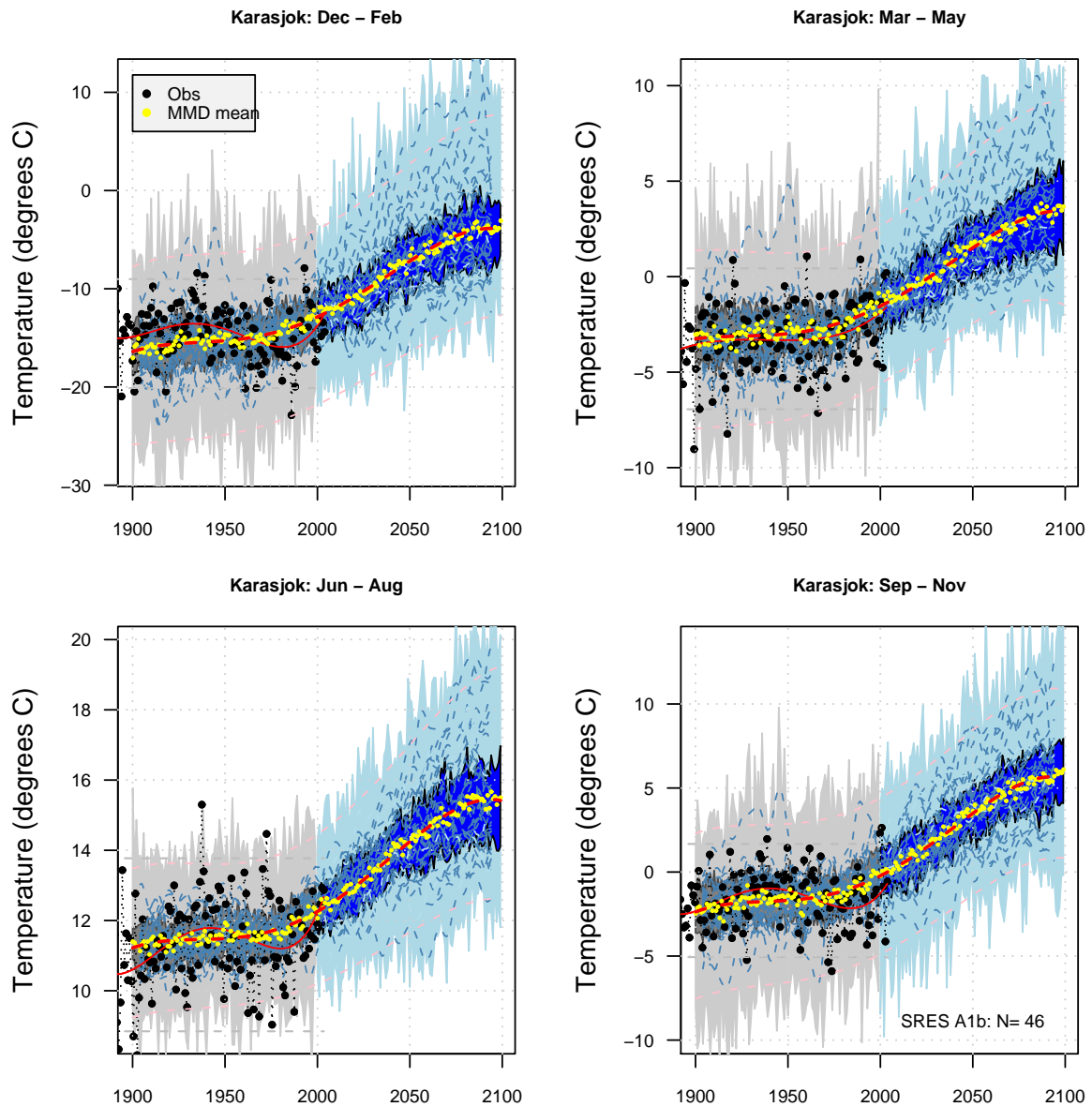


Figure 5: As in Figure 3, but for Karasjok (97250).

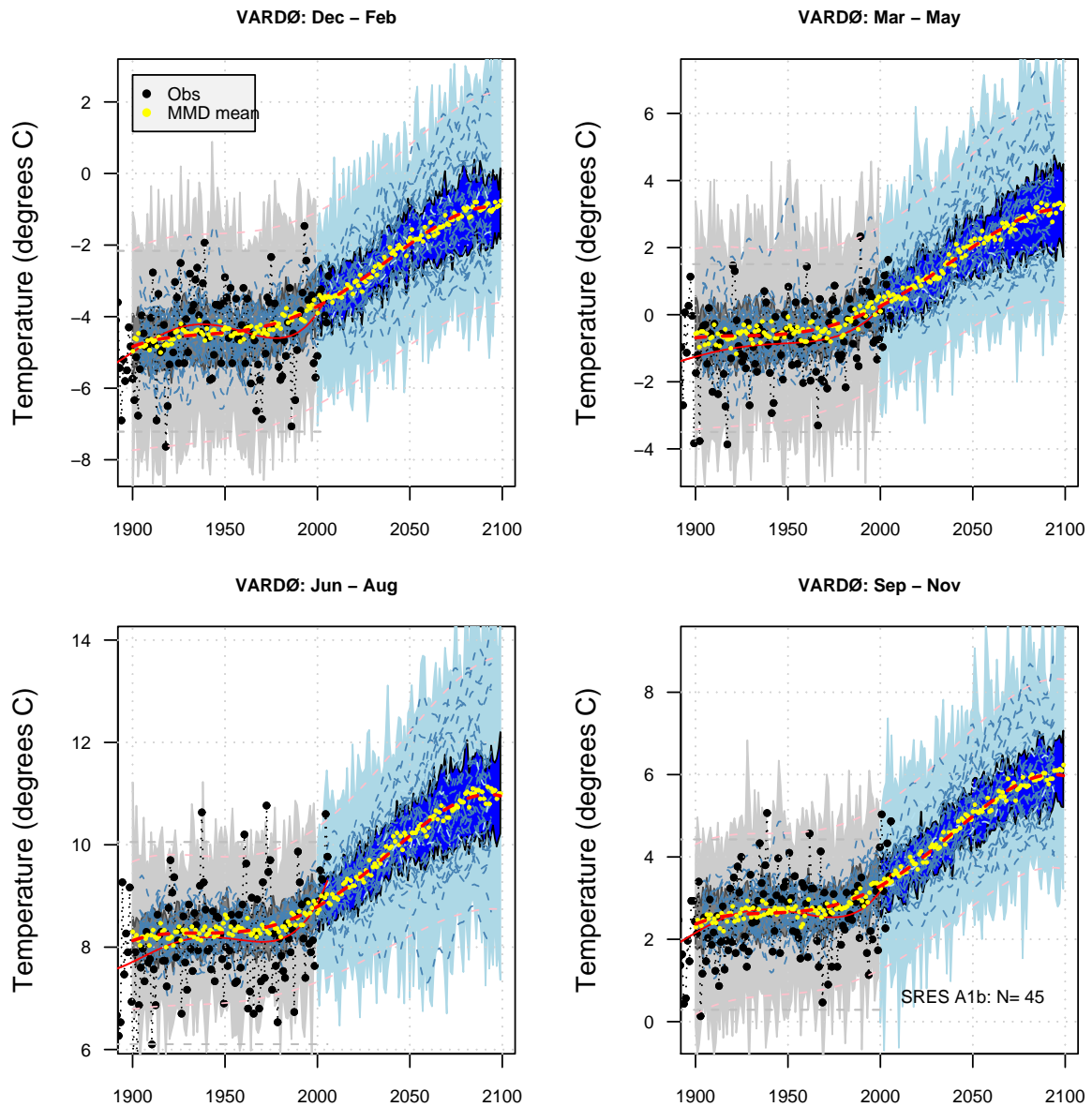


Figure 6: As in Figure 3, but for Vardø (98550).

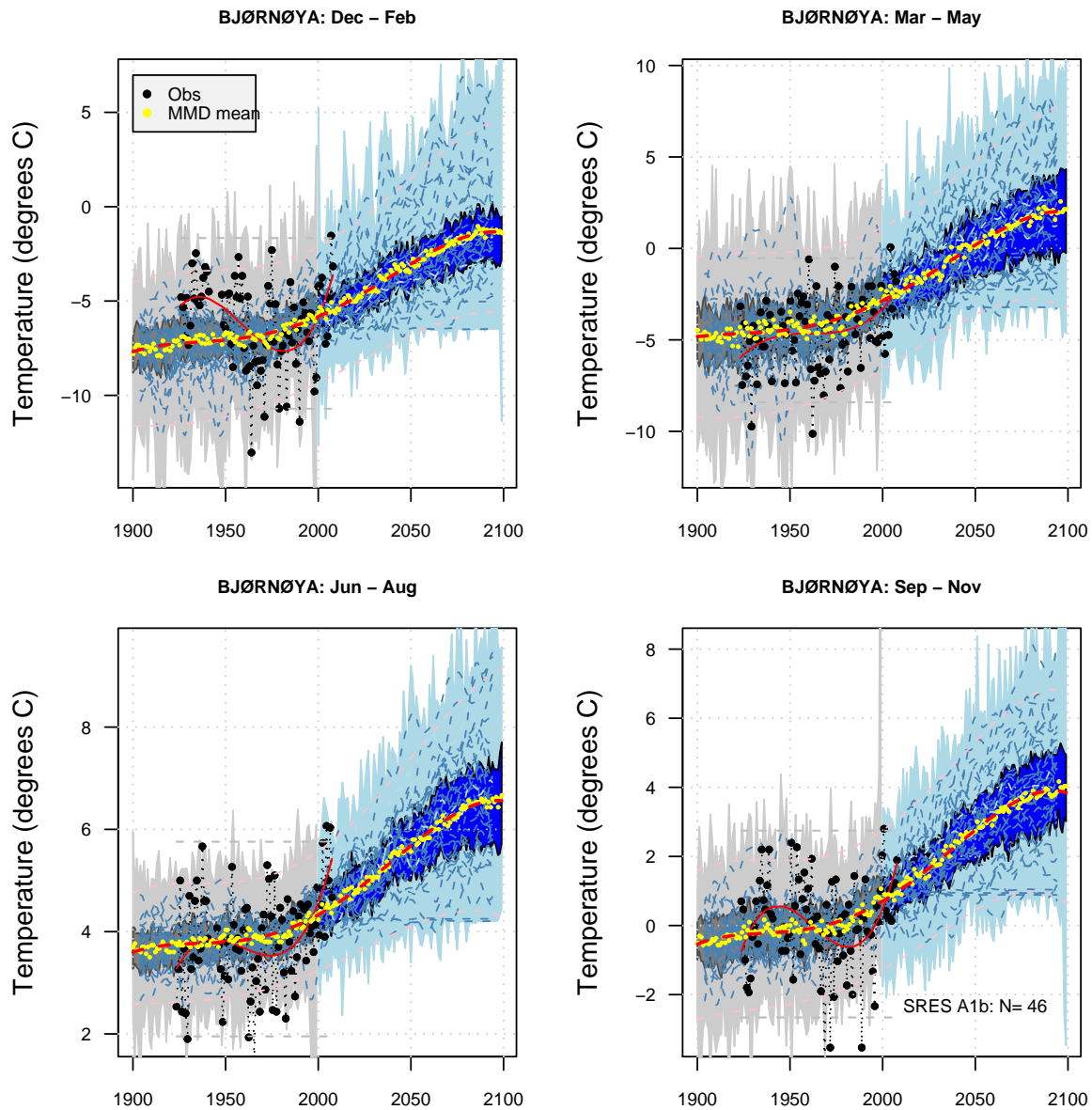


Figure 7: As in Figure 3, but for Bjørnøya (99710).

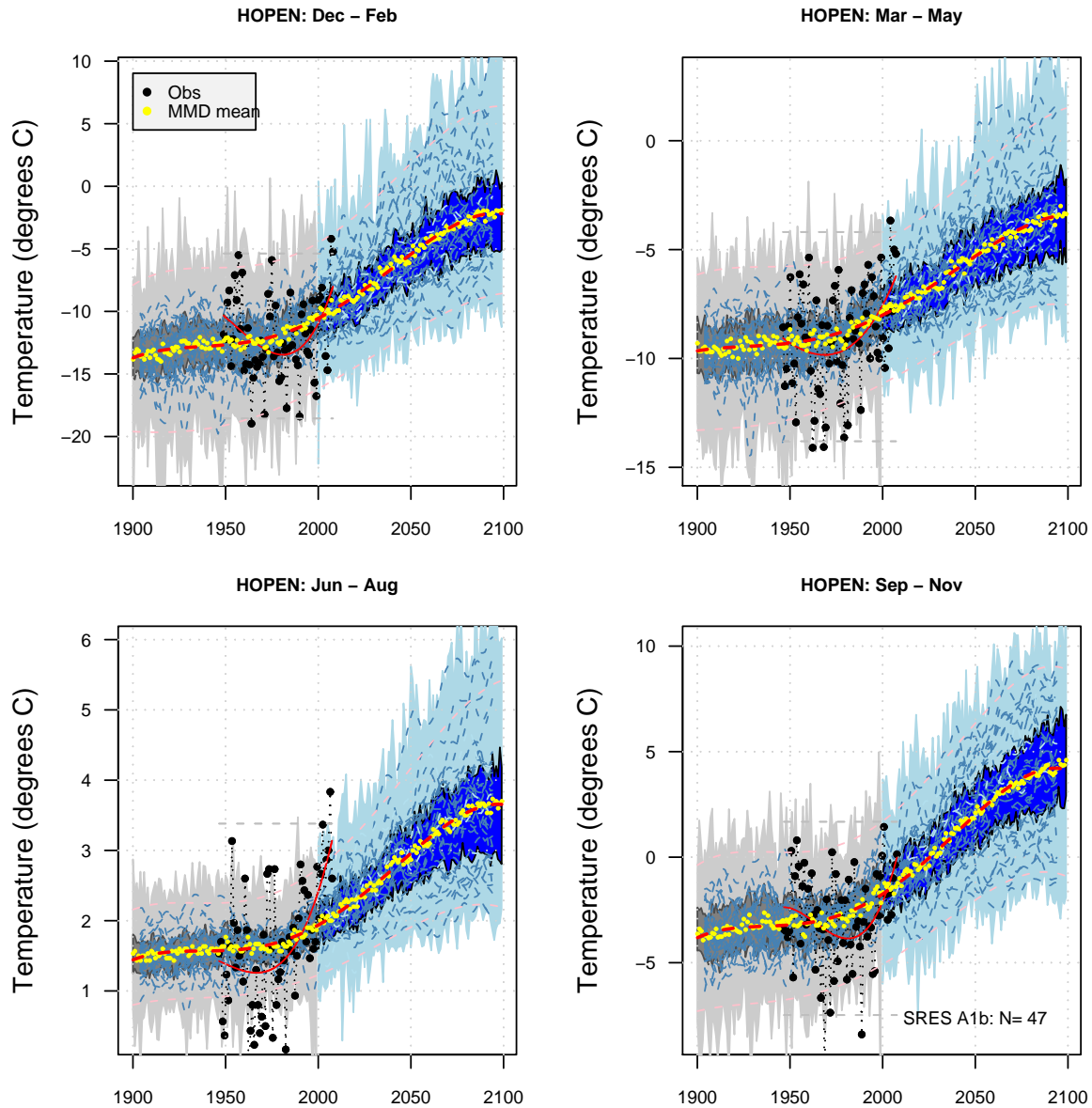


Figure 8: As in Figure 3, but for Hopen (99720).

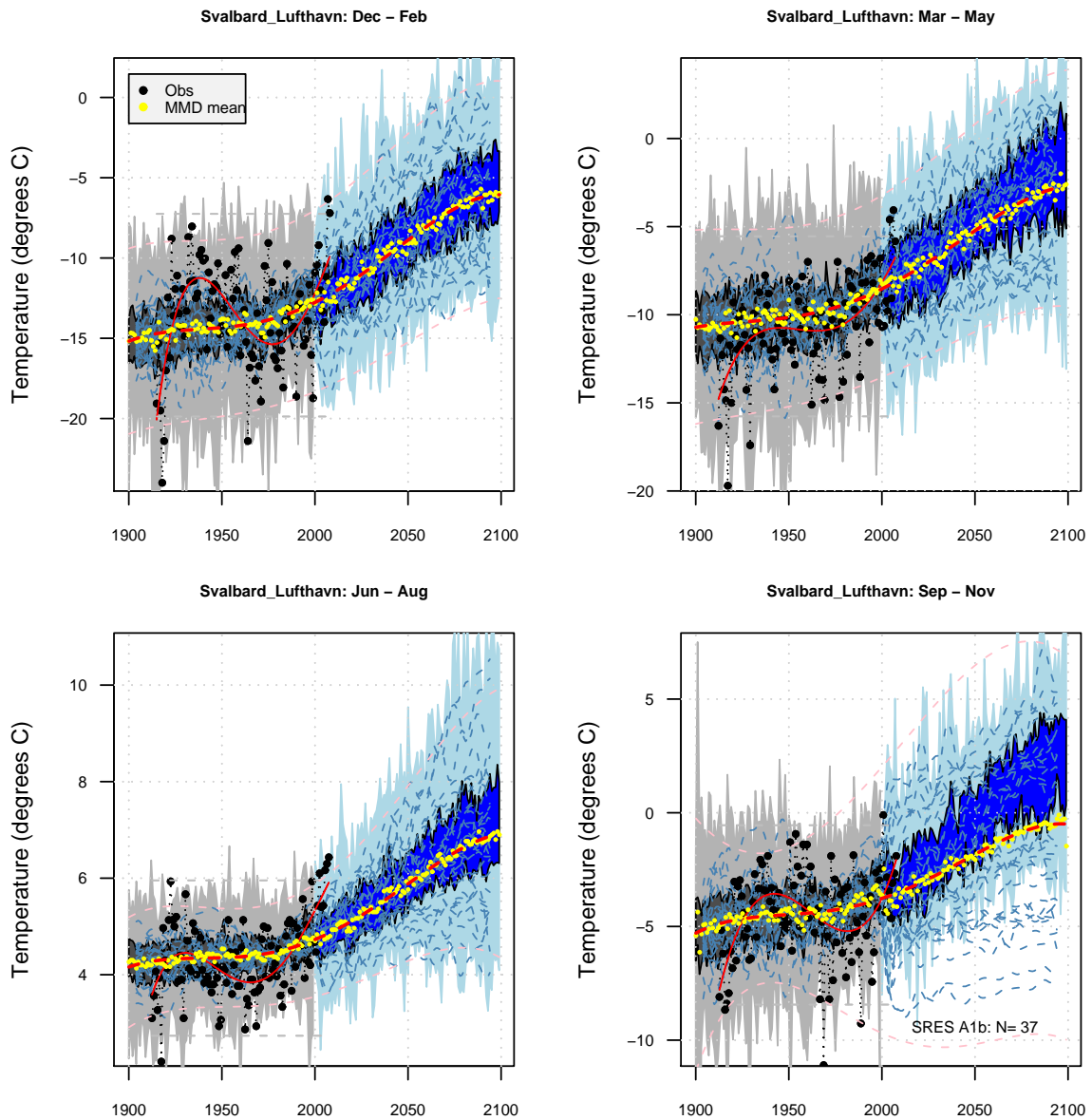


Figure 9: As in Figure 3, but for Svalbard lufthavn/Longyearbyen (99840).

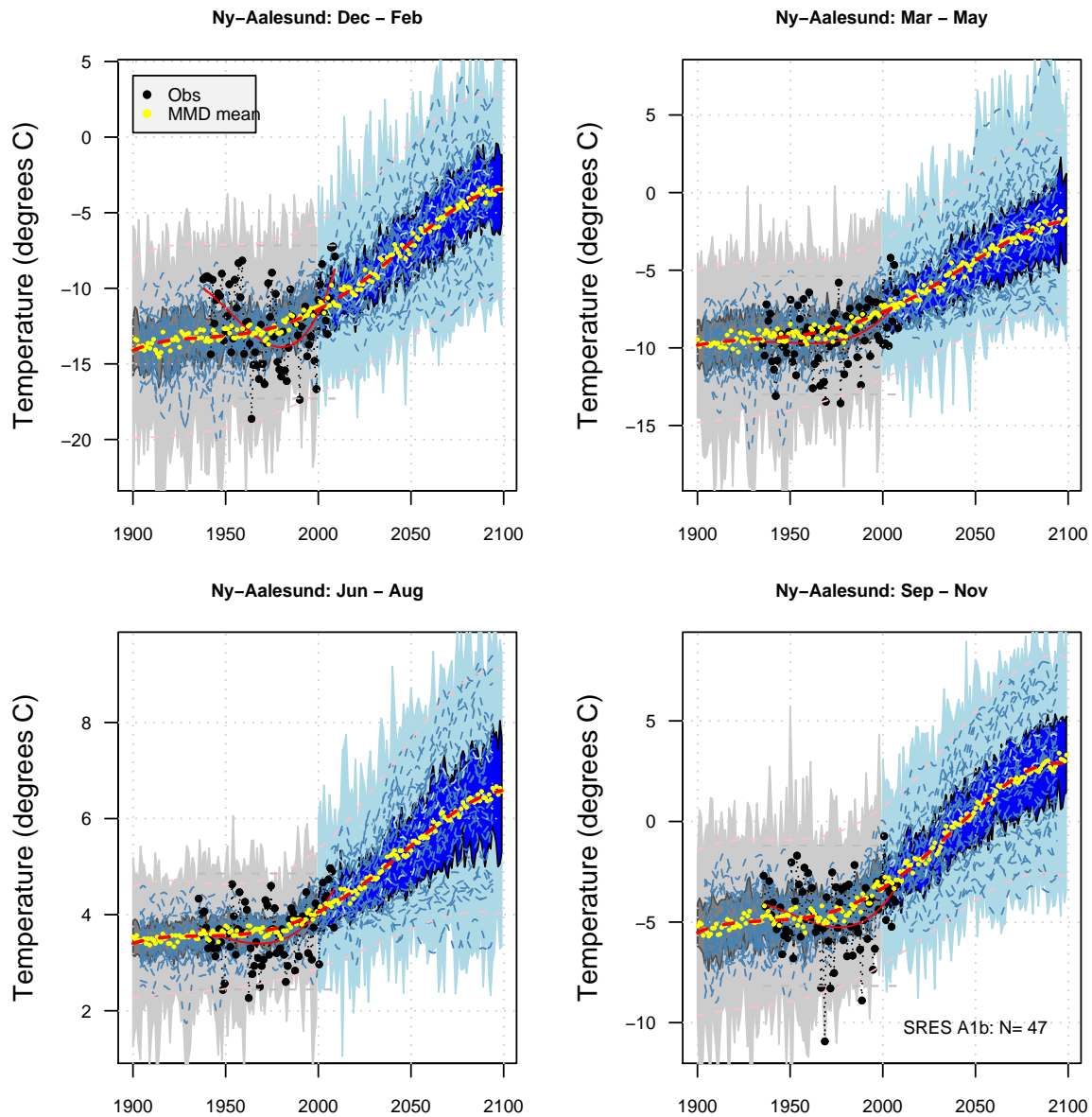


Figure 10: As in Figure 3, but for Ny Ålesund (99910).

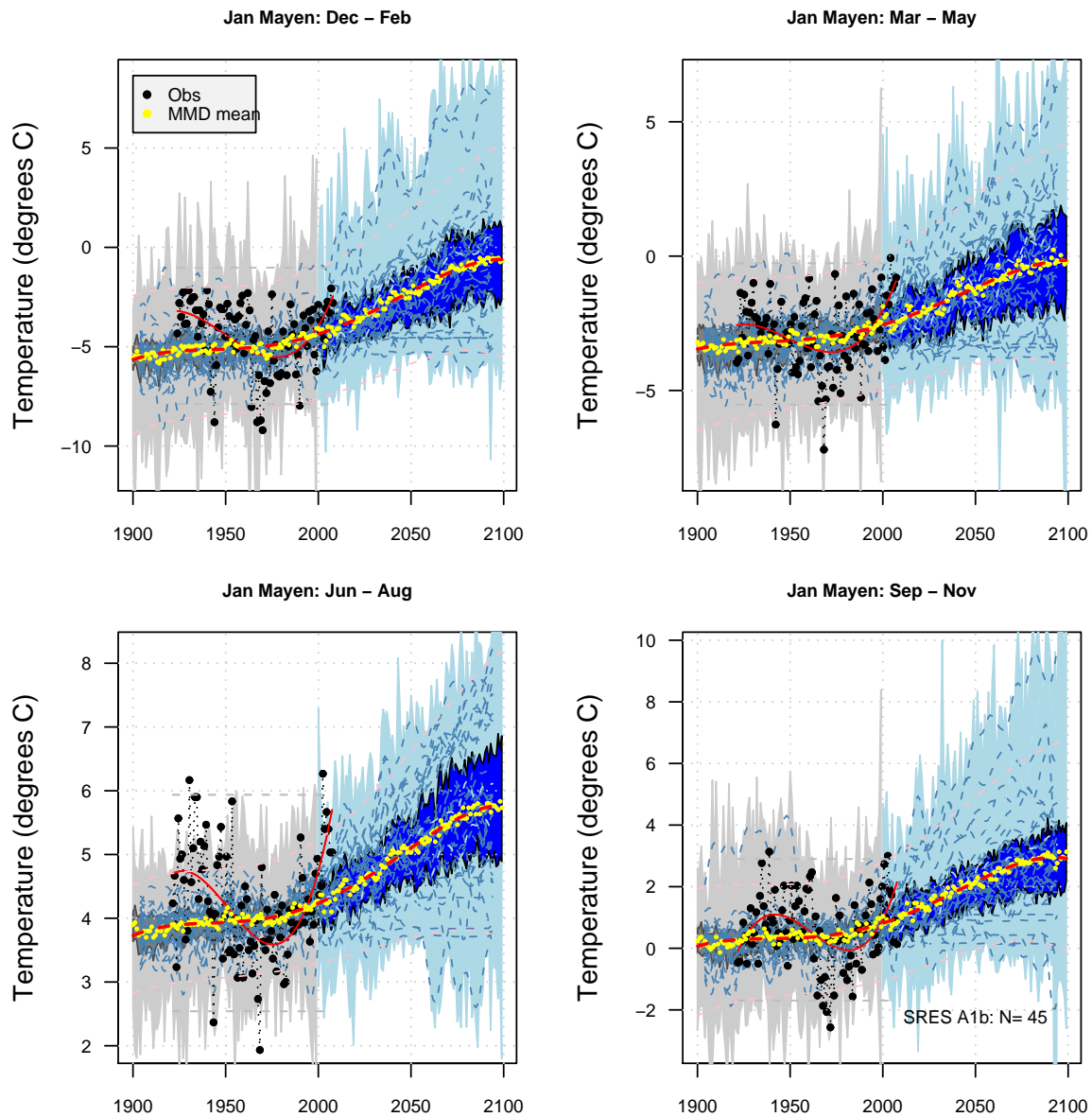


Figure 11: As in Figure 3, but for Jan Mayen (99950).

Table 1: Seasonal mean temperature (unit:  $^{\circ}\text{C}$ ): mean seasonal temperature over the reference climatology ('TAM(1961–1990)'), estimated for the future 2070–2099 interval ('TAM(2070–2099)'), and the difference between these two 30-year periods (' $\Delta\text{TAM}(2070–2099)$ ').

	St. nr.	Winter	Spring	Summer	Autumn
<b>TAM(1961–1990)</b>					
TROMSØ	90450	-4.0	0.8	10.5	2.7
KAUTOK	93700	-16.0	-5.2	10.7	-1.0
KARASJ	97250	-15.9	-3.2	11.3	-1.8
VARDØ	98550	-4.7	-0.7	8.2	2.6
KIRKEN	99370	-11.0	-2.3	10.4	0.2
BJØRNØ	99710	-7.6	-4.8	3.6	-0.5
HOPEN	99720	-13.3	-9.9	1.3	-3.7
SVALBA	99840	-14.8	-10.1	4.3	-5.0
NY-ÅLE	99910	-13.5	-9.3	3.5	-4.9
JAN MA	99950	-5.7	-3.5	3.7	-0.2
<b>TAM(2070–2099)</b>					
TROMSØ	90450	0.1±3.1	5.0±3.0	13.9±2.5	6.7±2.4
KAUTOK	93700	-4.6±7.9	1.8±4.4	14.7±2.6	3.7±3.3
KARASJ	97250	-4.9±8.0	3.0±4.3	15.1±2.7	5.5±4.2
VARDØ	98550	-1.2±2.3	2.9±2.5	10.8±2.0	5.8±1.9
KIRKEN	99370	-3.7±4.5	2.5±3.3	13.7±2.7	4.5±2.7
BJØRNØ	99710	-1.9±4.4	1.7±4.7	6.3±2.0	3.8±2.7
HOPEN	99720	-3.2±6.8	-3.8±3.9	3.5±1.4	3.9±4.4
SVALBA	99840	-5.9±5.0	-2.8±5.3	6.8±2.1	-0.9±4.7
NY-ÅLE	99840	-3.6±5.6	-2.4±5.1	6.4±2.2	2.8±4.8
JAN MA	99950	-0.9±4.3	-0.3±3.7	5.6±1.9	2.7±3.0
<b><math>\Delta\text{TAM}(2070–2099)</math></b>					
TROMSØ	90450	4.0±3.1	4.2±3.0	3.3±2.5	4.0±2.4
KAUTOK	93700	11.4±7.9	7.0±4.4	3.9±2.6	4.7±3.3
KARASJ	97250	11.0±8.0	6.2±4.3	3.7±2.7	7.3±4.2
VARDØ	98550	3.6±2.3	3.5±2.5	2.6±2.0	3.3±1.9
KIRKEN	99370	7.3±4.5	4.9±3.3	3.3±2.7	4.3±2.7
BJØRNØ	99710	5.6±4.4	6.5±4.7	2.8±2.0	4.3±2.7
HOPEN	99720	10.1±6.8	6.0±3.9	2.2±1.4	7.6±4.4
SVALBA	99840	8.9±5.0	7.4±5.3	2.4±2.1	4.1±4.7
NY-ÅLE	99910	10.0±5.6	6.9±5.1	2.9±2.2	7.7±4.8
JAN MA	99950	4.8±4.3	3.2±3.7	1.8±2.2	2.8±3.0

## 4.2 Precipitation

The results for the precipitation Figures 12–21 suggest that the downscaled (shaded areas) year-to-year variability (variance) is underestimated, and that there are also stronger secular variations in the actual observations (black symbols) than seen in the ESD results for the past (grey). A summary of estimated 2070–2099 climatology is provided in Table 2.

The first ESD results for Kautokeino, Bjørnøya, Hopen, and Ny Ålesund (not shown) were in general poor and not reliable, but a smaller domain gave more credible results. In some cases, the ESD-analysis in the first set of calculations (not shown) gave different standard deviations in the CTL and A1b runs, spurious spikes, or the quality check weeded out a large proportion of model runs with problems. One reason for this is that the statistical link between the local (rain gauges) and the large-scale (ERA40) precipitation is in general weak and of a very local nature (*Benestad et al., 2007*). The precipitation from ERA40 is also model-derived and may contain biases and systematic errors. In addition, some of the models may not reproduce the regional precipitation characteristics very well, thus introducing further errors and uncertainties in trying to identify the important spatial rainfall patterns in the GCMs.

### 4.2.1 Trends

The first set of predicted winter trends for Tromsø (not shown) suggested a decline in the future, in contrast to corresponding results for the Hålogaland region in *Benestad (2008a)*, but a re-calculation with a smaller predictor (Figure 12) domain gave more consistent results. The expected change in the future precipitation will be affected by changes in the mean zonal wind, humidity, and the storm tracks over the same region.

### 4.2.2 Quality checks

The ESD was derived from the large-scale precipitation pattern, and generally lower  $R^2$  values than for the temperature can be seen. In other words, the relationship between the large-scale (ERA40) and the local (station) precipitation is weaker than corresponding relationship for temperature.

A few spikes can be found, as in the results for the temperature, although all values less than zero were set to zero in the post-processing.

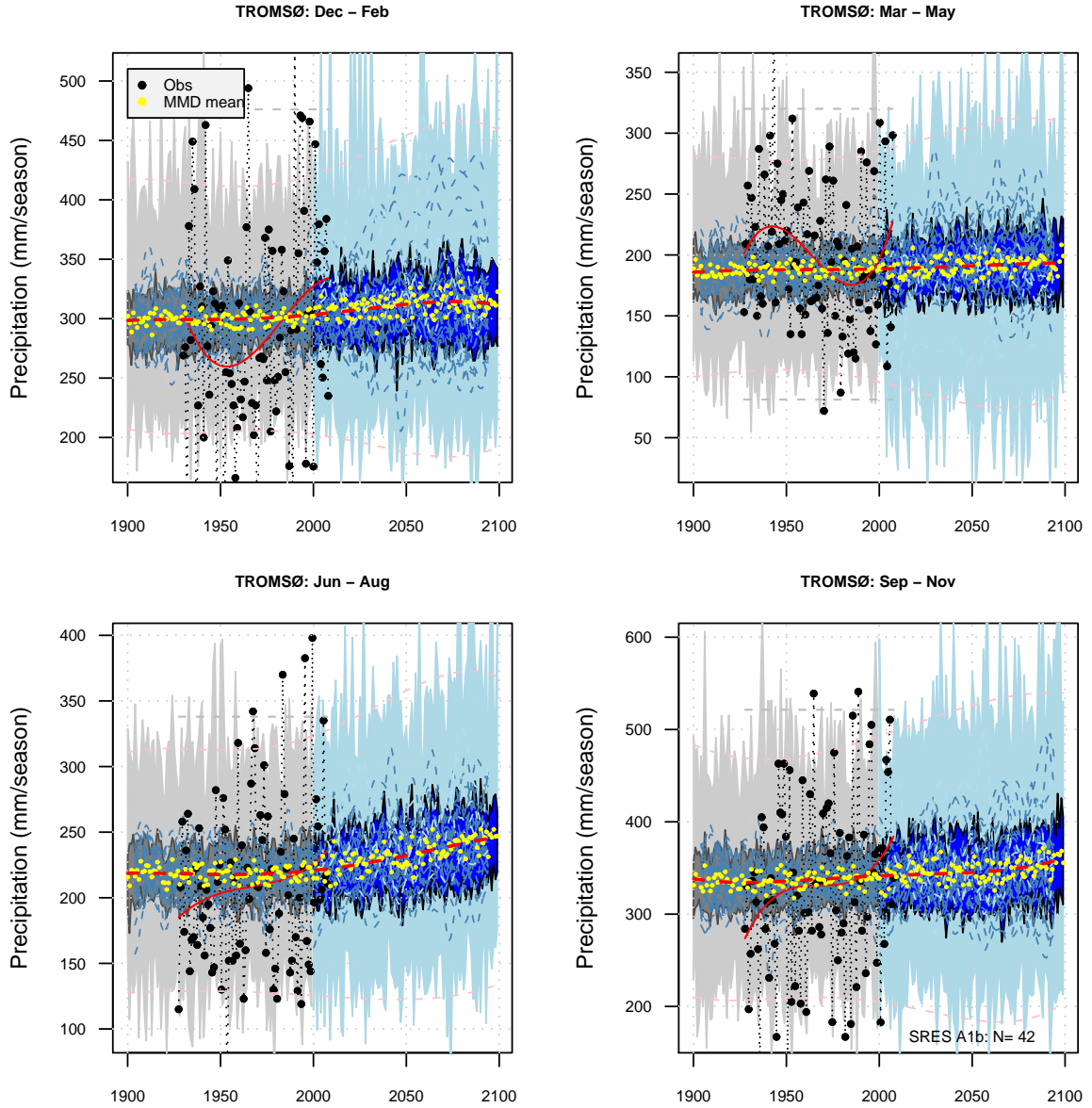


Figure 12: Plume plot for Tromsø (90450), showing the time evolution of the observed values (black), the 20th Century simulations (grey), and the future scenarios (blue). The light shading shows the minimum–maximum range for the ensemble, and the darker shading marks the inter-quantile range (25%–75%). The yellow symbols mark the ensemble mean values, and the thick red-dashed lines show the fitted polynomial trends. The thin pink lines show best-fit polynomial to the 5 and 95 percentiles, and the dashed blue lines show 10-year low-pass filtered (Gaussian filter) of the individual runs.

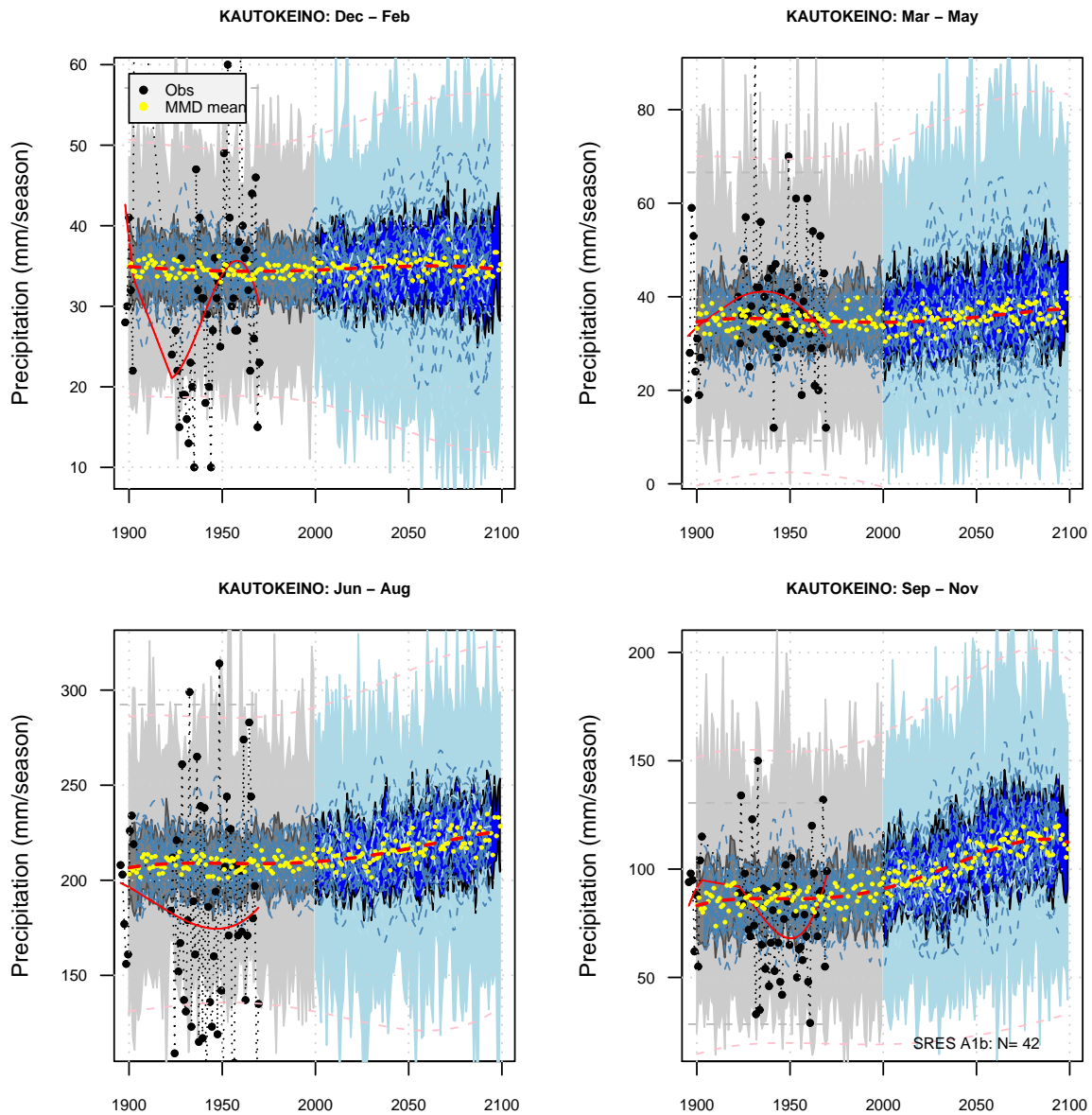


Figure 13: As in Figure 12, but for Kautokeino (93700).

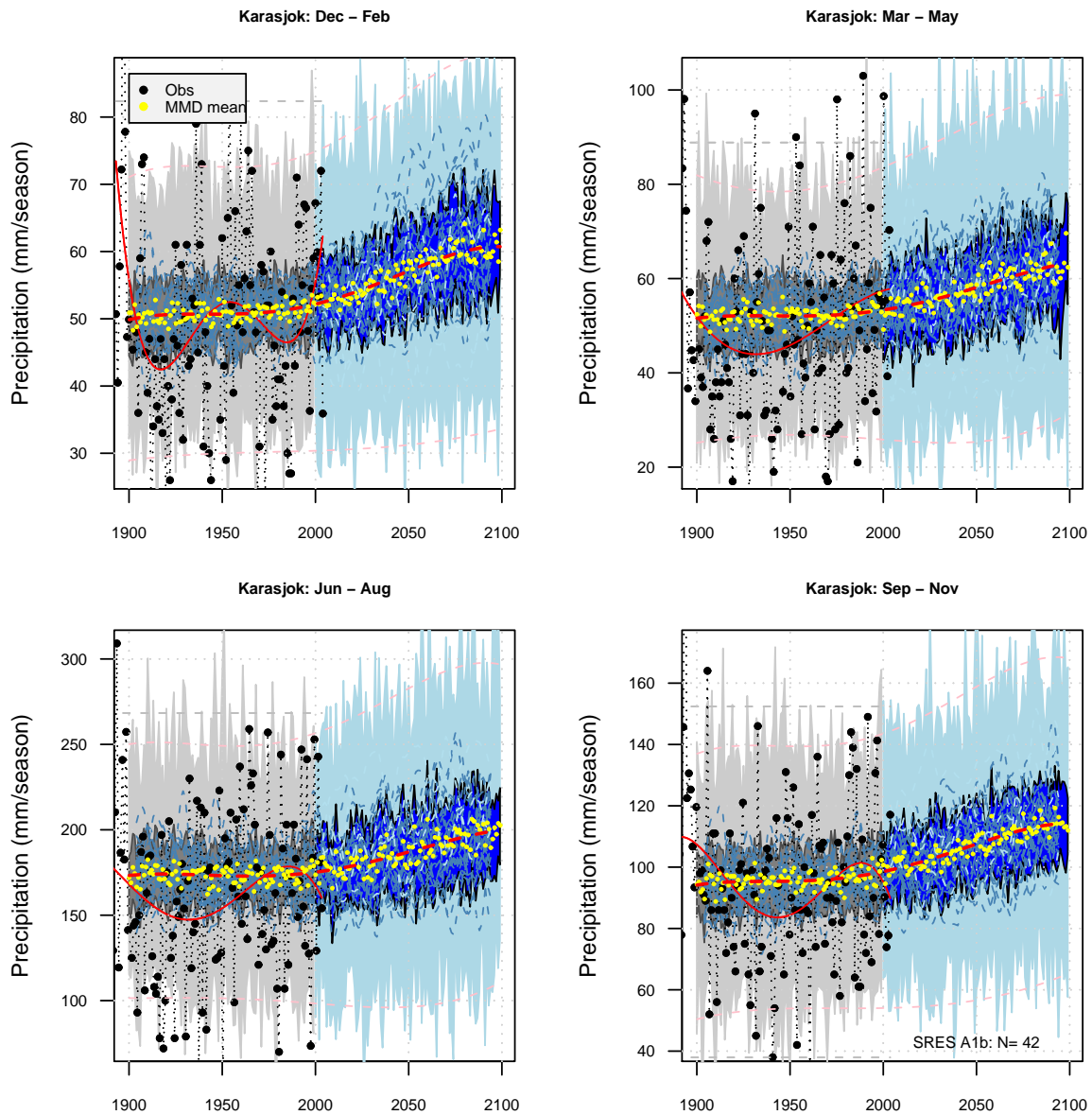


Figure 14: As in Figure 12, but for Karasjok (97250).

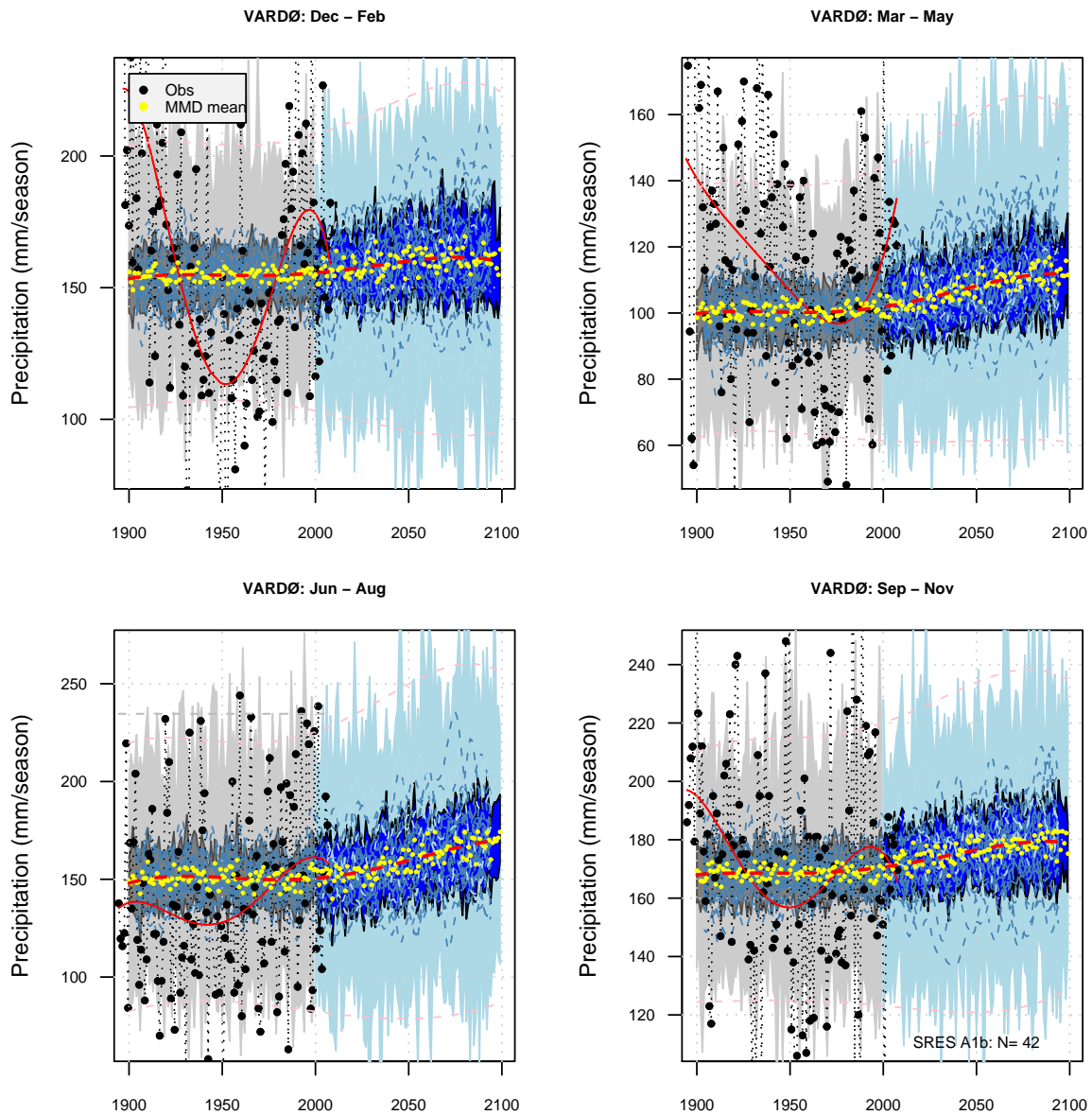


Figure 15: As in Figure 12, but for Vardø (98550).

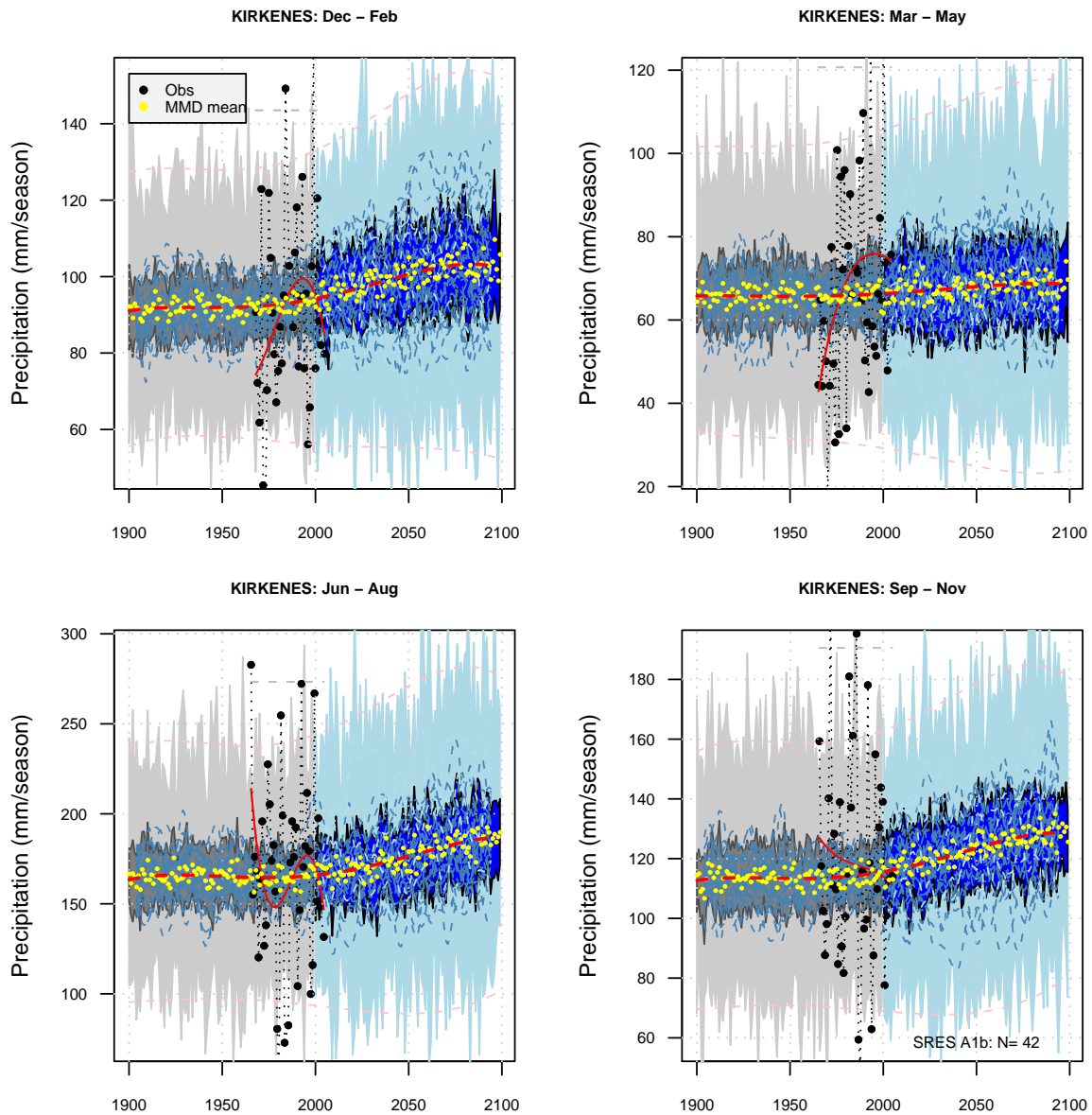


Figure 16: As in Figure 12, but for Kirkenes (99370).

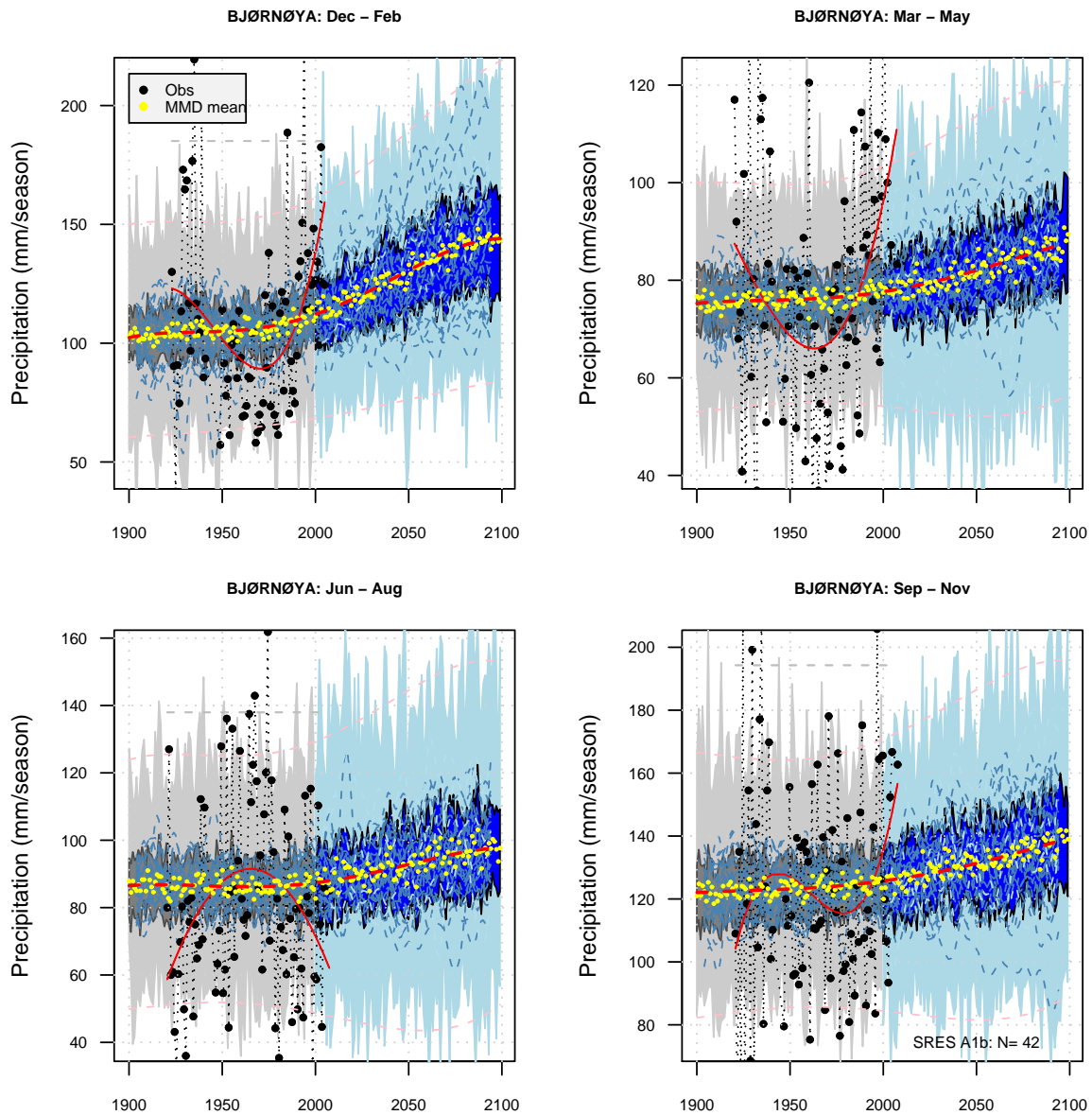


Figure 17: As in Figure 12, but for Bjørnøya (99710).

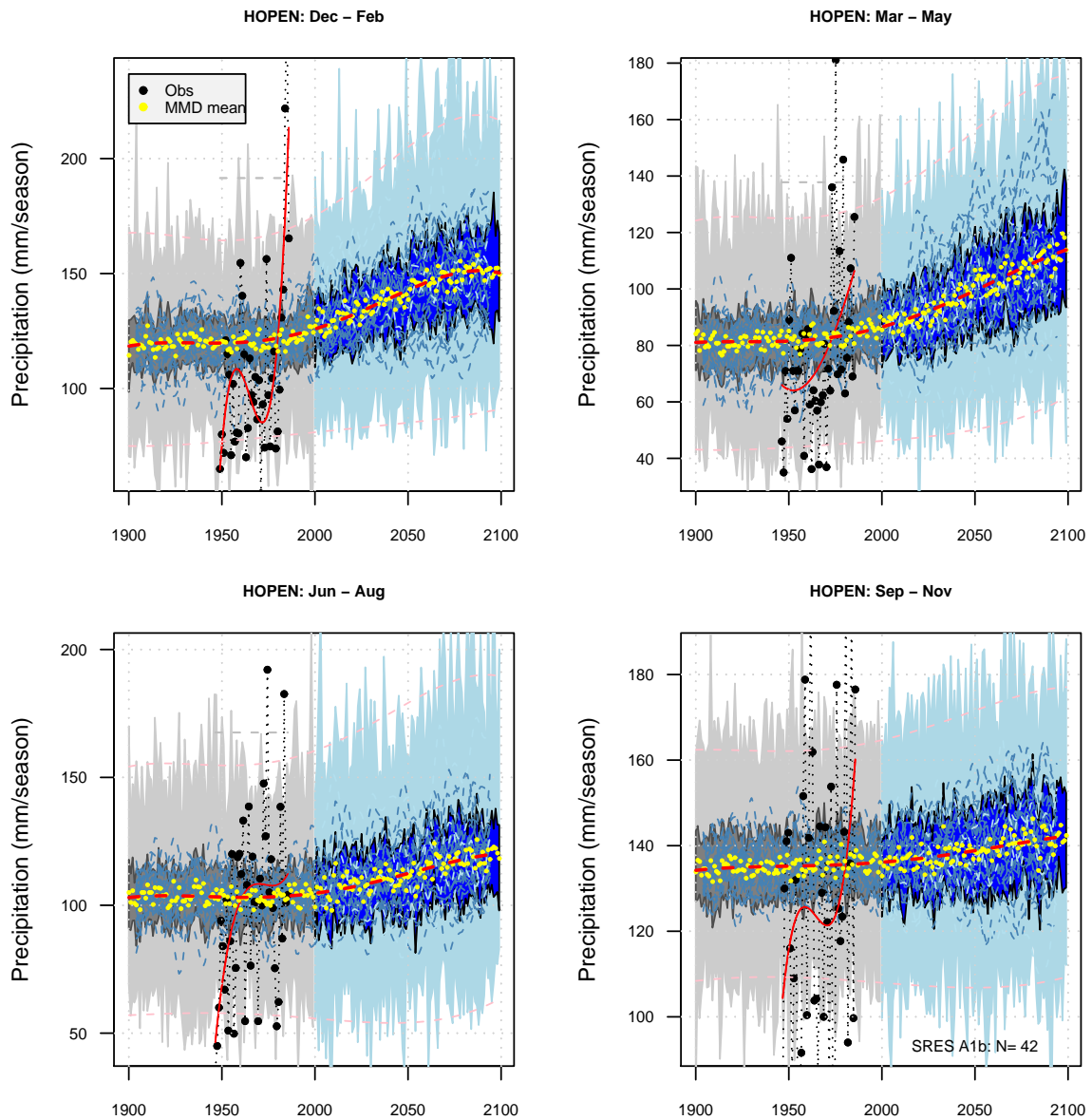


Figure 18: As in Figure 12, but for Hopen (99720).

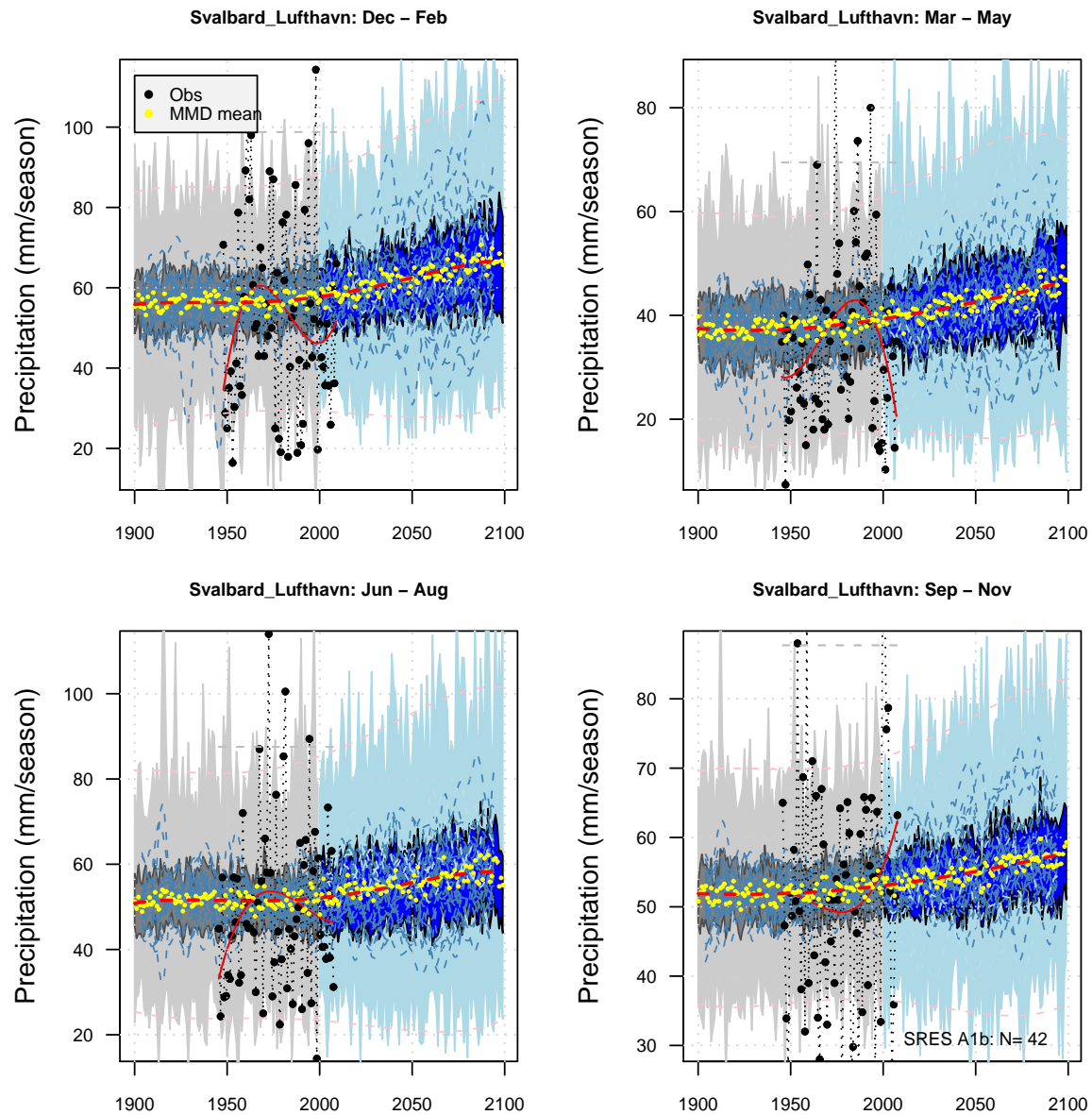


Figure 19: As in Figure 12, but for Svalbard airport (99840).

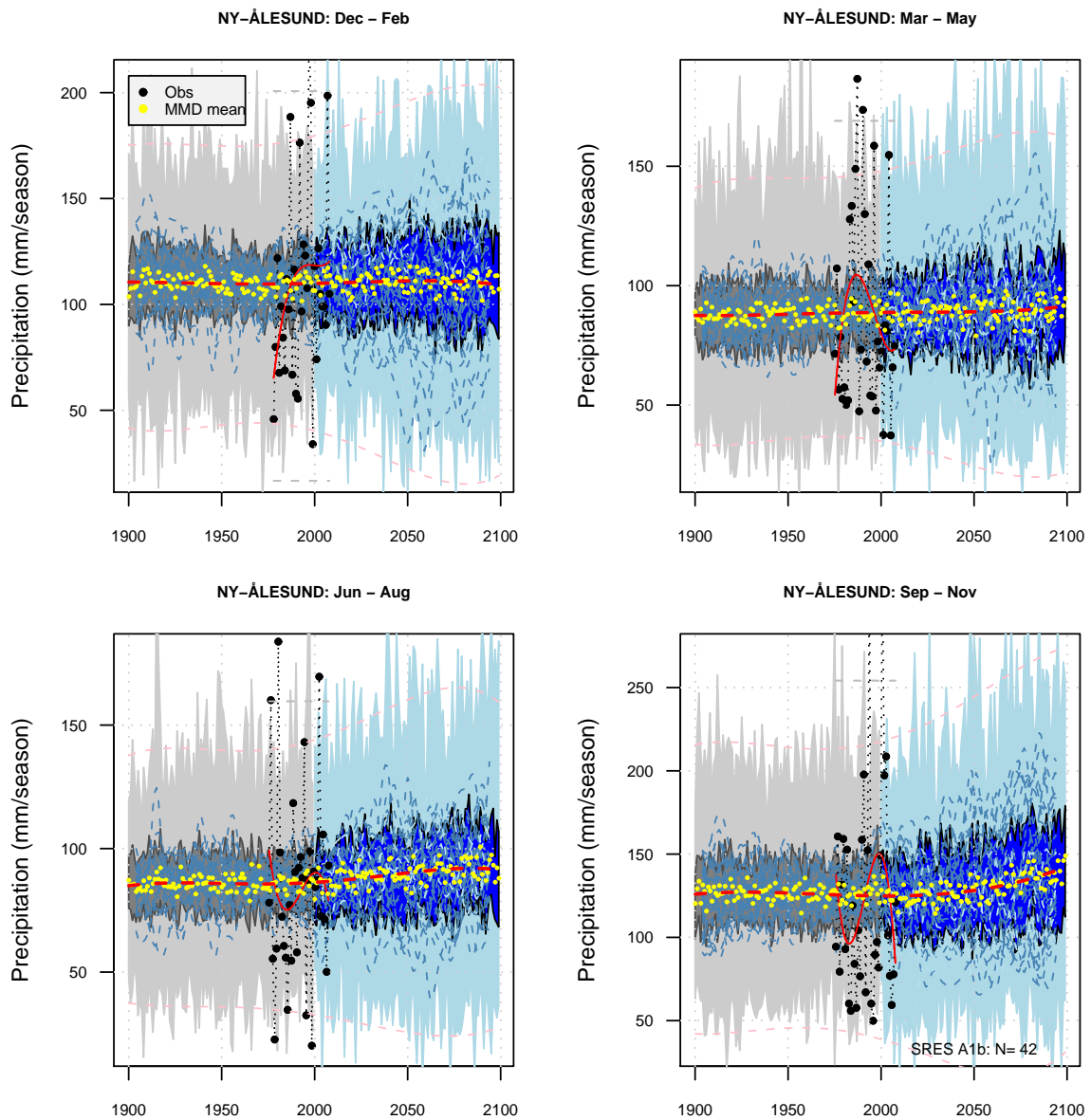


Figure 20: As in Figure 12, but for Ny Ålesund (99910).

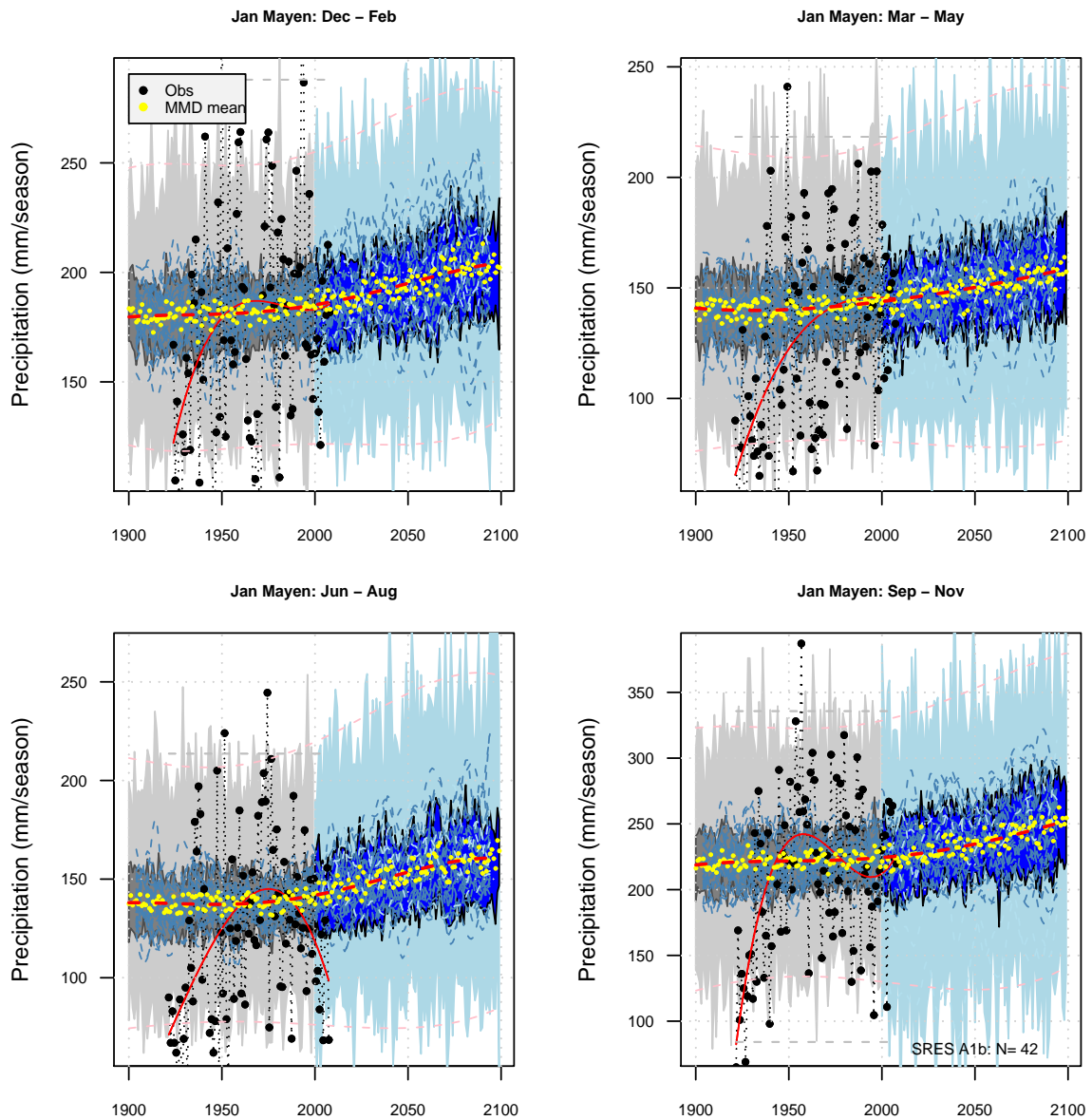


Figure 21: As in Figure 12, but for Jan Mayen (99950).

Table 2: Seasonal precipitation: seasonal total precipitation amount over the reference climatology ('RR(1961–1990)'), estimated for the future 2070–2099 interval ('RR(2070–2099)'), the difference between these two 30-year periods (' $\Delta RR(2070–2099)$ '), and estimated 2070–2099 expressed as the fraction of the 1961–1990 values (' $RR(2070–2099)/RR_{ref}$ '). The units for the three former are mm/season whereas for the latter the units are in %.

	St. nr.	Winter	Spring	Summer	Autumn
<b>RR(1961–1990):</b>					
TROMSØ	90450	288	185	218	340
KAUTOK	93700	30	32	194	92
KARASJ	97250	47	52	171	96
VARDØ	98550	149	98	146	171
KIRKEN	99370	89	65	162	116
BJØRNØ	99710	93	67	89	121
HOPEN	99720	119	84	102	134
SVALBA	99840	45	42	49	48
NY-ÅLE	99910	94	94	80	114
JAN MA	99950	174	135	145	229
<b>RR(2070–2099):</b>					
TROMSØ	90450	307±90	194±76	239±78	349±108
KAUTOK	93700	35±15	36±27	222±55	112±51
KARASJ	97250	60±18	62±24	196±62	113±33
VARDØ	98550	161±45	110±31	166±54	179±34
KIRKEN	99370	103±31	68±27	183±56	127±35
BJØRNØ	99710	140±47	86±22	96±32	136±35
HOPEN	99720	149±43	108±40	117±39	141±26
SVALBA	99840	65±27	44±21	57±25	56±15
NY-ÅLE	99910	109±59	89±48	91±44	135±76
JAN MA	99950	200±51	155±50	157±53	246±81

Table 2 continued...

$\Delta RR(2070-2099)$ :

TROMSØ	90450	20±90	9±76	21±78	9±108
KAUTOK	93700	5±15	4±27	29±55	20±51
KARASJ	97250	13±18	10±24	25±62	17±33
VARDØ	98550	12±45	13±31	21±54	8±34
KIRKEN	99370	14±31	3±27	21±56	11±35
BJØRNØ	99710	47±47	19±22	7±32	16±35
HOPEN	99720	30±43	23±40	15±39	7±26
SVALBA	99840	20±27	2±21	7±25	8±15
NY-ÅLE	99910	15±59	-6±48	11±44	20±76
JAN MA	99950	26±51	20±50	13±53	18±81

$RR(2070-2099)/RR_{ref}$ :

TROMSØ	90450	107±31	105±41	109±36	103±32
KAUTOK	93700	118±51	114±86	115±28	121±55
KARASJ	97250	128±39	120±46	115±37	118±34
VARDØ	98550	108±30	113±32	114±37	105±20
KIRKEN	99370	115±35	105±41	113±35	110±30
BJØRNØ	99710	151±50	128±32	108±36	113±29
HOPEN	99720	125±36	128±47	114±38	105±20
SVALBA	99840	144±60	106±50	115±51	117±31
NY-ÅLE	99910	116±63	94±50	113±56	118±66
JAN MA	99950	115±29	115±37	109±37	108±35

## 5 Discussion & Conclusions

Many of the Arctic series were short, which may have reduced the quality of the ESD analysis. The ESD for both the temperature and the precipitation yielded weak results (low  $R^2$ ) for some locations, and most of the precipitation at the Arctic stations exhibited secular variations which were not captured by the ESD.

The ESD for precipitation used large-scale precipitation as predictor, and a weak link between the local series and the predictor suggests that either the large-scale precipitation is not very accurate or that the secular variations are of very local nature which is not representative for the larger region. If the latter is true, then it is questionable whether one can expect a systematic change as a consequence of a future climate change, as this would entail a change in the local but not the regional characteristics. If the first explanation is true, then it implies that severe shortcomings limit the quality and reliability of the ESD results for the precipitation.

It is reasonable to expect that there still are severe shortcomings associated with the GCMs' description of the precipitation in the Arctic region and the statistical downscaling of these. Thus, the results for the precipitation presented here *must* be regarded with extreme caution.

*Benestad* (1999) argued that taking the difference between two different time periods is prone to additional uncertainties associated with chaotic internal decadal variability, and subsequent publications (*Benestad* (2001)–*Benestad* (2007)) have focused on the slope of linear fits to the SCE results. However, a recent analysis for Statnett (*Benestad*, 2008a) started to look at the question of what future climatological values would be compared with the present day, as opposed to the rate of warming, and efforts went into adjusting the SCE results to have matching mean levels for the 1995–2007 period in order to account for the present phase of decadal variability.

Subsequent work used a variety of this adjustment (*Engen-Skaugen* et al., 2008, 2007) whereby the entire ensemble was adjusted in order to fit the end of the CTL runs. In *Benestad* (2008b) a further improvement was sought by trying to match the individual CTL and SCE runs for the same GCM and the same integration, however, in retrospect this matching introduced further uncertainties associated with the individual runs. The effect of adjusting each downscaled GCM run individually, however, was small for the level for the entire ensemble (ensemble mean) compared to adjusting the whole set, but the effect was greater for the individual ESD results (the ensemble range). While the individual ESD curves would vary with the matching strategy, the associated rate of change (i.e. the slope of linear best-fit trend) used in the previous studies would remain constant.

Several rounds of ESD-analysis were performed, with different ways of adjusting SCE re-

sults and different predictor domain choices. Both the precipitation and temperature were sensitive to the domain size, due to (i) that the spatial scale of the precipitation in general is small (*Benestad et al., 2008*) or (ii) that the GCMs do not reproduce the spatial structure very well. The GCMs still have difficulties describing changes in the vicinity of the sea-ice edge, as reported in *Benestad et al. (2002)*.

## Acknowledgement

I'm grateful for valuable discussions with Inger Hanssen-Bauer and Eirik Førland. This analysis was partly funded by the NorACIA programme and several IPY-projects under the Norwegian Resource Council.

## References

- Anderson, D.L.T., & Carrington, D., 1994. Simulation of Tropical Variability as a Test of Climate Models. In: Speranza, A., & R. Fantechi, S. Tibaldi (eds), *Global Change. Environment and Quality of Life*, vol. EUR 15158 EN. European Commission.
- Benestad, R.E., 1999. *Pilot Studies of Enhanced Greenhouse Gas Scenarios for Norwegian Temperature and Precipitation from Empirical Downscaling*. Klima 16/99. DNMI, PO Box 43 Blindern, 0313 Oslo, Norway.
- Benestad, R.E., 2001. A comparison between two empirical downscaling strategies. *Int. J. Climatology*, **21**, 1645–1668. DOI 10.1002/joc.703.
- Benestad, R.E., 2003. *Downscaling analysis for daily and monthly values using clim.pact-V.0.9*. KLIMA 01/03. met.no, PO Box 43 Blindern, 0313 Oslo, Norway ([www.met.no](http://www.met.no)).
- Benestad, R.E., 2004. Empirical-Statistical Downscaling in Climate Modeling. *Eos, Volume* **85**(42), p. 417.
- Benestad, R.E., 2005. Climate change scenarios for northern Europe from multi-model IPCC AR4 climate simulations. *Geophys. Res. Lett.*, **32**(doi:10.1029/2005GL023401), L17704.
- Benestad, R.E., 2007. Novel Methods for Inferring Future Changes in Extreme Rainfall over Northern Europe. *Climate Research*, **34**(doi: 10.3354/cr00693), 195–210.
- Benestad, R.E., 2008a. *Downscaled regional Norwegian temperature and precipitation series: Analysis for Statnett and CES*. Climate 7. met.no, [www.met.no](http://www.met.no).
- Benestad, R.E., 2008b. *Empirical-Statistical Downscaling of Russian and Norwegian temperature series*. Climate 13. met.no, [www.met.no](http://www.met.no).
- Benestad, R.E., 2008c. *Heating degree days, Cooling degree days and precipitation in Europe: Analysis for the CELECT-project*. Climate 4. met.no, [www.met.no](http://www.met.no).
- Benestad, R.E., Hanssen-Bauer, I., & Førland, E.J., 2002. Empirically downscaled temperature scenarios for Svalbard. *Atmospheric Science Letters*, **3**, Issue 2-4(doi:10.1006/asle.2002.0051), 71–93.
- Benestad, R.E., Hanssen-Bauer, I., & Førland, E.J., 2007. An Evaluation of Statistical Models for Downscaling Precipitation and Their Ability to Capture Long-Term Trends. *International Journal of Climatology*, **27**(10.1002/joc.1421), 649–665.
- Benestad, R.E., Chen, D., & Hanssen-Bauer, I., 2008. *Empirical-Statistical Downscaling*. Singapore: World Scientific Publishing.

- Bengtsson, L., 1996. The Climate response to the Changing Greenhouse Gas Concentration in the Atmosphere. In: Anderson, D.L.T., & Willebrand, J. (eds), *Decadal Variability*. NATO ASI series, vol. 44. Springer.
- Bengtsson, L., Hodges, K.I., & Hagemann, S., 2004. Sensitivity of the ERA40 reanalysis to the observing system: determination of the global atmospheric circulation from reduced observations. *Tellus*, **56A**, 456–471.
- Christensen, J.H., & Christensen, O.B., 2002. Severe summertime flooding in Europe. *Nature*, **421**, 805.
- Christensen, J.H., Räisänen, J., Iversen, T., Bjørge, D., Christensen, O. B., & Rummukainen., 2001. A synthesis of regional climate change simulations - A Scandinavian perspective. *Geophys. Res. Lett.*, **28**(6), 1003.
- Christensen, J.H., Hewitson, B., Busuioc, A., A. Chen, X. Gao, Held, I., Jones, R., Kolli, R.K., Kwon, W.-T., Laprise, R., na Rueda, V. Maga Mearns, L., Menéndez, C.G., Räisänen, J., Rinke, A., Sarr, A., & Whetton, P., 2007a. *Climate Change: The Physical Science Basis*. United Kingdom and New York, NY, USA: Cambridge University Press. Chap. Regional Climate Projections.
- Christensen, J.H., Hewitson, B., Busuioc, A., A. Chen, X. Gao, Held, I., Jones, R., Kolli, R.K., Kwon, W.-T., Laprise, R., na Rueda, V. Maga Mearns, L., Menéndez, C.G., Räisänen, J., Rinke, A., Sarr, A., & Whetton, P., 2007b. *Climate Change: The Physical Science Basis*. United Kingdom and New York, NY, USA: Cambridge University Press. Chap. Regional Climate Projections.
- Christensen, O.B., J.H., Christensen, Machenhauer, B., & Botzet, M., 1998. Very High-Resolution Climate Simulations over Scandinavia - Present Climate. *Journal of Climate*, **11**, 3204–3229.
- Crane, R.G., & Hewitson, B.C., 1998. Doubled CO<sub>2</sub> Precipitation Changes for the Susquehanna Basin: Downscaling from the Genesis General Circulation Model. *International Journal of Climatology*, **18**, 65–76.
- Easterling, D.R., 1999. Development of regional climate scenarios using a downscaling approach. *Climatic Change*, **41**, 615–634.
- Engen-Skaugen, T., Benestad, R.E., & Roald, L.A., 2007. *Empirically downscaling of runoff in Norway; Is it feasible?* Climate 15. met.no, www.met.no.
- Engen-Skaugen, T., Benestad, R.E., & Førland, E.J., 2008. *Empirically downscaled precipitation and temperature representing Norwegian catchments*. Climate in progress. met.no, www.met.no.
- Fleagle, R.G., & Businger, J.A., 1980. *An Introduction to Atmospheric Physics*. 2 edn. International Geophysics Series, vol. 25. Orlando: Academic Press.

- Førland, E.J., Hanssen-Bauer, I., Haugen, J.E., Benestad, R., & Aadlandsvik, B., 2008. *NorACIAS klimascenarier for norsk Arktis*. Climate 09/08. met.no, www.met.no. in Norwegian.
- Fowler, H.J., Blenkinsop, S., & Tebaldi, C., 2007. Linking climate change modelling to impacts studies: recent advances in downscaling techniques for hydrological modelling. *International Journal of Climatology*, **27**, 1547–1578.
- Hanssen-Bauer, I., Achberger, C., Benestad, R.E., Chen, D., & Førland, E.J., 2005. Statistical downscaling of climate scenarios over Scandinavia: A review. *Climate Research*, **29**, 255–268.
- Haugen, J.E., & Ødegaard, V., 2003. Evaluation of MPI and Hadley simulations with HIRHAM, and sensitivity to integration domains. *Pages 19–29 of:* Iversen, T., & Lystad, M. (eds), *RegClim*. General Technical report, no. 7. <http://regclim.met.no/>: NILU.
- Haugen, J.E., Bjørge, D., & Nordeng, T.E., 2000. Dynamical downscaling PT1: Further results. *Pages 79–82 of:* Iversen, T., & Høiskar, B.A.K. (eds), *RegClim*. General Technical report, no. 4. <http://www.nilu.no/regclim/>: NILU.
- Houghton, J.T., 1991. *The physics of atmospheres*. Cambridge, U.K.: Cambridge University Press.
- Houghton, J.T., Ding, Y., Griggs, D.J., Noguer, M., van der Linden, P.J., Dai, X., Maskell, K., & Johnson, C.A., 2001. *Climate Change 2001: The Scientific Basis*. Contribution of Working Group I to the Third Assessment Report of IPCC. International Panel on Climate Change, (Available from [www.ipcc.ch](http://www.ipcc.ch)).
- IPCC., 1990. Climate Change: The Scientific Assessment. IPCC. Cambridge University Press.
- IPCC., 1995. *The Second Assessment Report*. Technical Summary. WMO & UNEP, [http://www.ipcc.ch/pub/sa\(E\).pdf](http://www.ipcc.ch/pub/sa(E).pdf).
- Meehl, G.A., Covey, C., Delworth, T., Latif, M., McAvaney, B., Mitchell, J.F.B., Stouffer, R.J., & Taylor, K.E., 2007. THE WCRP CMIP3 Multimodel Dataset: A New Era in Climate Change Research. *Bull. Amer. Meteor. Soc.*, **88**, 1383–1394.
- Meehls, G.A., Stocker, T.F., W.D. idlingstein, Gaye, A.T., Gregory, J.M., Kitoh, A., Knutti, R., murphy, J.M., Noda, A., Raper, S.C.B., Watterson, I.G., Weaver, A.J., & Zhao, Z.-C., 2007. *Climate Change: The Physical Science Basis*. United Kingdom and New York, NY, USA: Cambridge University Press. Chap. Global Climate Projections.
- Nakicenovic, N, J, Alcamo, G, Davis, de Vries B, J, Fenmann, S, Gaffin, K, Gregory, A, Grübler, T, Young Jung, T, Kram, EL, La Rover, L, Michaelis, Mori S, Morita T, W, Pepper, H, Pitcher, L, Price, K, Rihai, A, Roehrl, HH, Rogner, A, Sankovski, M, Schlesinger, P, Shukla, S, Smith, R, Swart, van Rooijen S, N, Victor, & Z, Dadi (eds.), 2000. *Special report on emission scenarios. A special report*

*of working group III of the intergovernmental Panel on Climate Change.* Cambridge University Press, Cambridge. Chap. 4.

Peixoto, J.P., & Oort, A.H., 1992. *Physics of Climate.* N.Y.: AIP.

Philander, S.G., 1989. *El Niño, La Niña, and the Southern Oscillation.* N.Y.: Academic Press.

Press, W.H., Flannery, B.P., Teukolsky, S.A., & Vetterling, W.T., 1989. *Numerical Recipes in Pascal.* Cambridge University Press.

Robinson, P.J., & Finkelstein, P.L., 1991. The development of impact-oriented scenarios. *Bull. Am. Met. Soc.*, 4, 481–490.

Rummukainen, M., 1997. *Methods for Statistical downscaling of GCM simulations.* SWECLIM 80. SMHI.

Sarachik, E.S., Winton, M., & Yin, F.L., 1996. Mechanisms for Decadal-to-Centennial Climate Variability. In: Anderson, D.L.T., & Willebrand, J. (eds), *Decadal Variability.* NATO ASI series, vol. 44. Springer.

Simmons, A.J., & Gibson, J.K., 2000. *The ERA-40 Project Plan.* ERA-40 Project Report Series 1. ECMWF, [www.ecmwf.int](http://www.ecmwf.int).

Solomon, S., Quin, D., Manning, M., Chen, Z., Marquis, M., Averyt, K.B., Tignor, M., & Miller, H.L. (eds)., 2007. *Climate Change: The Physical Science Basis. Contribution of Working Group I to the Fourth Assessment Report of the Intergovernmental Panel on Climate Change.* United Kingdom and New York, NY, USA: Cambridge University Press.

Strang, G., 1988. *Linear Algebra and its Application.* San Diego, California, USA: Harcourt Brace & Company.

Trenberth, K.E., Koike, T., & Onogi, K., 2008. Progress and Prospects for Reanalysis for Weather and Climate. *Eos*, 89(26), 234–235.

Treut, H. Le., 1994. Cloud Representation in Large-Scale Models: Can we Adequately Constrain them through Observed Data? In: Speranza, A., & nd R. Fantechi, S.Tibaldi (eds), *Global Change. Environment and Quality of Life*, vol. EUR 15158 EN. European Commission.

von Storch, H., Zorita, E., & Cubasch, U., 1993a. Downscaling of Global Climate Change Estimates to Regional Scales: An Application to Iberian Rainfall in Wintertime. *Journal of Climate*, 6, 1161–1171.

von Storch, H., Zorita, E., & Cubasch, U., 1993b. Downscaling of Global Climate Change Estimates to Regional Scales: An Application to Iberian Rainfall in Wintertime. *Journal of Climate*, 6, 1161–1171.

- Weart, S., 2003. *Discovery of Global Warming*. Harvard University Press.
- Wilby, R.L., Hassan, H., & Hanaki, K., 1998. Statistical downscaling of hydrometeorological variables using general circulation model output. *Journal of Hydrology*, **205**, 1–19.
- Wilby, R.L., Charles, S.P., Zorita, E., Timbal, B., Whetton, P., & Mearns, L.O., 2004. *Guidelines for Use of Climate Scenarios Developed from Statistical Downscaling Methods*. Supporting material of the Intergovernmental Panel on Climate Change. Task group on Data and Scenario Support for Impacts and Climate Analysis.
- Zorita, E., & von Storch, H., 1997. *A survey of statistical downscaling results*. Tech. rept. 97/E/20. GKSS.

# Appendix

## Boxplots

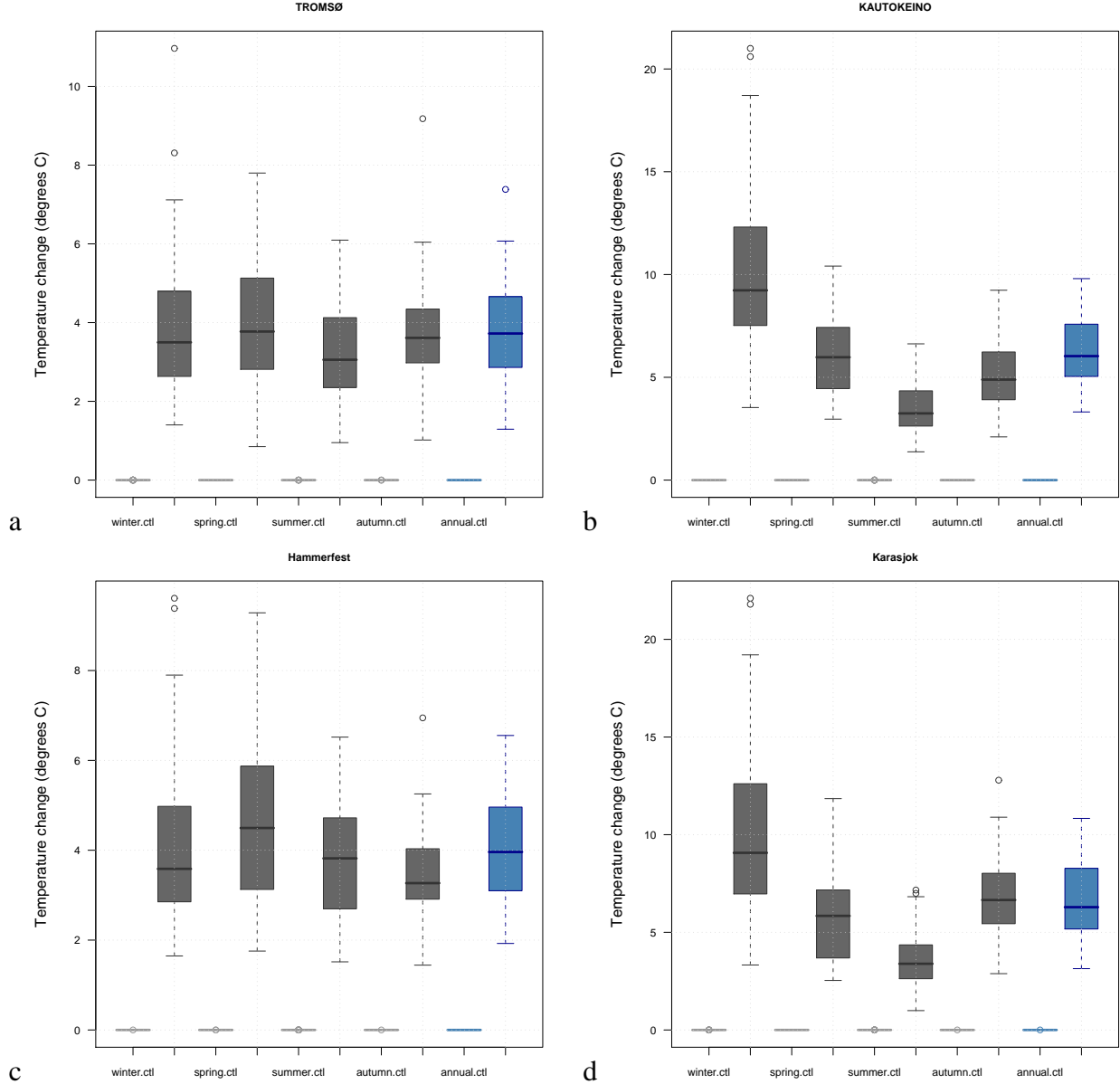


Figure 22: Box-plots for temperature scenarios. Stations 90450, 93700, 94260, and 97250.

## Quality evaluation of downscaling of temperature

In order to get a feeling for uncertainties involved in the ESD, the  $R^2$ -statistics from the regression analysis was checked for two arbitrary selected regions. Figure 28 shows how the

$R^2$ -statistics varies between GCMs (left) and the calendar month (right) for temperature regions 1 and 2. These results support the impression from Figures 3–7 which show corresponding variance in the observations and the downscaled results (indicative of a high  $R^2$ -score). The variance captured by the ESD model was high except for summer (June–Aug:  $\approx 40\text{--}60\%$ ).

Because the various GCMs may differ in their ability to provide an exact representation of the spatio-temporal structure of the temperature or precipitation modes, the common EOFs may differ somewhat from GCM to GCM. Thus the  $R^2$ -statistics may vary with the GCM, although the variation in the  $R^2$ -statistics should be small for realistic GCMs (large deviations in the  $R^2$ -statistics may be an indicator of model problems).

Additional quality control ensuring smooth variation in the trend estimates throughout the year was not used here (*Benestad, 2004*), but the change in the trend characteristics through the year can then be used to assess the quality of the results.

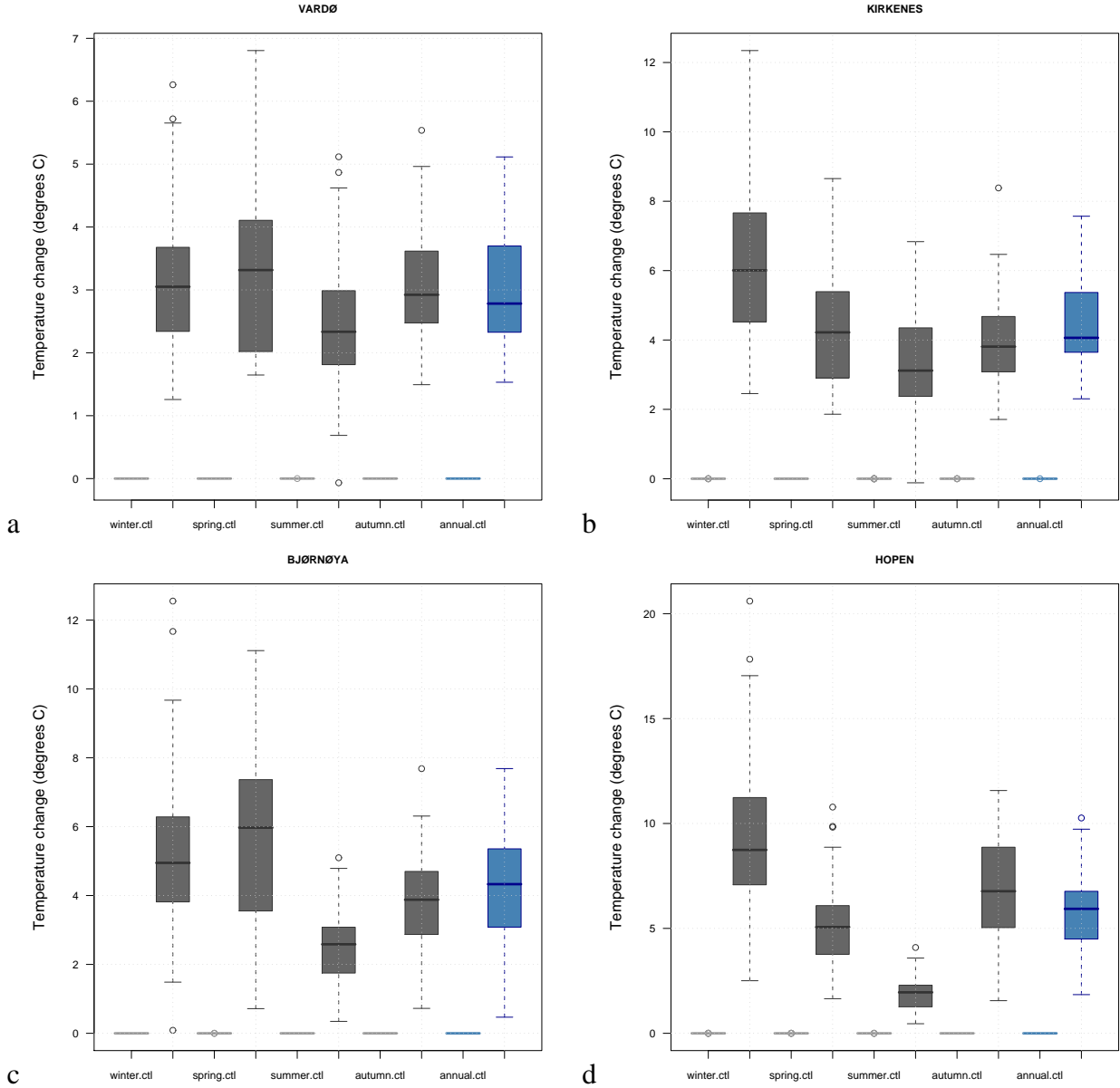


Figure 23: Box-plots for temperature scenarios. Stations 98550, 99370, 99710, and 99720.

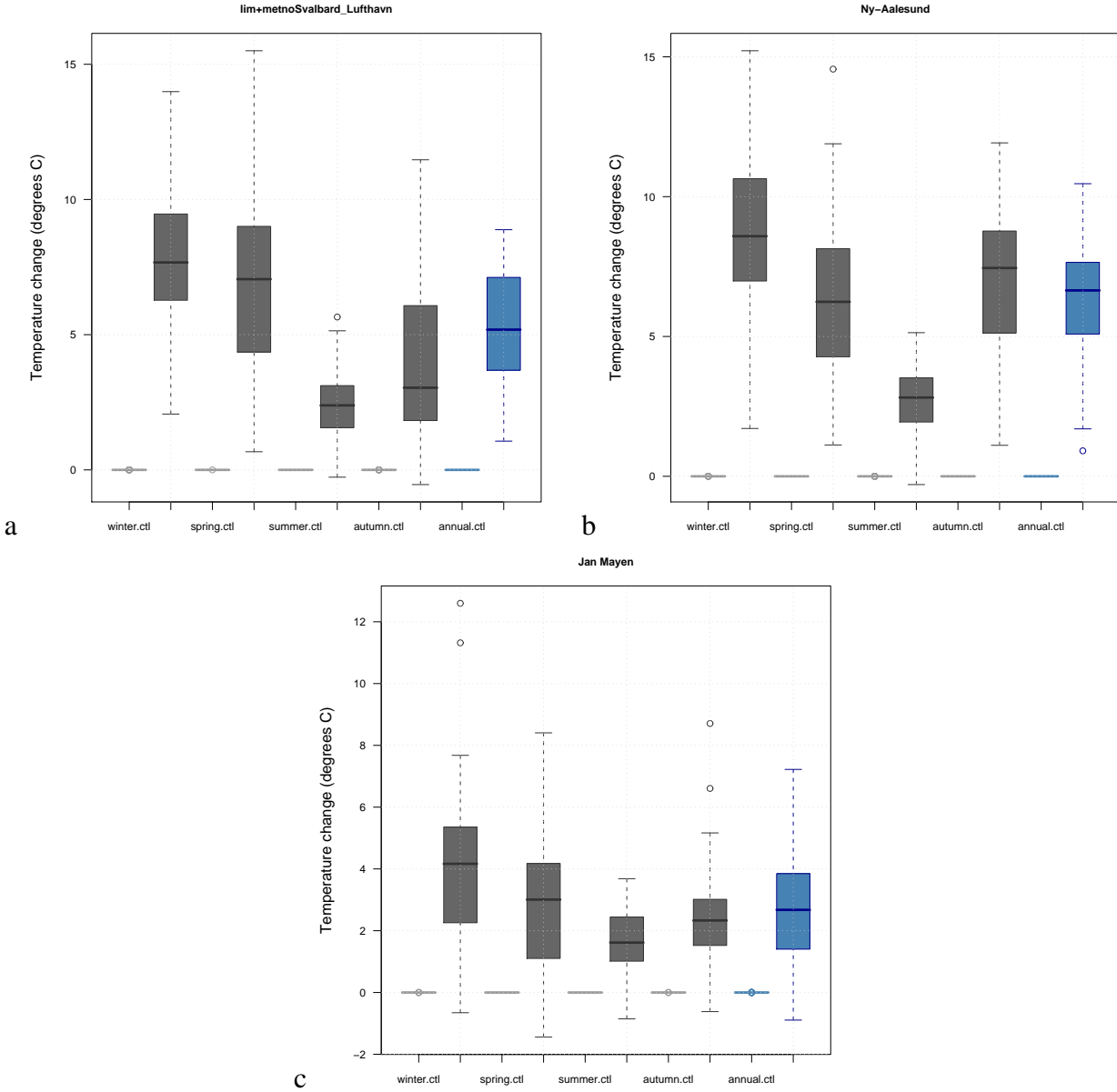


Figure 24: Box-plots for temperature scenarios. Stations 99840, 99910, and 99950.

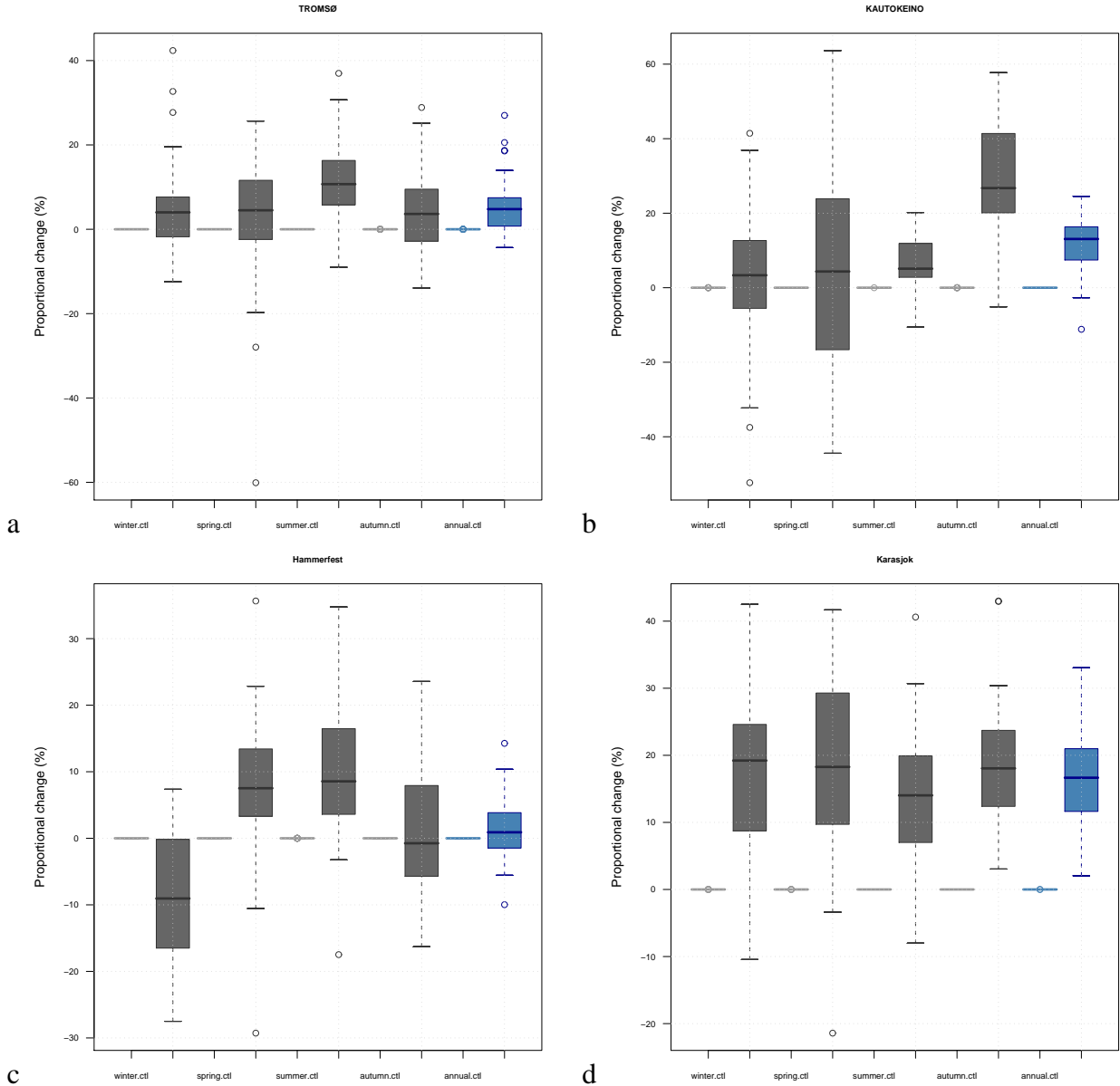


Figure 25: Box-plots for precipitation scenarios. Stations 90450, 93700, 94260, and 97250.

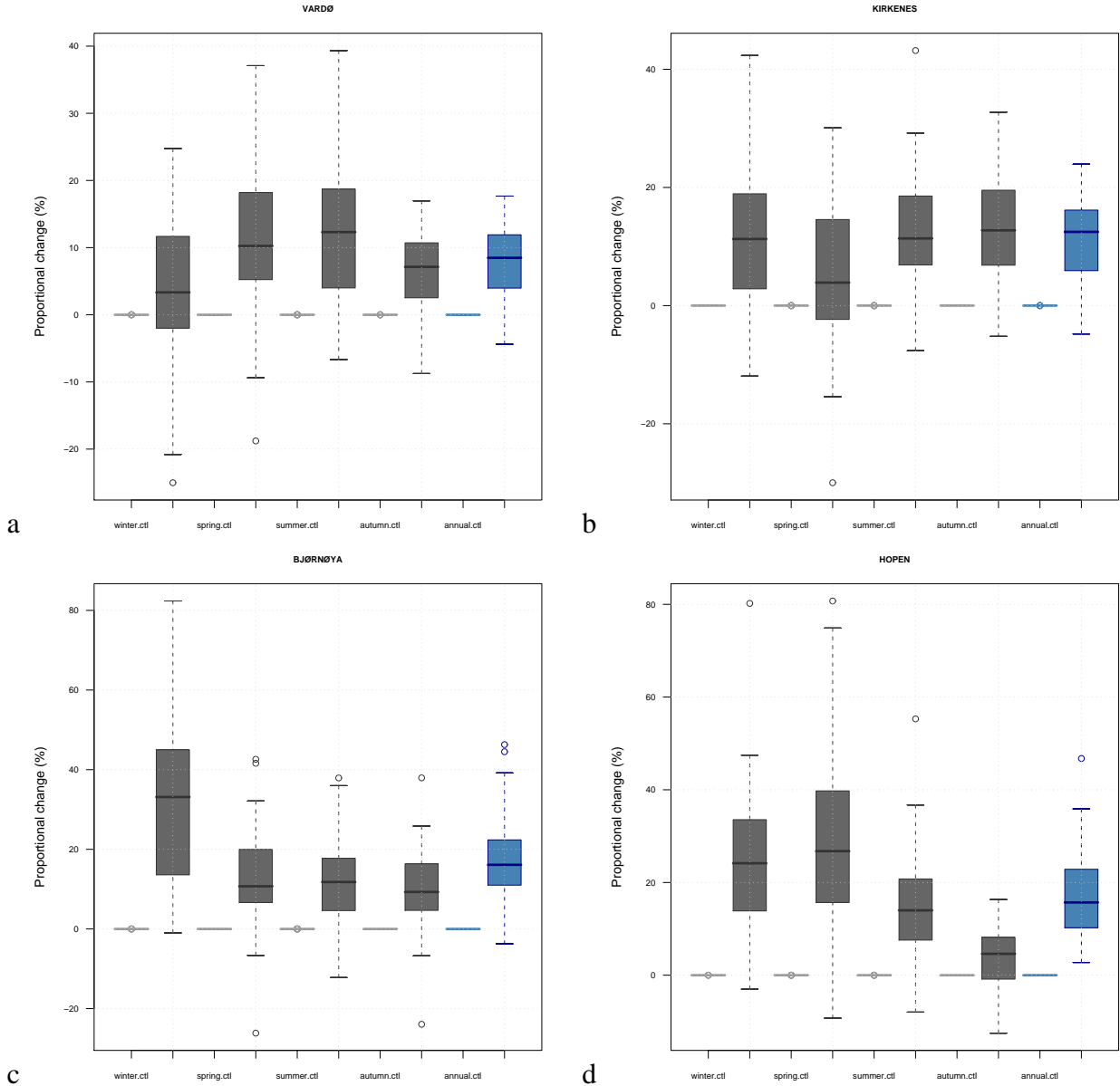


Figure 26: Box-plots for precipitation scenarios. Stations 98550, 99370, 99710, and 99720.

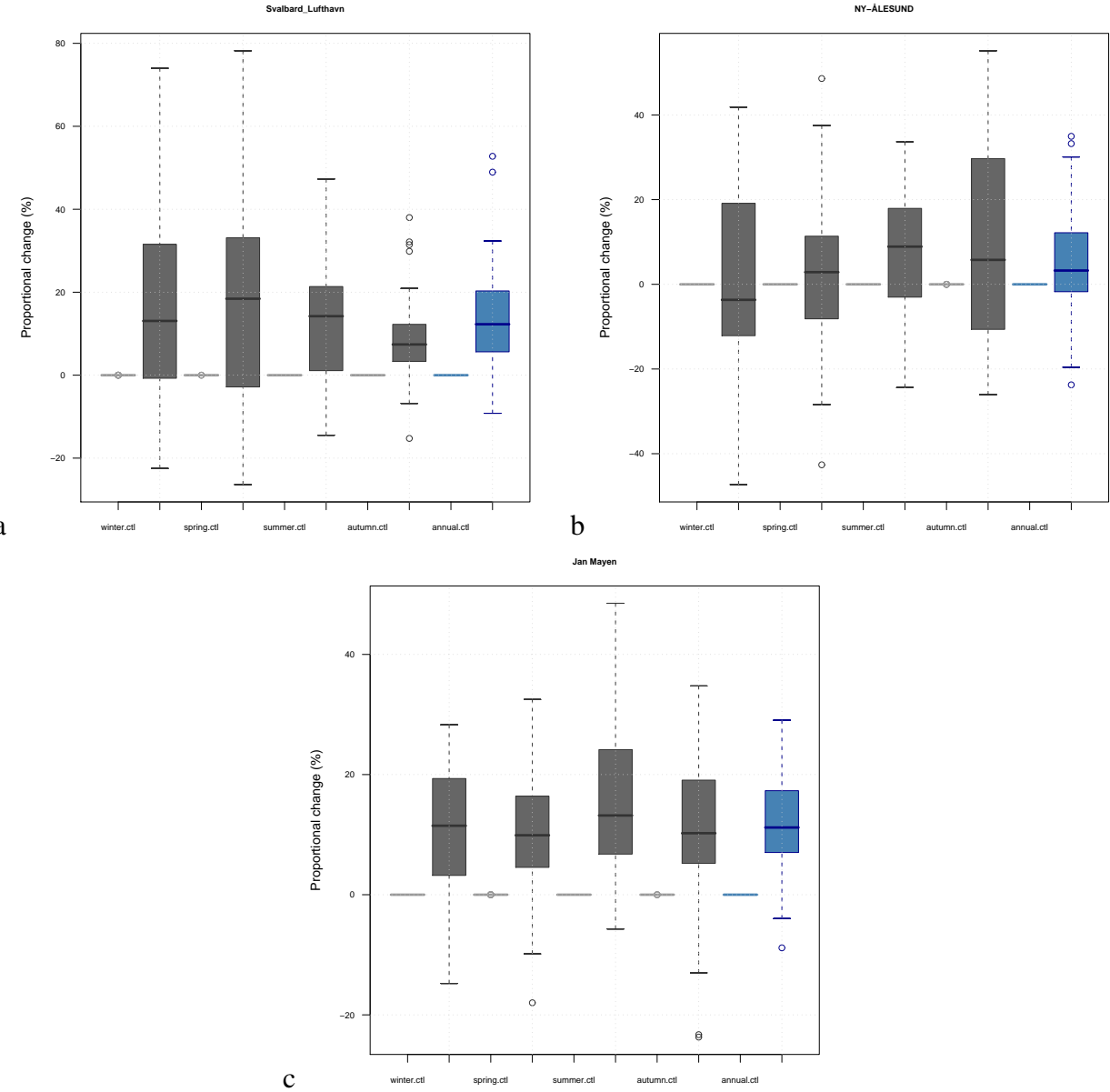


Figure 27: Box-plots for precipitation scenarios. Stations 99840, 99910, and 99950.

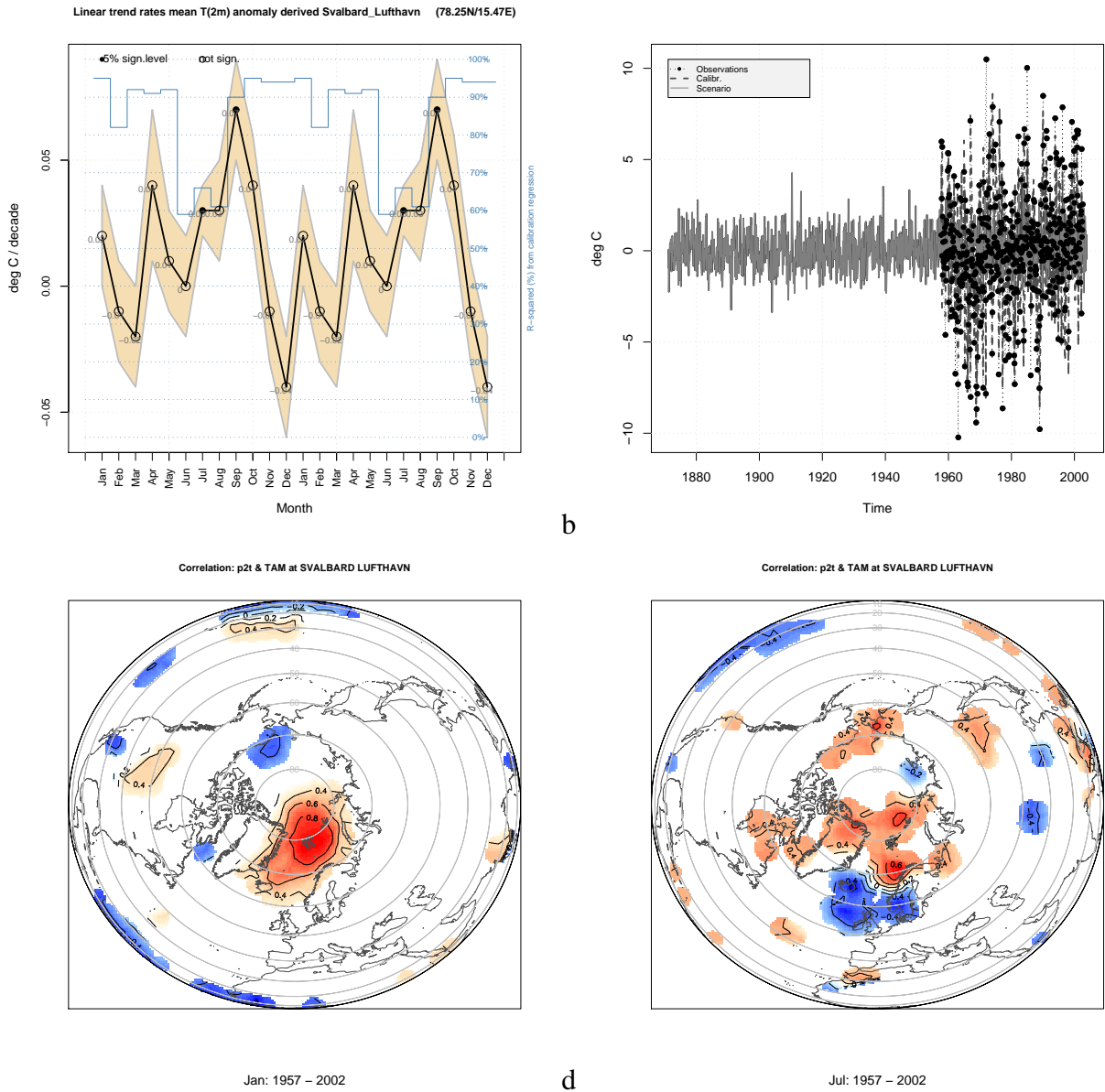
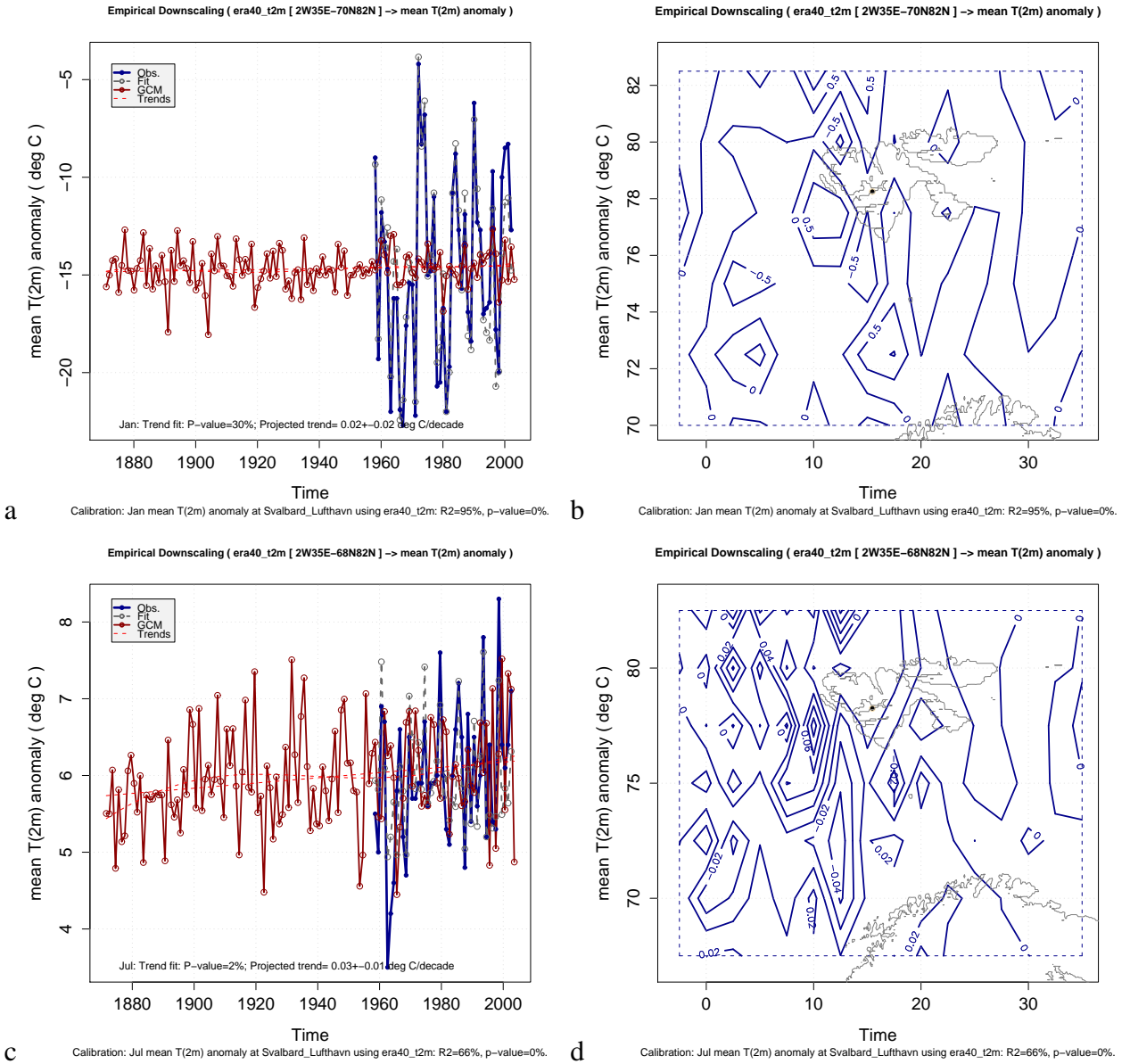


Figure 28: Diagnostics from the downscaling of the temperature at Svalbard Lufthavn (99840) for the 20th century. The blue curve in panel a shows the  $R^2$  statistics from the regression, indicating values less than 20% for all months. Panel b shows the annual time series, whereas c–d show the correlation maps between January and July temperature at 99840 and the large-scale temperature from ERA40.



**Figure 29:** Diagnostics from the downscaled temperature at 99840 for the 20th century: (a) the downscaled January time series, (b) January predictor pattern, (c) July time series, and (d) July predictor pattern.

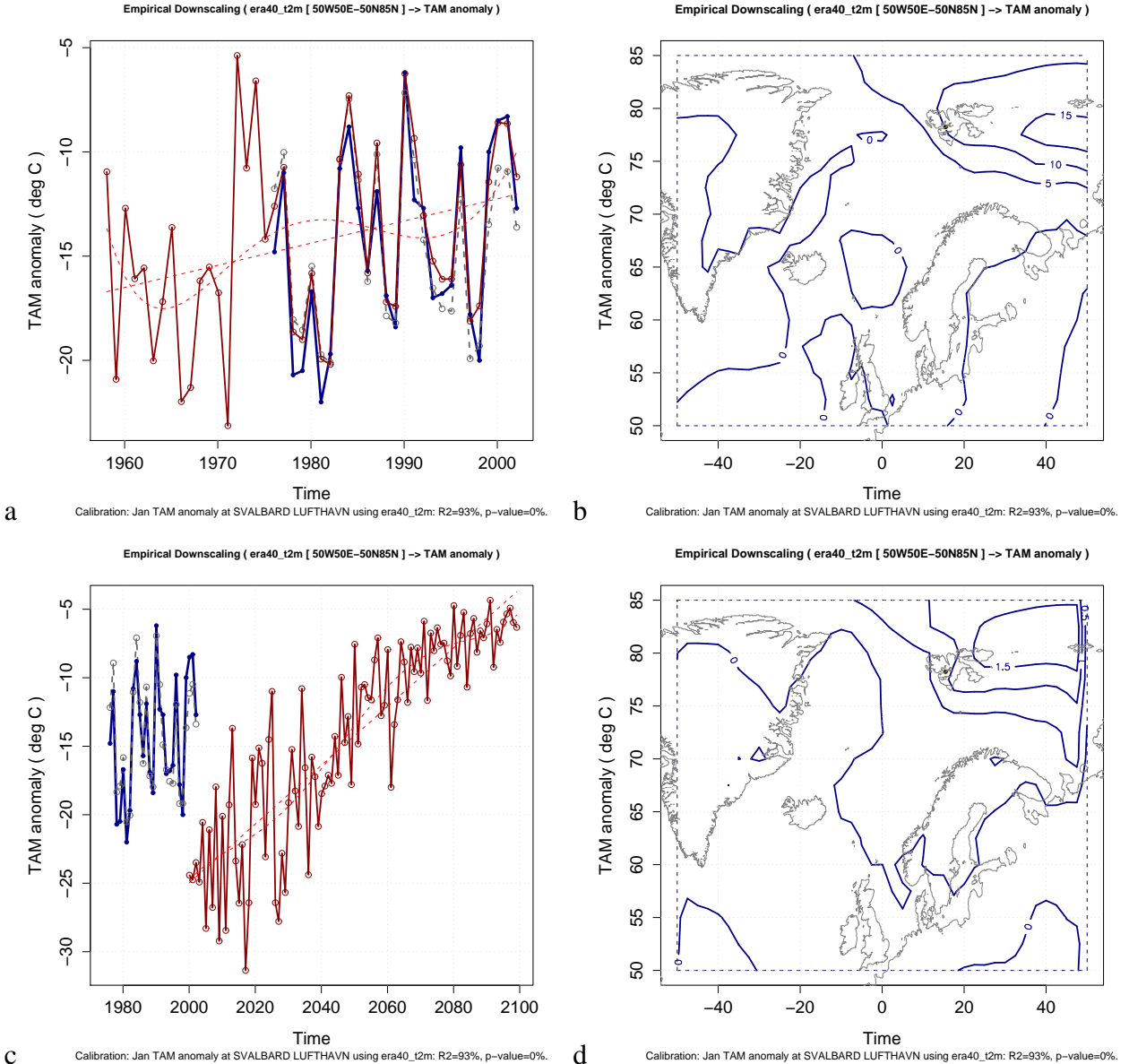


Figure 30: Diagnostics from the downscaled temperature at 99840 for the 20th and 21st centuries: (a) the downscaled 1950–2000 January time series, and (b) corresponding January predictor pattern, (c) downscaled 2000–2100 January time series, and (d) corresponding predictor pattern.

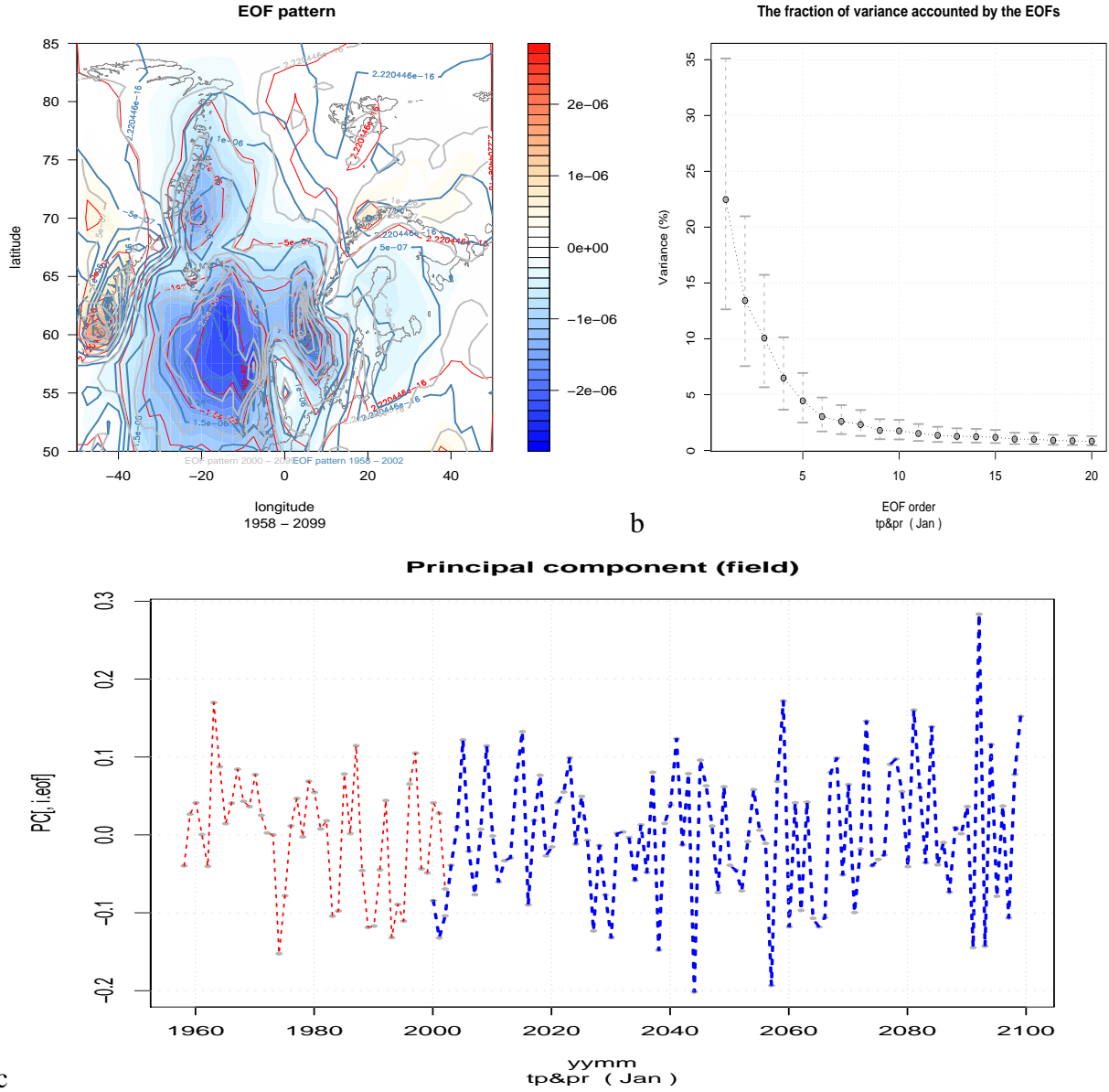


Figure 31: Diagnostics from the EOFs for the January temperature over the Greenland-Iceland-Norwegian Sea region. Panel a compares the leading common EOF (shading/red) with the leading EOFs derived from the ERA40 (blue) and HadGEM1 SRES A1b (grey). Panel b shows the variances associated with the common EOFs, and c shows the time series.

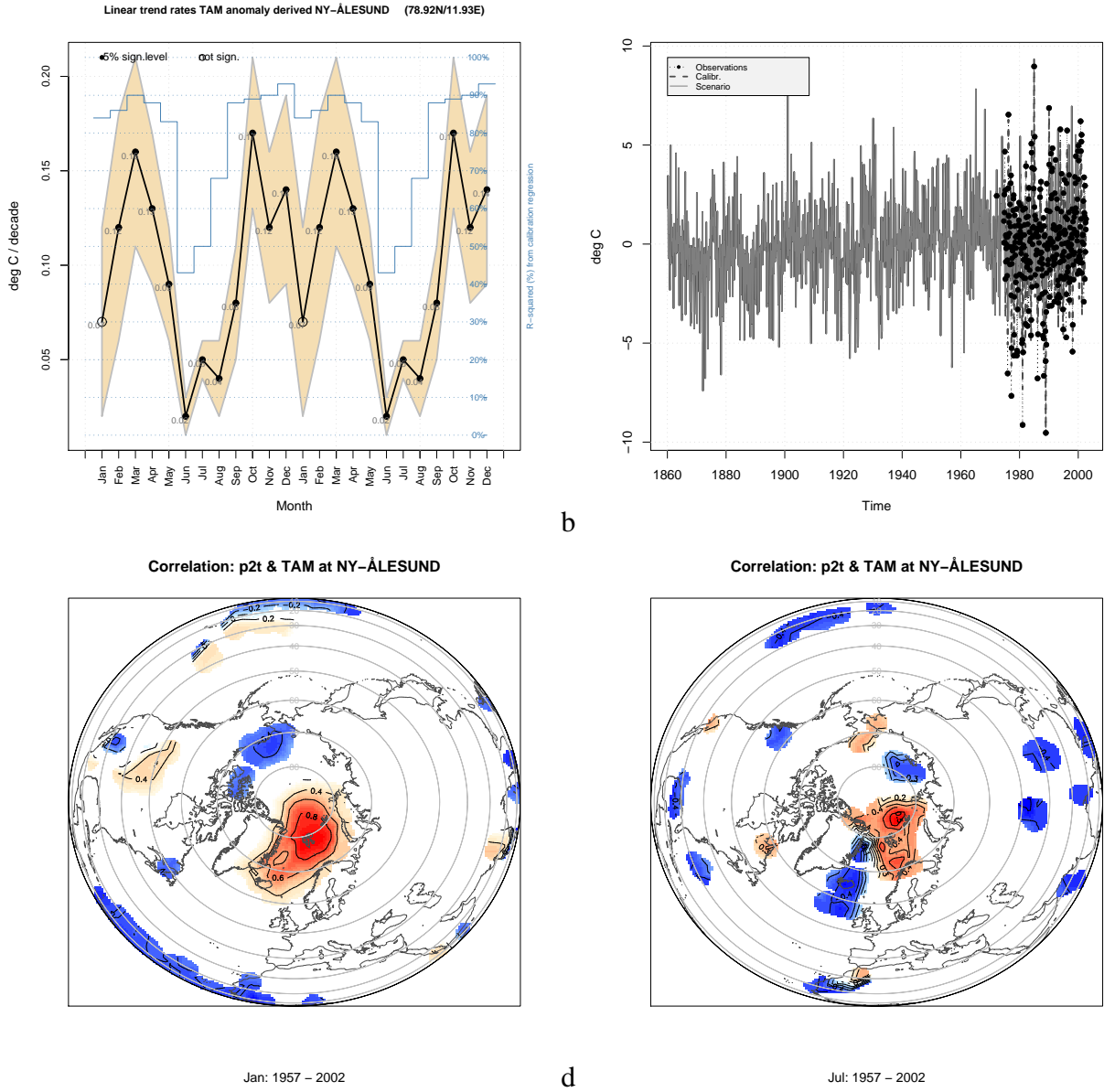


Figure 32: Diagnostics from the downscaling of the temperature at 99910. The blue curve in panel a shows the  $R^2$  statistics from the regression, indicating values less than 20% for all months. Panel b shows the annual time series, whereas c-d show the correlation maps between January and July temperature at 99910 and the large-scale temperature from ERA40.

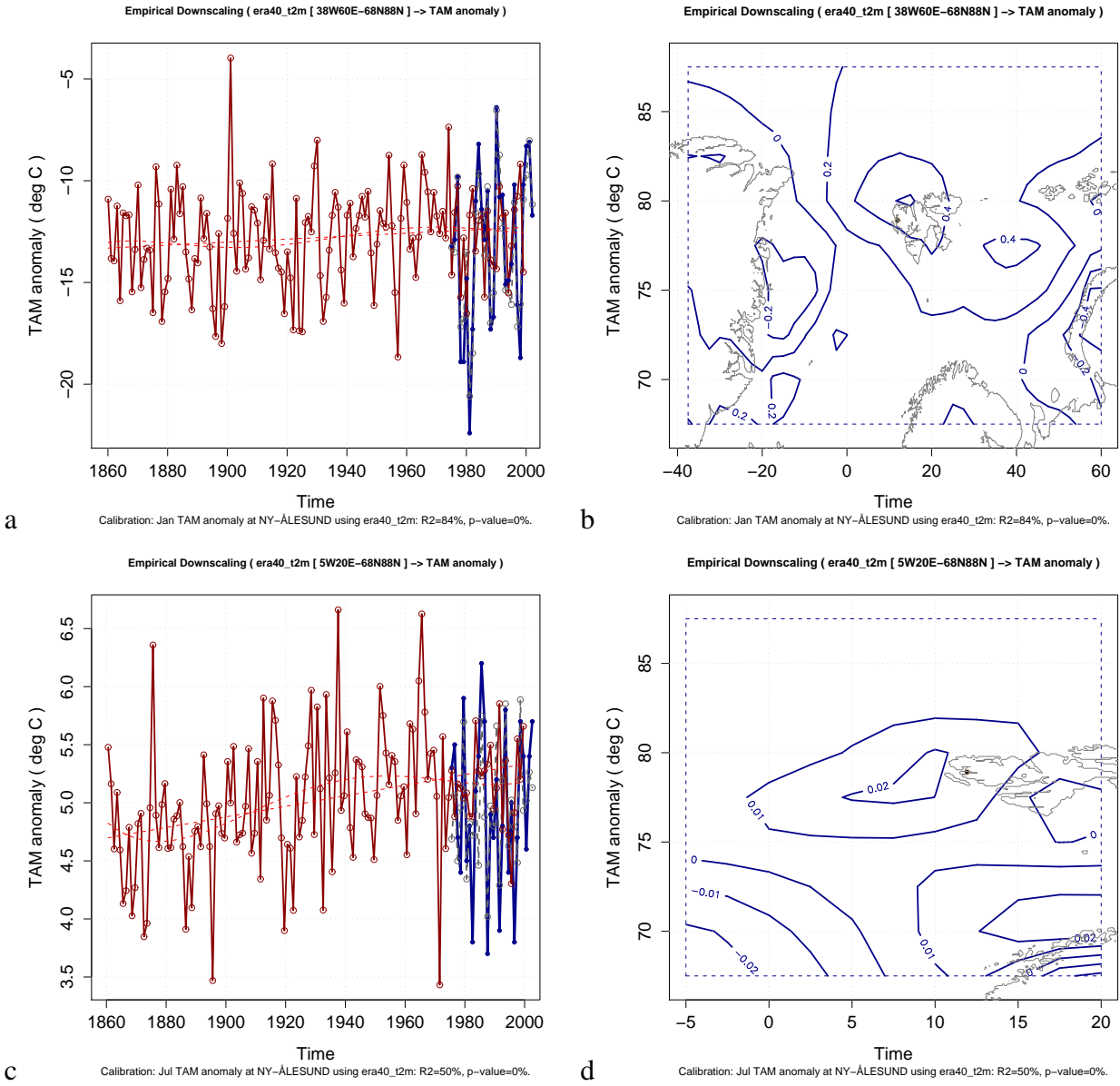


Figure 33: Diagnostics from the downscaling of the temperature at 99910 for the 20th century: (a) the downscaled January time series, (b) January predictor pattern, (c) July time series, and (d) July predictor pattern.

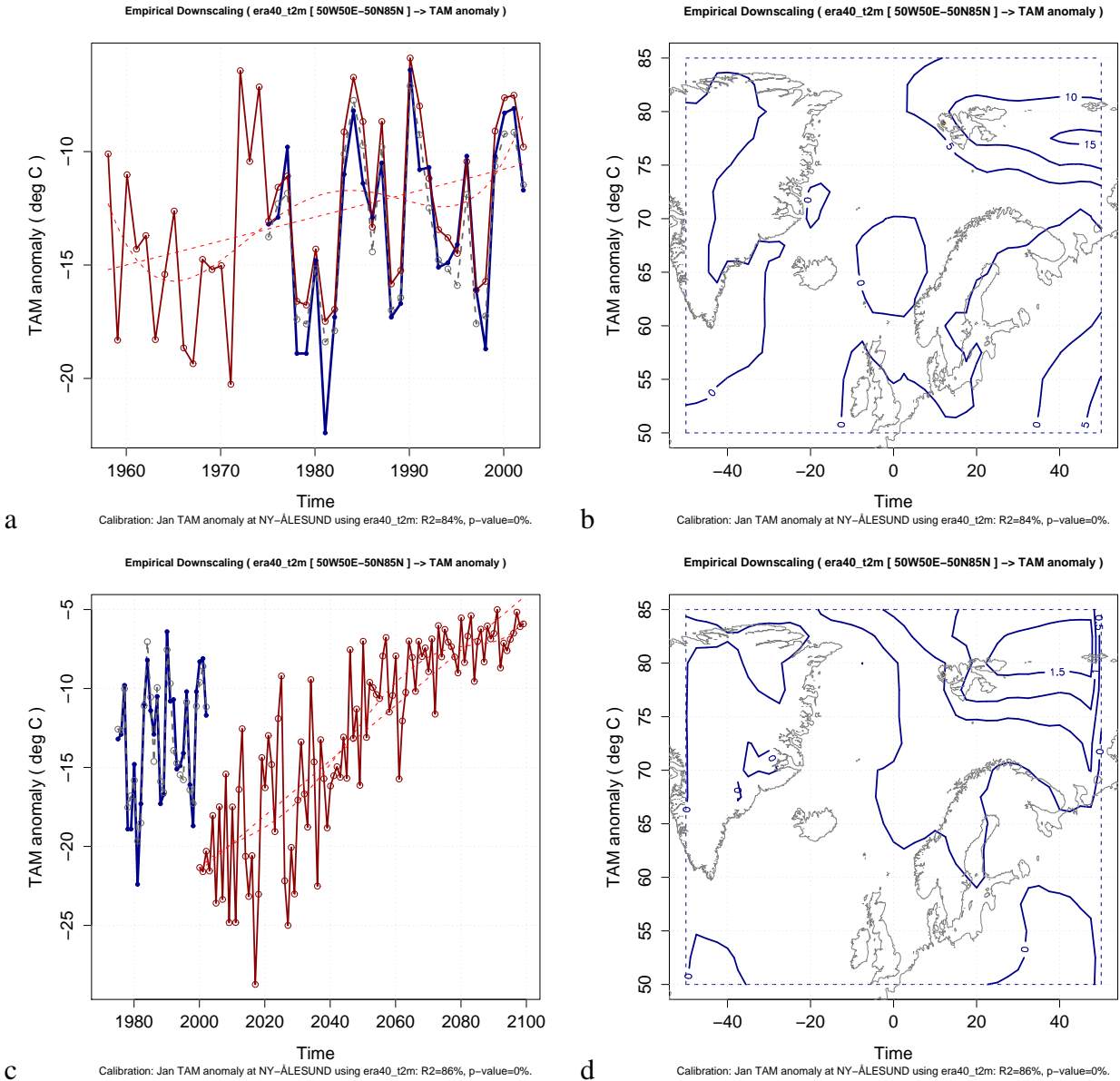


Figure 34: Diagnostics from the downscaled temperature at 99910 for the 20th and 21st centuries: (a) the downscaled 1950–2000 January time series, and (b) corresponding January predictor pattern, (c) downscaled 2000–2100 January time series, and (d) corresponding predictor pattern.

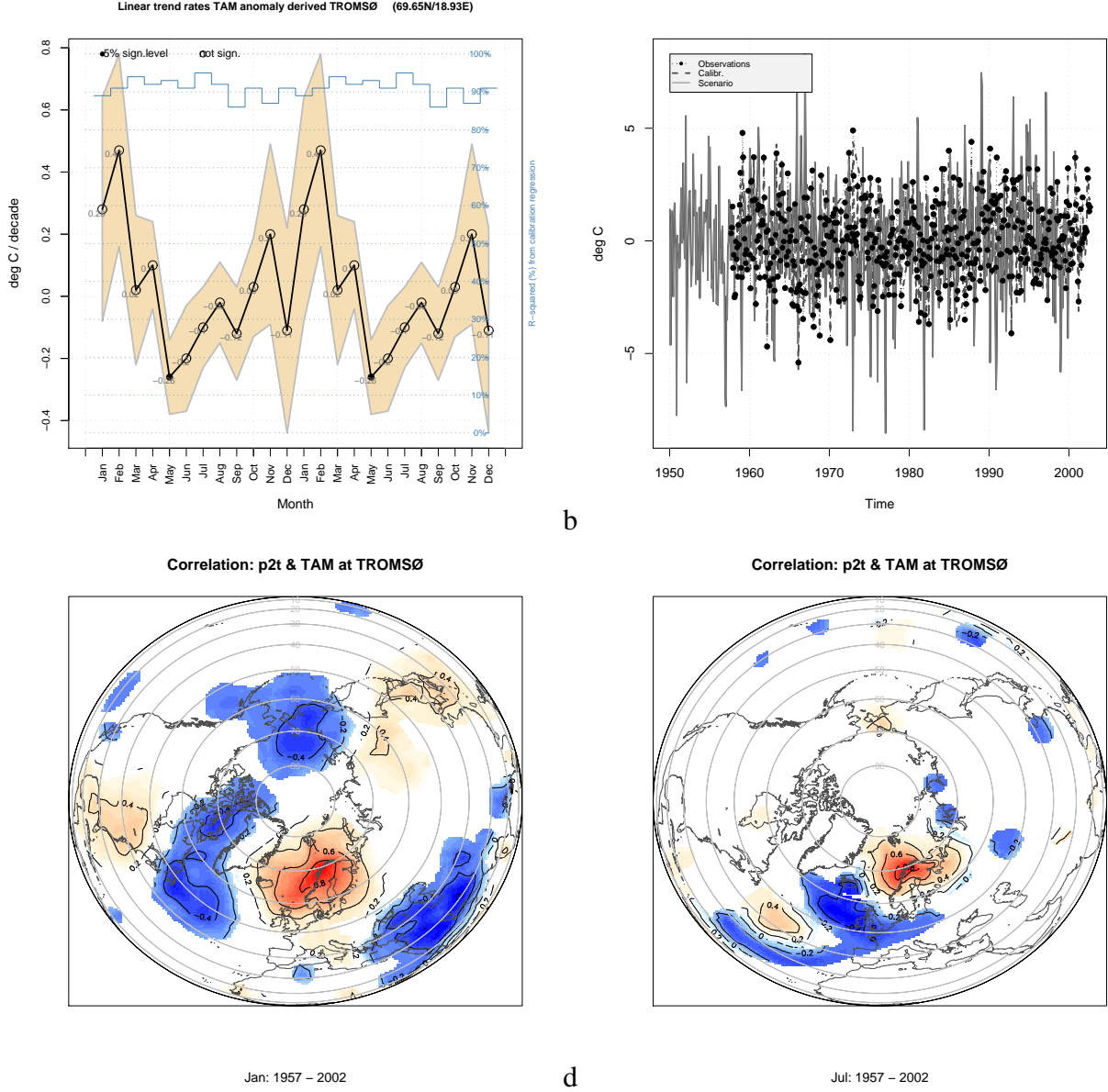


Figure 35: Diagnostics from the downscaling of the temperature at 90450. The blue curve in panel a shows the  $R^2$  statistics from the regression, indicating values less than 20% for all months. Panel b shows the annual time series, whereas c–d show the correlation maps between January and July temperature at 90450 and the large-scale temperature from ERA40.

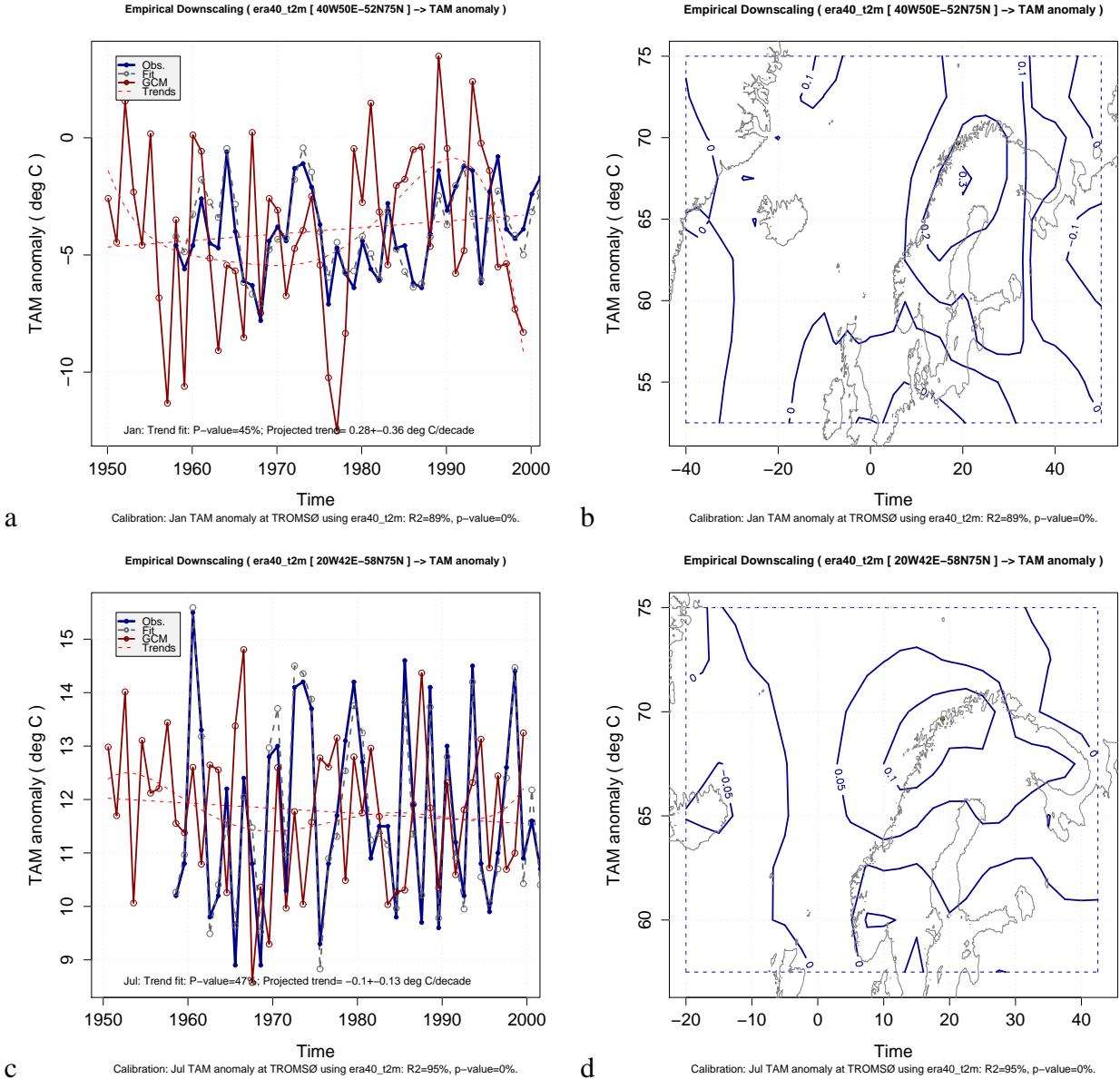


Figure 36: Diagnostics from the downscaling of the temperature at 90450 for the 20th century: (a) the downscaled January time series, (b) January predictor pattern, (c) July time series, and (d) July predictor pattern.

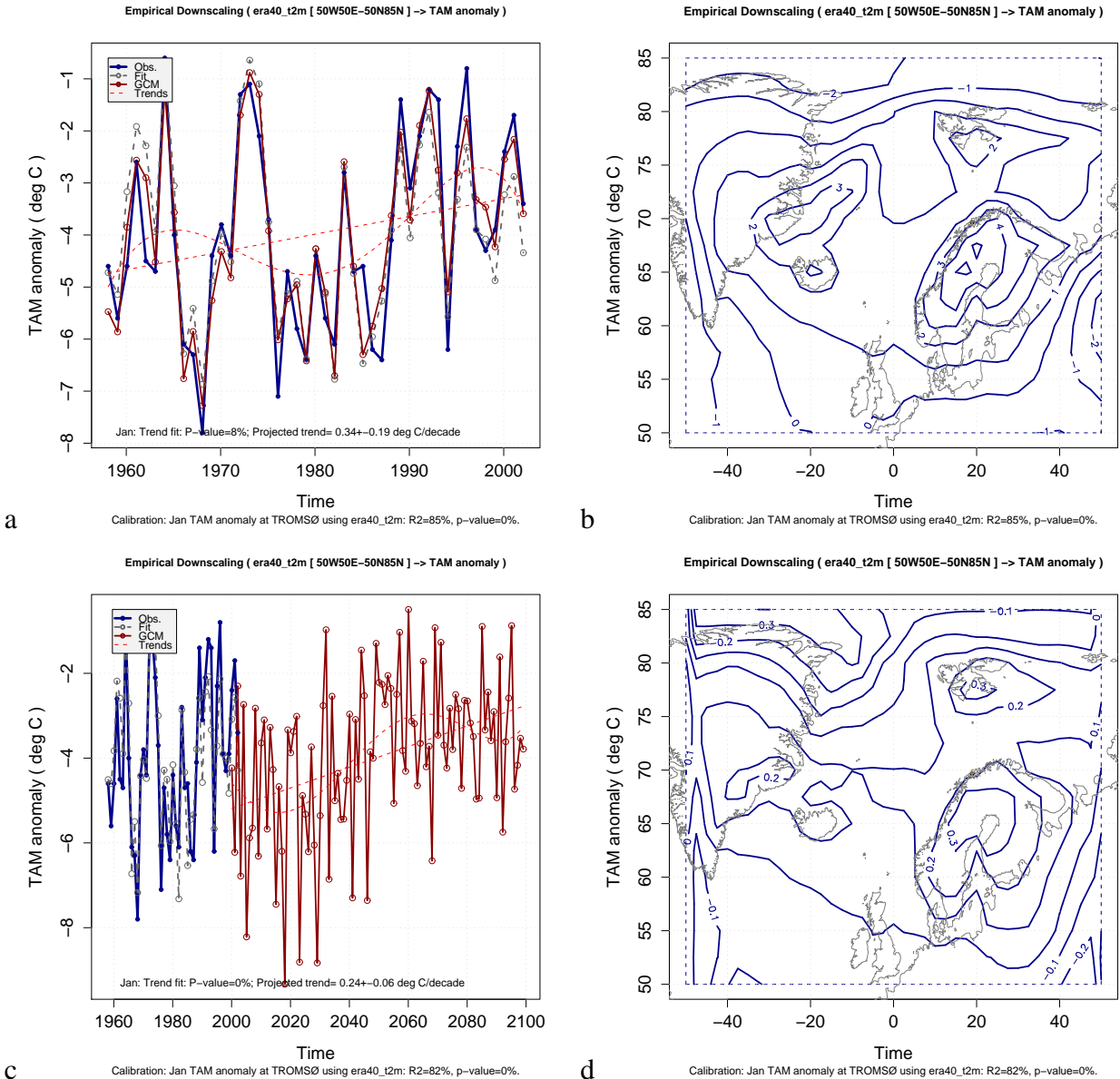


Figure 37: Diagnostics from the downscaled temperature at 90450 for the 20th and 21st centuries: (a) the downscaled 1950–2000 January time series, and (b) corresponding January predictor pattern, (c) downscaled 2000–2100 January time series, and (d) corresponding predictor pattern.

## Quality evaluation of downscaling of precipitation

The ESD analysis yielded low values (30–40%) for  $R^2$  during spring (Figure 38a), although the correlation analysis did suggest positive correlations in January and July. The spatial correlation structure for precipitation has in general substantially smaller spatial extent than for temperature, making ESD more tricky for the former (Benestad et al., 2008).

The July results for one of the A1b run with HadGEM1 did not reproduce any of the variability for large domain choice (not shown), but captured a good part of the variance for the smaller domain (Figure 40c). The differences can be explained by different spatial characteristics in the projected results and the reanalysis (i.e. the EOF analysis yields different modes, see Figure 41). Although the model roughly reproduces the maximum variability between the British Isles and Greenland, there are important differences in the vicinity of Svalbard and the Barents Sea, to which these results may be sensitive.

The values for the precipitation in reanalysis (Trenberth et al., 2008) products are derived from model assimilation, and are thus prone to biases, especially at high latitudes with sparse observational network. Only one example is shown here (HadGEM1), but these caveats are expected to depend on the choice of GCM (the scatter in the plume plots indicate substantial variations amongst the different runs).

The diagnostics of the ESD-results for Hopen reveals similar problems as for Bjørnøya (Figure 43). Figure 44 shows a comparison between results from ESD exercises, carried out with the ERA40 calibration predictors, and a set of arbitrary GCM-predictors respectively. From Figure 44a, we can learn that the weak statistical relationship between the predictand and predictor results in an underestimate of the variance (possibly due to discrepancies in the ERA40 or errors in the station series). There are no clear and dominant spatial structure (Figure 40b and 44b). Figures 44c–d suggest that the GCM produces similar levels of variance as the re-analysis, but that the spatial structure associated with these Figure 44d now differs from the ERA40-only ESD results (Figure 44b).

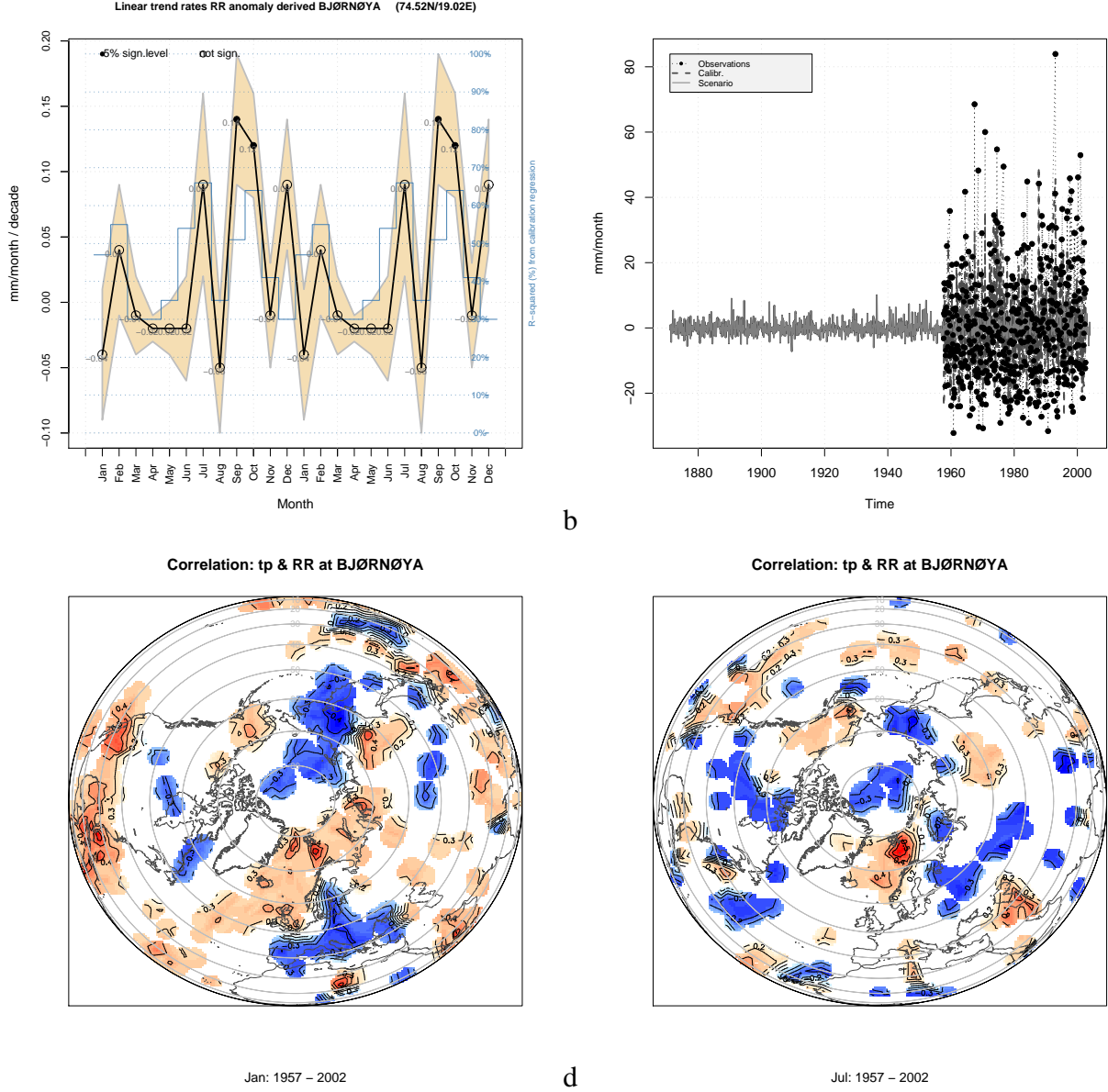


Figure 38: Diagnostics from the downscaling precipitation at 99710. The blue curve in panel a shows the  $R^2$  statistics from the regression, indicating values less than 20% for all months. Panel b shows the annual time series, whereas c–d show the correlation maps between January and July precipitation at 99710 and the large-scale precipitation from ERA40.

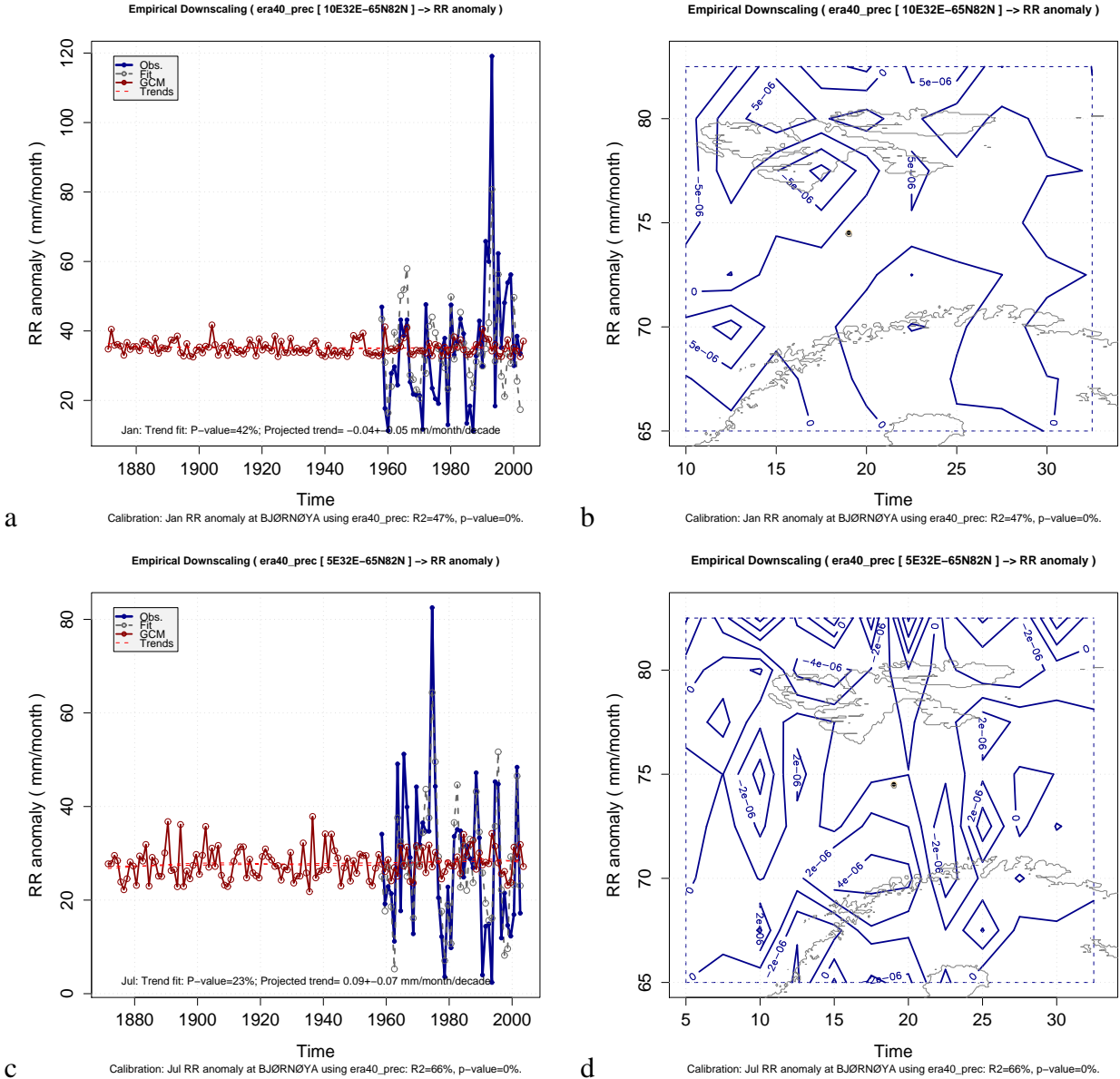


Figure 39: Diagnostics from the downscaling precipitation at 99710 for the 20th century: (a) the downscaled January time series, (b) January predictor pattern, (c) July time series, and (d) July predictor pattern.

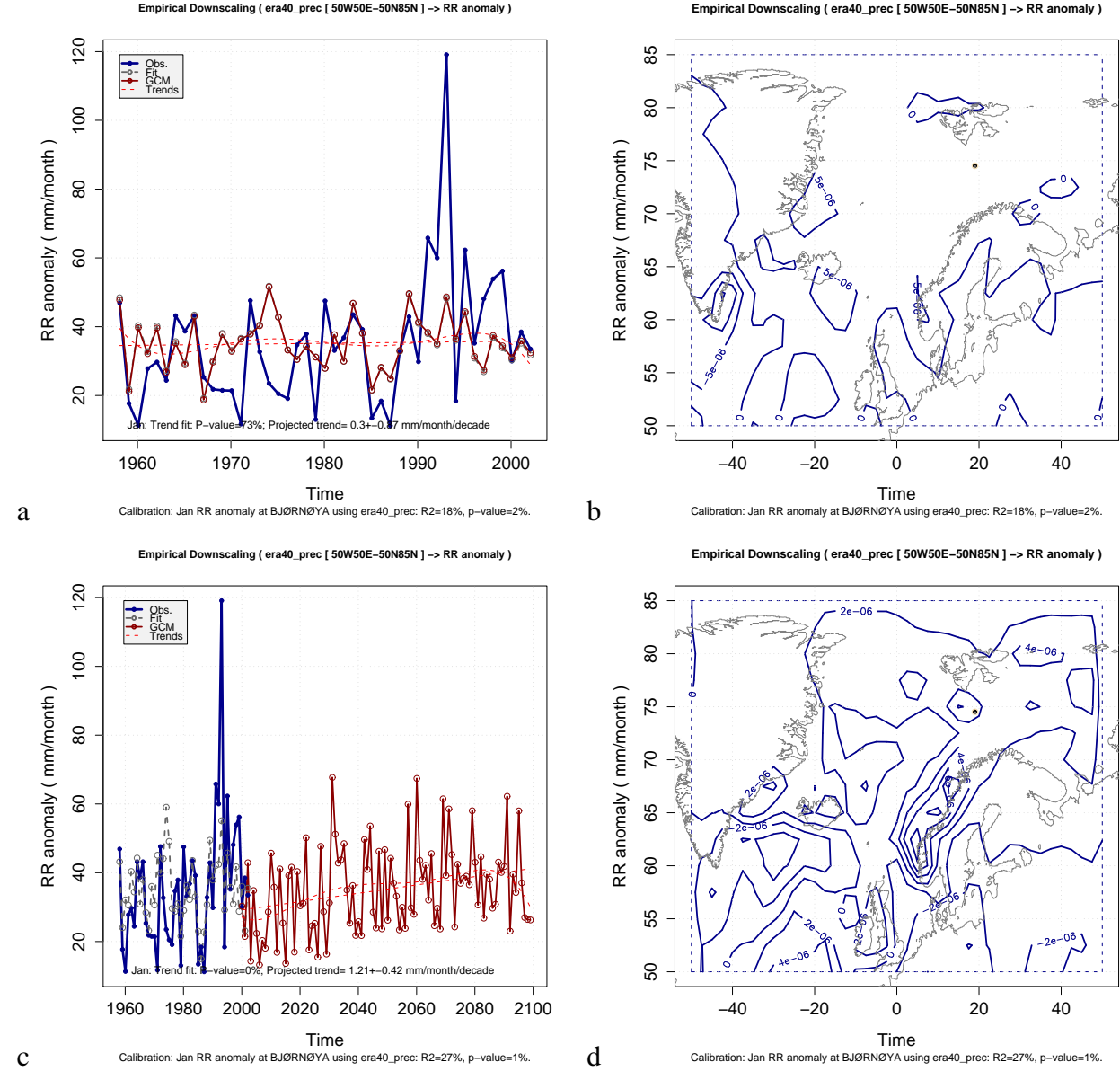


Figure 40: Diagnostics from the downscaling precipitation at 99710 for the 20th and 21st century: (a) the downscaled January time series based on ERA40 (dependent data), (b) predictor pattern corresponding to the results in panel a, (c) the downscaled January time series based on HadGEM1 SRES A1b (independent data), and (d) predictor pattern corresponding to the results in panel c.

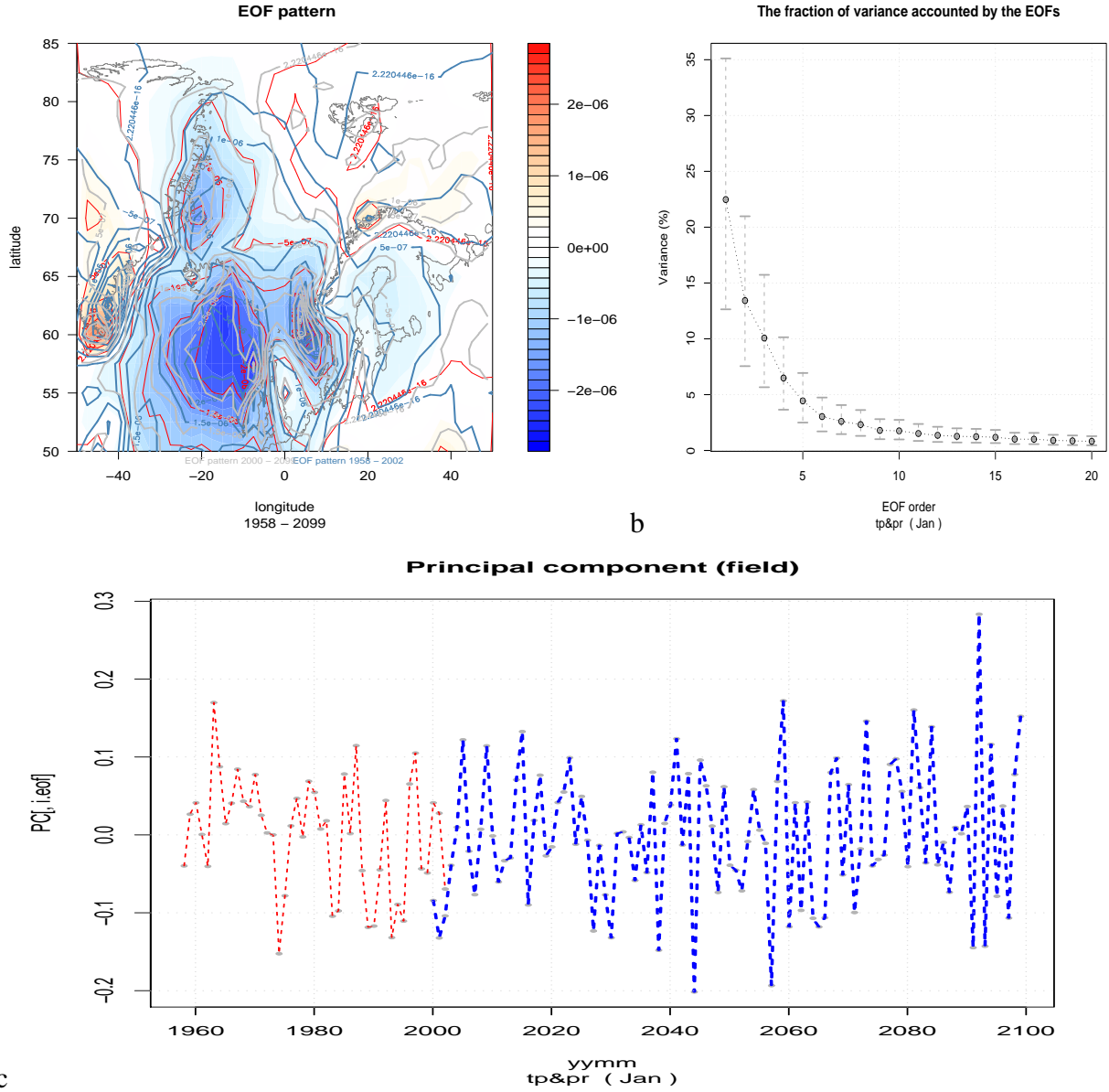


Figure 41: Diagnostics from the EOFs for the January precipitation over the Greenland-Iceland-Norwegian Sea region. Panel a compares the leading common EOF (shading/red) with the leading EOFs derived from the ERA40 (blue) and HadGEM1 SRES A1b (grey). Panel b shows the variances associated with the common EOFs, and c shows the time series.

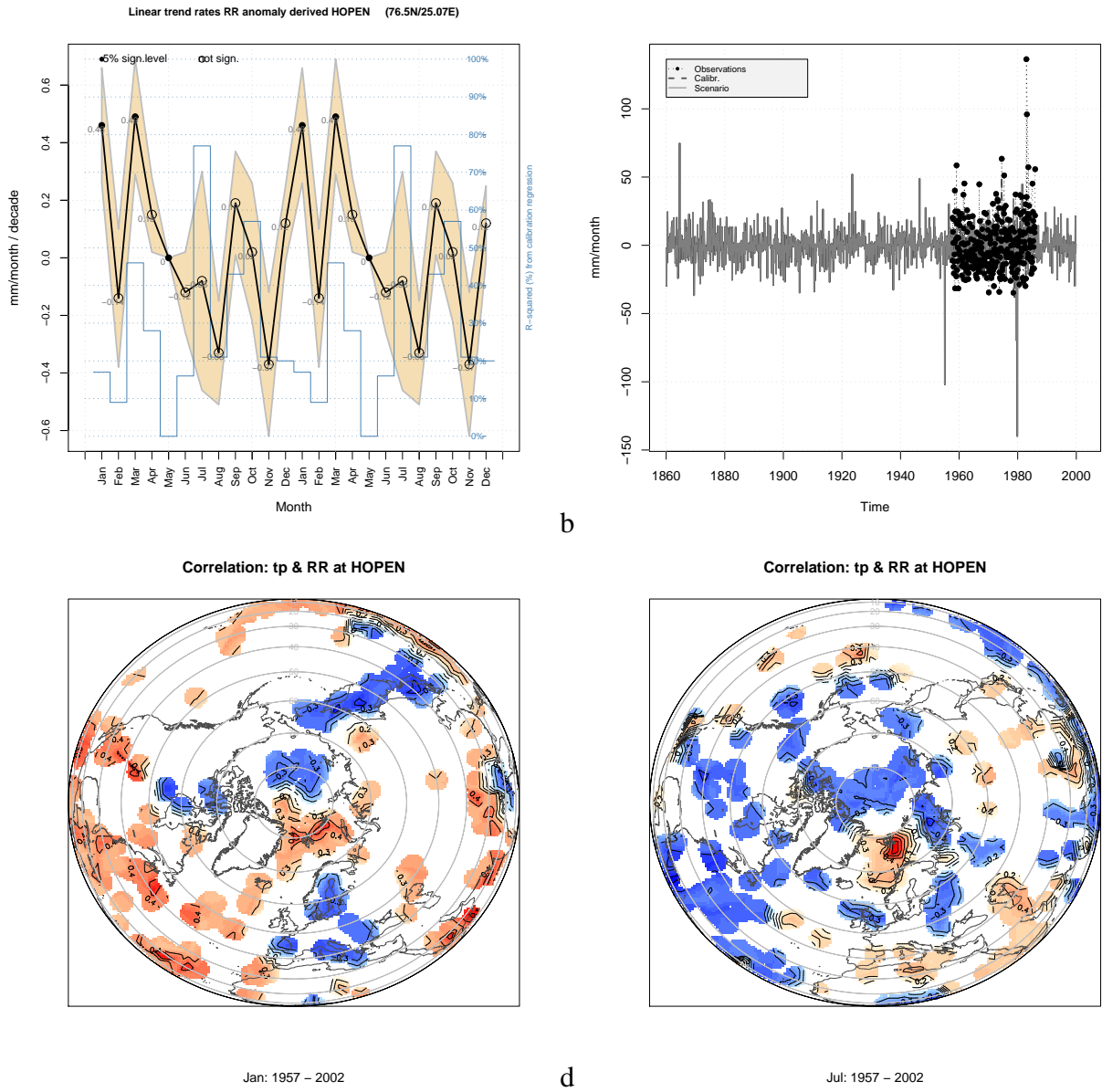


Figure 42: Diagnostics from the downscaling precipitation at Hopen (99720). The blue curve in panel a shows the  $R^2$  statistics from the regression, indicating values less than 20% for all months. Panel b shows the annual time series, whereas c-d show the correlation maps between January and July precipitation at 99720 and the large-scale precipitation from ERA40.

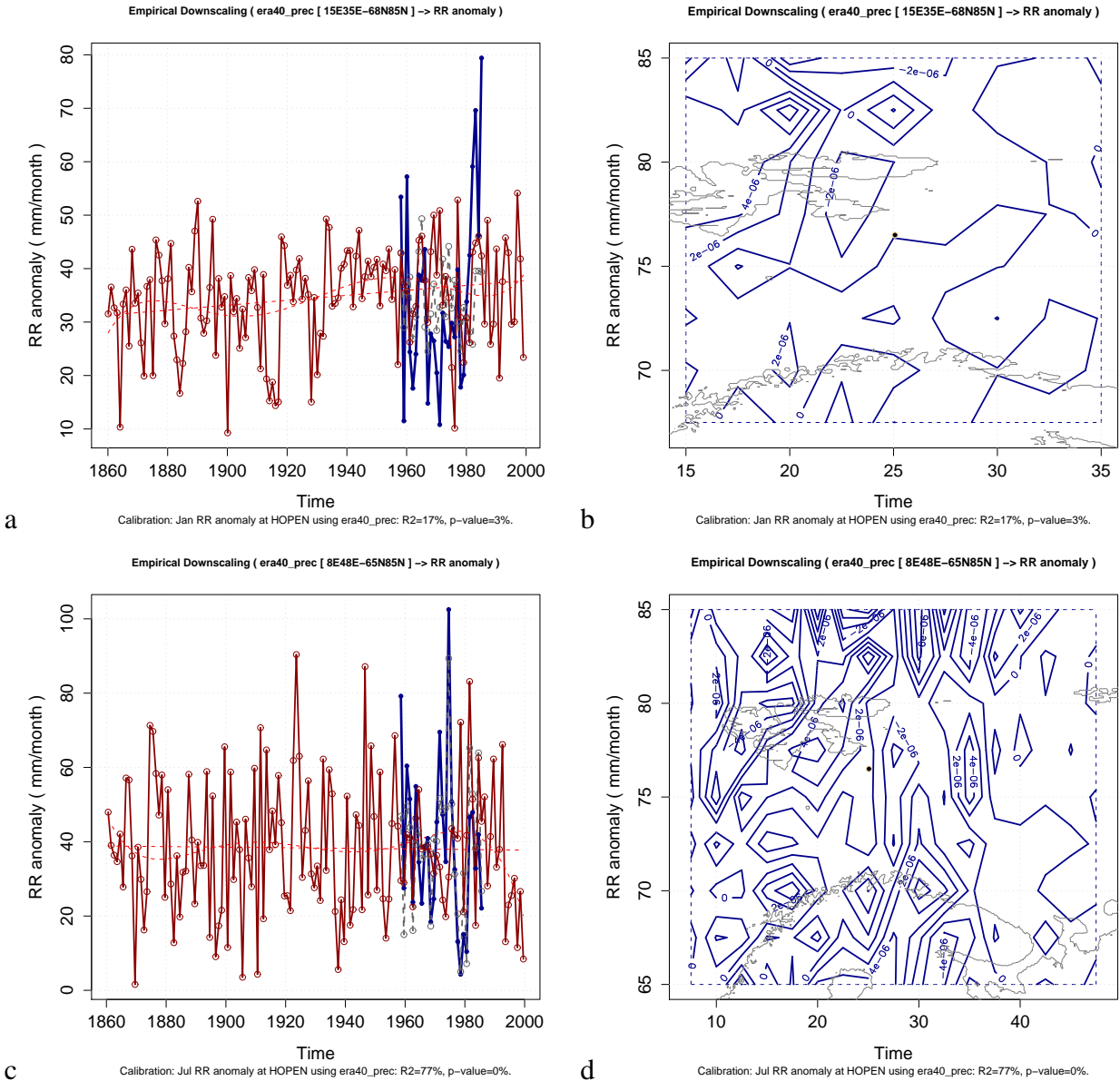


Figure 43: Diagnostics from the downscaling precipitation at Hopen (99720) for the 20th century: (a) the downscaled January time series, (b) January predictor pattern, (c) July time series, and (d) July predictor pattern.

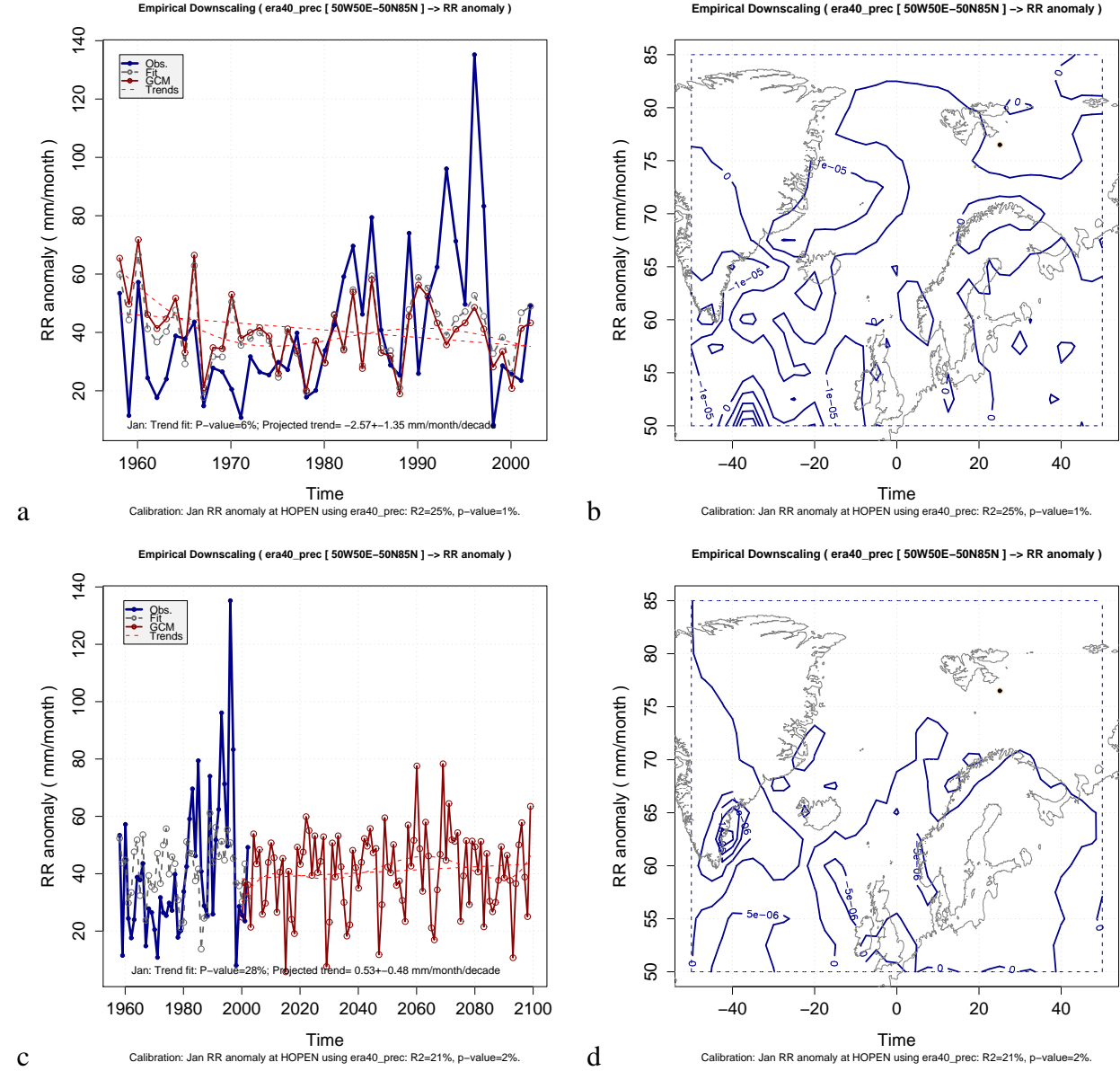


Figure 44: Diagnostics from the downscaling precipitation at 99720 for the 20th and 21st century: (a) the downscaled January time series based on ERA40 (dependent data), (b) predictor pattern corresponding to the results in panel a, (c) the downscaled January time series based on HadGEM1 SRES A1b (independent data), and (d) predictor pattern corresponding to the results in panel c.

Table 3: List of the GCMs and the scenario simulations used as input for the ESD-based scenario production. The choice of runs was arbitrary in the sense that only those results that were available at the time of the downloading were selected.

Temperature:		
GCM	c20	SRES A1b
bcc_cm1	1–2	
bccr_bcm2_0	1	1
cccma_cgcm3_1	1	1
cccma_cgcm3_1_t63	1	1
cnrm_cm3	1	1
csiro_mk3_0	1	1
gfdl_cm2_0	1	1
gfdl_cm2_1	1–3	1
giiss_aom	1–2	1–2
giiss_model_e_h	1–5	1–3
giiss_model_e_r	1–5	1–5
iap_fgoals1_0_g	1	1,3
ingv_echam4	1	1
inmcm3_0	1	1
ipsl_cm4	1	1
miroc3_2_hiress	1	1
miroc3_2_medres	1–3	1–3
miub_echo_g	1–5	1–3
mpi_echam5	1–3	1–4
mri_cgcm2_3_2a	1–5	1–5
ncar_ccsm3_0	1,3,6,9	1–3,5–7, 9
ncar_pcm1	2–4	1–3
ukmo_hadcm3	1–2	1
ukmo_hadgem1	1–2	
sum	55	50

### List of GCMs

Table 4: List of the GCMs and the scenario simulations used as input for the ESD-based scenario production. The choice of runs was arbitrary in the sense that only those results that were available at the time of the downloading were selected.

Precipitation:		
GCM	c20	SRES A1b
bcc_cm1	1–2	0
bccr_bcm2_0	1	1
cccma_cgcm3_1	1	1
cccma_cgcm3_1_t63	1	1
cnrm_cm3	1	1
csiro_mk3_0	1	1
gfdl_cm2_0	1	1
gfdl_cm2_1	1–3	1
giss_aom	1–2	1–2
giss_model_e_h	1,3–5	1–3
giss_model_e_r	1–5	2,4
iap_fgoals1_0_g	1	0
ingv_echam4	1	1
inmcm3_0	1	1
ipsl_cm4	1	1
miroc3_2_hires	1	0
miroc3_2_medres	1–3	1–3
miub_echo_g	1–5	1–3
mpi_echam5	1–3	1,2–3
mri_cgcm2_3_2a	1–5	1–5
ncar_ccsm3_0	1,3,5–7,9	1–3,5–7,9
ncar_pcm1	2–4	1–3
ukmo_hadcm3	1–2	1
ukmo_hadgem1	1–2	1
<b>sum</b>	<b>54</b>	<b>43</b>

## Meta data

## R-script

Listing of the R-script used to derive these results (file name is NorAcia.R):

```

library(clim.pact)
library(met.no) # met.no_1.1-0.tar.gz
source("ds_one.R")

do.esd <- function(param="TAM",LINPACK=TRUE,economic=FALSE,predictand="metno",
                    a=c(90450,93700,94260,97250,98550,99370,99710,99720,99840,99910,99950),
                    dlon=c(-50,50),dlat=c(-30,10)) {

ele <- switch(param,"TAM"=101,"RR"=601)
if (is.null(a)) a <- stnr()

for (i in 1:length(a)) {
  print(a[i])
  obs <- KDVH4DS(a[i],param=param)
  if (a[i]==94260) {obs$location <- "Hammerfest"; obs$lon <- 23.6667; obs$lat <- 70.6833; obs$alt <- 69} else
  if (a[i]==97250) {obs$location <- "Karasjok"; obs$lon <- 25.5030; obs$lat <- 69.4670; obs$alt <- 129}

  if ( (param=="RR") & is.element(a[i],c(93700,99720)) ) {
    # Ignore the last part of the Hopen RR-record: station displacement and break in series.
    # Ignore the last part of the Kautokeino RR-record: inhomogeneity.
    obs$val[obs$yy > 1989,] <- NA
    #plotStation(obs)
  }
  if ( (param=="TAM") & (a[i]==99840) ) {
    # Include earlier part of the Svalbard series.
    old.predictand <- predictand; predictand="nordklim+metno"
    obs2 <- obs
    obs1 <- getnordklim(obs2$location,ele=ele)
    obs <- mergeStation(obs1,obs2)
  }

  if ( (sum(is.element(obs$yy,1950:2000))>=25) & (sum(is.finite(obs$val))>=250) ) {
    print(paste("Downscaling",a$location))
    ds.one(ele=ele,cmons=1:12,silent=TRUE,do.a1b=TRUE,do.rcm=0,
           qc=FALSE,station=obs,predictand=predictand,LINPACK=LINPACK,
           lon=obs$lon+dlon,lat=obs$lat+dlat,economic=economic)
  } else {
    print("The series was considered to be too short")
    print(c(sum(is.element(obs$yy,1950:2000)),sum(is.finite(obs$val))))
  }
  while (dev.cur()>1) dev.off()
  if ( (param=="TAM") & (a[i]==99840) ) {predictand <- old.predictand; rm(old.predictand)}
}
}

#remove.Rdata.files(path="STATNETT")

testplot <- function() {
  finalPlot(station=99720)
}

Figures <- function(ele=101,remove.bad.sd=TRUE,
                     station=c(90450,93700,94260,97250,98550,99370,99710,99720,99840,99910,99950)) {
  bad.start.cri <- switch(as.character(ele),"101"=3,"601"=7)
#  finalPlot(station=c(90450,93700,94260,97250,98550,99370,99710,99720,99840,99910,99950),ele=ele)
  finalPlot(station=station,ele=ele,remove.bad.sd=remove.bad.sd)
}

tables <- function(ele=101,inflation=FALSE,period=2070:2099,absolute=TRUE,prop.chng=FALSE,pattern="metno",
                   locations=c(90450,93700,94260,97250,98550,99370,99710,99720,99840,99910,99950)) {
  seasons <- matrix(c(12,1,2,3:5,6:8,9:11),3,4)
  dig <- switch(as.character(ele),"101"=1,"601"=0)
  param <- switch(as.character(ele),"101"="TAM","601"="RR")
  M <- rep(NA,101*4); dim(M) <- c(101,4); Q1 <- M; Q2 <- M
}

```

```

m <- rep(NA,101*4); dim(m) <- c(101,4); q1 <- m; q2 <- m
trend <- rep(NA,201*4); dim(trend) <- c(201,4)
n <- length(locations)
sce.2000.2040 <- rep("NA",n*4); dim(sce.2000.2040) <- c(n,4); sce.0.2000.2040 <- sce.2000.2040
clim <- rep(NA,4*n); dim(clim) <- c(n,4)

colnames(sce.2000.2040) <- c("Winter","Spring","Summer","Autumn")
colnames(clim) <- c("Winter","Spring","Summer","Autumn")
Clim <- clim

locs <- rep("?",n)
for (i in 1:n) {
  t <- 2000:2100
  obs <- KDVH4DS(locations[i],param=param)
  if (locations[i]==94260) {obs$location <- "Hammerfest"; obs$lon <- 23.6667; obs$lat <- 70.6833; obs$alt <- 69} else
    if (locations[i]==97250) {obs$location <- "Karasjok"; obs$lon <- 25.5030; obs$lat <- 69.4670; obs$alt <- 129}

  locs[i] <- obs$location
  print(paste("locs[i]=",locs[i]))
  esd <- showall(locations[i],predictand=pattern,ele=ele,plot=TRUE)
  N <- length(esd$scen.files.a1b)
  z <- rep(NA,101*N*4); dim(z) <- c(101,N,4)
  X <- obs$yy

  for (igcm in 1:N) {
    for (is in 1:4) {
      if (ele==101) {
        y <- colMeans(esd$sce[igcm,seasons[,is],],na.rm=TRUE)
        clim[i,is] <- mean(obs$val[is.element(obs$yy,1961:1990),seasons[,is]],na.rm=TRUE)
      } else if (ele==601) {
        y <- colSums(esd$sce[igcm,seasons[,is],],na.rm=TRUE)
        clim[i,is] <- mean(rowSums(obs$val[is.element(obs$yy,1961:1990),seasons[,is]]),na.rm=TRUE)
        obs$unit <- "mm/season"
      }
      x <- esd$yy.21c
      if (ele==601) { y[y < 0] <- 0 }
      iiii <- is.element(2000:2100,x)
      iiii2 <- is.element(x,2000:2100)
      z[iiii,igcm,is] <- y[iiii2]
    }
  }

  for (is in 1:4) {
    for (it in 1:101) {
      M[it,is] <- median(z[it,,is],na.rm=TRUE)
      Q1[it,is] <- quantile(z[it,,is],0.05,na.rm=TRUE)
      Q2[it,is] <- quantile(z[it,,is],0.95,na.rm=TRUE)
    }
  }

  trendM <- lm(M[,is] ~ t + I(t^2) + I(t^3)+ I(t^4) + I(t^5))
  trendQ1 <- lm(Q1[,is] ~ t + I(t^2) + I(t^3)+ I(t^4) + I(t^5))
  trendQ2 <- lm(Q2[,is] ~ t + I(t^2) + I(t^3)+ I(t^4) + I(t^5))

  good <- c(is.finite(M[,is]))
  m[good,is] <- round(predict(trendM),2)
  q1[good,is] <- round(predict(trendQ1),2)
  q2[good,is] <- round(predict(trendQ2),2)
}

#print(c(length(t),NA,dim(m)))
intv <- is.element(t,period)

for (is in 1:4) {
  if ((absolute) & (!prop.chng))   sce.2000.2040[i,is] <- paste(round(mean(m[intv,is],na.rm=TRUE),dig),"+/-",
                                round(0.5*(mean(q2[intv,is],na.rm=TRUE)-mean(q1[intv,is],na.rm=TRUE)),dig),sep="")
  if ((! absolute) & (!prop.chng)) sce.2000.2040[i,is] <- paste(round(mean(m[intv,is],na.rm=TRUE)-clim[i,is],dig),"+/-",
                                round(0.5*(mean(q2[intv,is],na.rm=TRUE)-mean(q1[intv,is],na.rm=TRUE)),dig),sep="")
  if ((absolute) & (prop.chng))   sce.2000.2040[i,is] <-
}

```

```

        paste(round(100*mean(m[intv,is])/clim[i,is],na.rm=TRUE),dig),"+/-",
        round(50*(mean(q2[intv,is],na.rm=TRUE)-mean(q1[intv,is],na.rm=TRUE))/clim[i,is],dig),
              sep="") else
    if ((!absolute) & (prop.chng)) sce.2000.2040[i,is] <-      # not really used...
        paste(round(100*(mean(m[intv,is],na.rm=TRUE)-clim[i,is])/clim[i,is],dig),"+/-",
        round(50*(mean(q2[intv,is],na.rm=TRUE)-mean(q1[intv,is],na.rm=TRUE))/clim[i,is],dig),
              sep=""))
    }
}

rownames(sce.2000.2040) <- substr(locs,1,6)
rownames(clim) <- substr(locs,1,6)
write.table(sce.2000.2040,file=paste("Esd_",__ele,"_",min(period),"-",max(period),
                                         ".txt",sep=""),quote=FALSE,sep="\t")
write.table(round(clim,dig),file=paste("Clim_",__ele,"_1961-1990.txt",sep=""),quote=FALSE,sep="\t")
invisible(sce.2000.2040)
}

kart <- function(locations=c(90450,93700,94260,97250,98550,99370,99710,99720,99840,99910,99950)) {
  data(addland2)
  lat.cont[lat.cont < 0] <- NA
  x11()
  par(col.axis="white")
  plot(c(-0.3,0.3),c(-0.5,0),type="n",main="Locations",xlab="",ylab="")
  par(col.axis="black")
  grid()
  for (i in seq(0,0.5,length=10)) {
    colour <- paste("grey",round(90+i*20),sep="")
    polygon((1-i)*cos(seq(0,2*pi,length=360))+0.3*i,(1-i)*sin(seq(0,2*pi,length=360))+0.3*i,col=colour,border=colour)
  }
  for (i in seq(0,80,by=10)) {
    r <- sin(pi * (90 - i)/180)
    lines(r*cos(seq(0,2*pi,length=360)),r*sin(seq(0,2*pi,length=360)),col="grey80",lwd=1,lty=2)
  }
  for (i in seq(0,360,by=10)) {
    lines(c(0,cos(2*pi*i/360)),c(0,sin(2*pi*i/360)),col="grey80",lwd=1,lty=2)
  }

  r <- sin(pi * (90 - lat.cont)/180)
  x.cont <- r * sin(pi * lon.cont/180)
  y.cont <- -r * cos(pi * lon.cont/180)
  lines(x.cont, y.cont, col = "grey30")

  for (StNr in locations) {
    obs <- KDVH4DS(StNr)
    r <- sin(pi * (90 - obs$lat)/180)
    x <- r * sin(pi * obs$lon/180)
    y <- -r * cos(pi * obs$lon/180)
    points(x,y,pch=19,cex=0.7)
    text(x,y-0.04,StNr,cex=0.4)
  }

  dev.copy2eps(file="kart.eps")
}

# plots for the abstract

qual.check1 <- function(path="output/nordklim+metnoSvalbard_Lufthavn99840101") {
  rfiles <- list.files(path=path, pattern=".Rdata", full.names=TRUE)
  load(rfiles[1])
  plotDSobj(ds.station,figs=c(1,4))
  stnr <- x$station
  #print(stnr)
  dev.copy2eps(file=paste("qual.check-",x$station,"_",x$ele,"-1.eps",sep="")); dev.off()
  dev.copy2eps(file=paste("qual.check-",x$station,"_",x$ele,"-2.eps",sep="")); dev.off()

  plotDS(ds.station$Jan)
}

```

```

dev.copy2eps(file=paste("qual.check-",x$station,"_",x$ele,"-jan1.eps",sep="")); dev.off()
dev.copy2eps(file=paste("qual.check-",x$station,"_",x$ele,"-jan2.eps",sep="")); dev.off()

plotDS(ds.station$Jul)
dev.copy2eps(file=paste("qual.check-",x$station,"_",x$ele,"-jul1.eps",sep="")); dev.off()
dev.copy2eps(file=paste("qual.check-",x$station,"_",x$ele,"-jul2.eps",sep="")); dev.off()

}

qual.check2 <- function(StNr=99840,param="TAM",field.file="ERA40_t2m_mon.Rdata",field.name="t2m") {
  load(field.file)
  field <- eval(parse(text=field.name))
  obs <- KDVH4DS(StNr,param=param)
  m <- corField(field,obs,mon=1)
  stereogr(m,dr=0.05)
  dev.copy2eps(file=paste("qual.check-",StNr,"_",param,"-jan-cor.eps",sep=""))

  m <- corField(field,obs,mon=7)
  stereogr(m,dr=0.05)
  dev.copy2eps(file=paste("qual.check-",StNr,"_",param,"-jul-cor.eps",sep=""))
}

qual.check3 <- function(era.file="ERA40_t2m_mon.Rdata",field.name="t2m",StNr=99840,param="TAM",v.nam="tas",
  gcm.name="/klimadata/rasmusb/data/ipcc_FoAR/GCMs/pcmdi.ipcc4.ukmo_hadgem1.sresa1b.run1.monthly.tas_A1_2000_Jan_to_2099_Nov"
  load(era.file)
  field <- eval(parse(text=field.name))
  gcm <- retrieve.nc(gcm.name,x.rng=c(-50,50),y.rng=c(50,85),v.nam=v.nam)
  cfield <- catFields(field,gcm,lon=c(-50,50),lat=c(50,85),mon=1)
  eof12 <- EOF(cfield,mon=1)
  eof1 <- EOF(field,lon=c(-50,50),lat=c(50,85),mon=1)
  eof2 <- EOF(gcm, lon=c(-50,50),lat=c(50,85),mon=1)
  m1 <- plotEOF(eof1); while (dev.cur()>1) dev.off()
  m2 <- plotEOF(eof2); while (dev.cur()>1) dev.off()
  m <- plotEOF(eof12)
  dev.copy2eps(file=paste("qual.check-eof12-1.eps",sep="")); dev.off()

  map(m,col="red")
  map(m1,add=TRUE,col="steelblue",lwd=2)
  m2$date <- paste(m2$date,"")
  map(m2,add=TRUE,col="grey",lwd=2)
  dev.copy2eps(file=paste("qual.check-eof12-3.eps",sep="")); dev.off(); dev.off()
  dev.copy2eps(file=paste("qual.check-eof12-2.eps",sep="")); dev.off()

  obs <- KDVH4DS(StNr,param=param)
  ds1 <- DS(obs,eof1)
  dev.copy2eps(file=paste("qual.check-ds1-",StNr,"_eof1.eps",sep="")); dev.off()
  dev.copy2eps(file=paste("qual.check-ds2-",StNr,"_eof1.eps",sep="")); dev.off()
  ds2 <- DS(obs,eof12)
  dev.copy2eps(file=paste("qual.check-ds1-",StNr,"_eof12.eps",sep="")); dev.off()
  dev.copy2eps(file=paste("qual.check-ds2-",StNr,"_eof12.eps",sep="")); dev.off()

}

gcm.table <- function(StNr=90450,ele=101,scenario="sresa1b") {
  esd <- showall(StNr,ele=ele)
  #print(summary(esd))
  names <- switch(scenario,"sresa1b"=esd$scen.files.a1b,"c20"=esd$scen.files.20c)
  N <- length(names)
  gcms <- rep("NA",N); runs <- gcms
  for (i in 1:N) {
    dots <- instring(".",names[i])
    sce <- instring(scenario,names[i])
    rn <- instring("run",names[i])
    gcms[i] <- substr(names[i],dots[2]+1,sce[1]-1)
    runs[i] <- substr(names[i],rn[1]+3,rn[1]+3)
  }
  results <- data.frame(gcm=gcms,run=runs)
  print(table(results))
  print(N)
  invisible(results)
}

```

```
}

re.do <- function(param="TAM",economic=FALSE,a=c(99710,99720,99840,99910,99950),LINPACK=FALSE,
                 dlon=c(-20,20),dlat=c(-20,5)) {
  do.esd(param=param,LINPACK=LINPACK,economic=economic,a=a,dlon=dlon,dlat=dlat)
}
```